NACA

RESEARCH MEMORANDUM

WIND-TUNNEL MEASUREMENTS AT SUBSONIC SPEEDS OF THE STATIC AND DYNAMIC-ROTARY STABILITY DERIVATIVES OF A TRIANGULAR-WING AIRPLANE MODEL HAVING A TRIANGULAR VERTICAL TAIL

By Benjamin H. Beam, Verlin D. Reed, and Armando E. Lopez

Ames Aeronautical Laboratory
Moffett Field, Calif.

NATIONAL ADVISORY COMMITTEE FOR AERONAUTICS

WASHINGTON

April 25, 1955

NATIONAL ADVISORY COMMITTEE FOR AERONAUTICS

RESEARCH MEMORANDUM

WIND-TUNNEL MEASUREMENTS AT SUBSONIC SPEEDS OF THE STATIC AND DYNAMIC-ROTARY STABILITY DERIVATIVES OF A TRIANGULAR-WING AIRPLANE MODEL HAVING A TRIANGULAR VERTICAL TAIL[1]

By Benjamin H. Beam, Verlin D. Reed,
and Armando E. Lopez

SUMMARY

Oscillation tests were conducted in a wind tunnel to measure the dynamic-rotary stability derivatives of an airplane model at high subsonic speeds. The model wing was approximately triangular with an aspect ratio of 2.2 and the vertical tail was triangular. The Mach number range was from 0.25 to 0.95 and the basic Reynolds number was 1,500,000. The angle-of-attack range was from -8° to $+18^{\circ}$ at low speeds but was more restricted at high speeds because of model safety considerations. The oscillation frequency for the majority of the tests was approximately 8 cycles per second; however, some data are included for an oscillation frequency of approximately 4 cycles per second. The oscillation amplitude was approximately 2°.

Measurements included the damping in pitch, damping in yaw, damping in roll, the rolling moment due to yawing velocity, and the yawing moment due to rolling velocity. The static force and moment characteristics of the model are also presented. Comparisons have been made between experimental values of the stability derivatives and values estimated by current semiempirical methods using the wind-tunnel static-force data.

Generally fair agreement between estimation and experiment was obtained at low angles of attack for Mach numbers below 0.92. Some sizable differences were noted but these could be accounted for by simple modifications to existing methods of computation. For Mach numbers of 0.94 and 0.95 the damping in pitch and damping in yaw were considerably lower than at a Mach number of 0.92, and for angles of attack above 10° at high Mach numbers the rolling derivatives were violently affected by flow irregularities on the wings.

[1]Corrected version supersedes original version which was found to contain a computing error in the yawing-moment coefficients measured during static-force tests.

INTRODUCTION

The calculation and prediction of dynamic stability has assumed considerable importance in recent years and, in fact, has become a necessary part of nearly all current airplane design. The phase of these calculations which is normally subject to the greatest uncertainty is the estimation of the dynamic stability derivatives for high speeds. The methods used in evaluating these derivatives include both theoretical and experimental techniques. A large number of purely theoretical reports have been published of which references 1 and 2 are examples. Wind-tunnel measurements include data taken at low speeds in the Langley stability tunnel (ref. 3), tests with a steadily rolling model at high speeds (ref. 4), and experiments with oscillating models (refs. 5 and 6). Flight measurements include tests with both piloted airplanes (refs. 7, 8, and 9) and rocket-propelled or freely falling models of aircraft (ref. 10). The literature on this subject is extensive and the above references are only representative examples of the different techniques. Summaries of the unclassified research on dynamic stability and estimation of the stability derivatives can be found in references 11 and 12.

The method used to obtain the data in this report represents a new approach to the measurement of dynamic stability derivatives in a wind tunnel (ref. 13). The technique should have considerable appeal to designers confronted with the problem of evaluating the dynamic performance of an airplane. The necessary stability derivatives are measured on a scale model at high speeds and under oscillatory conditions. With these experimental data and supplementary static-force test data it is shown herein that reasonably accurate estimates of the longitudinal and the lateral-directional dynamic stability characteristics can be made. Thus the most uncertain part of the dynamic stability estimate - the evaluation of the derivatives - becomes amenable to wind-tunnel research. It is believed that methods such as this will permit the same assurance in estimating the oscillatory characteristics as wind-tunnel static-force tests have provided in static stability and control calculations.

Results of tests on an airplane model having a triangular wing and a triangular vertical tail are presented in this report. The principal emphasis has been placed on the presentation and discussion of the wind-tunnel data, and comparison with existing methods of estimating the stability derivatives. Some typical dynamic stability calculations are presented for a representative airplane to illustrate the application of the data.

SYMBOLS

Forces and moments are referred to the stability system of axes shown in figure 1. The various stability derivatives are defined as follows:

C_{L_α} $\dfrac{\partial C_L}{\partial \alpha}$

$C_{L_{\dot{\alpha}}}$ $\dfrac{\partial C_L}{\partial\left(\dfrac{\dot{\alpha}\bar{c}}{2V}\right)}$

C_{L_q} $\dfrac{\partial C_L}{\partial\left(\dfrac{q\bar{c}}{2V}\right)}$

C_{L_δ} $\dfrac{\partial C_L}{\partial \delta}$

C_{m_α} $\dfrac{\partial C_m}{\partial \alpha}$

$C_{m_{\dot{\alpha}}}$ $\dfrac{\partial C_m}{\partial\left(\dfrac{\dot{\alpha}\bar{c}}{2V}\right)}$

C_{m_q} $\dfrac{\partial C_m}{\partial\left(\dfrac{q\bar{c}}{2V}\right)}$

C_{m_δ} $\dfrac{\partial C_m}{\partial \delta}$

C_{Y_p} $\dfrac{\partial C_Y}{\partial\left(\dfrac{pb}{2V}\right)}$

C_{Y_r} $\dfrac{\partial C_Y}{\partial\left(\dfrac{rb}{2V}\right)}$

C_{Y_β} $\dfrac{\partial C_Y}{\partial \beta}$

C_{l_p} $\dfrac{\partial C_l}{\partial\left(\dfrac{pb}{2V}\right)}$

C_{l_r} $\dfrac{\partial C_l}{\partial\left(\dfrac{rb}{2V}\right)}$

C_{l_β} $\dfrac{\partial C_l}{\partial \beta}$

$C_{l_{\dot{\beta}}}$ $\dfrac{\partial C_l}{\partial\left(\dfrac{\dot{\beta}b}{2V}\right)}$

C_{n_p} $\dfrac{\partial C_n}{\partial\left(\dfrac{pb}{2V}\right)}$

C_{n_r} $\dfrac{\partial C_n}{\partial\left(\dfrac{rb}{2V}\right)}$

C_{n_β} $\dfrac{\partial C_n}{\partial \beta}$

$C_{n_{\dot{\beta}}}$ $\dfrac{\partial C_n}{\partial\left(\dfrac{\dot{\beta}b}{2V}\right)}$

The following additional symbols are used in the report:

C_L lift coefficient, $\frac{\text{lift}}{\frac{1}{2}\rho V^2 S}$

C_D drag coefficient, $\frac{\text{drag}}{\frac{1}{2}\rho V^2 S}$

C_Y side-force coefficient, $\frac{\text{side force}}{\frac{1}{2}\rho V^2 S}$

C_l rolling-moment coefficient, $\frac{\text{rolling moment}}{\frac{1}{2}\rho V^2 S b}$

C_m pitching-moment coefficient, $\frac{\text{pitching moment}}{\frac{1}{2}\rho V^2 S \bar{c}}$

C_n yawing-moment coefficient, $\frac{\text{yawing moment}}{\frac{1}{2}\rho V^2 S b}$

M Mach number

R Reynolds number

S wing area

S_t tail area

$T_{1/2}$, $T_{1/10}$ time to damp to one-half and one-tenth amplitude, respectively

V	velocity
b	wing span
c	local chord
$\bar{c}$	wing mean aerodynamic chord
$\bar{c}_t$	tail mean aerodynamic chord
f	frequency of oscillation, cps
l	tail length
p	rolling velocity
q	pitching velocity
r	yawing velocity
t	time
ΔX_{cg}	chordwise distance of aerodynamic center behind the center of gravity
α	angle of attack, radians except where noted
β	angle of sideslip, radians except where noted
δ	flap deflection angle, positive downward, deg

ρ	air density
ω	circular frequency of oscillation, $2\pi f$
$(\dot{})$	$\frac{d()}{dt}$

Symbols used only in the appendix are defined in the appendix.

MODEL

The model wing used in this investigation was approximately triangular and the vertical tail was triangular. Figure 2 is a three-view drawing of the model showing some of the important dimensions. A front quarter view of the model mounted on the oscillation apparatus in the wind tunnel is shown in the photograph, figure 3(a). Additional geometric and dimensional model data are given in table I.

The wing was provided with split flaps which could be set to angles of -4°, -8°, -12°, and -16°, and with a removable chordwise fence at 65-percent semispan on each wing panel. The fence extended from the wing leading edge to the flap hinge line and was 0.04c in height above the wing surface between chordwise stations of 0.1c and 0.5c. The flap and fence installation is shown in the photograph in figure 3(b).

Construction details of the model are of interest because of the unique problems presented in dynamic testing. Although the weight of the model did not have a direct bearing on the accuracy of the measured aerodynamic data, it was desirable to keep the weight as low as practicable because in this way other design and vibration problems in the model support and oscillation mechanism were minimized. Structural rigidity in the model was also felt to be desirable to minimize flutter and aeroelastic distortion although no quantitative measurements were made to evaluate their possible effects.

The model was built of aluminum alloy in four major parts: the wing, the vertical tail, the body shell, and the case which enclosed the oscillation mechanism or the strain-gage balance and to which the other parts were attached. The wing and vertical tail were of sandwich construction. Aluminum honeycomb was used as a core material and inserted into a one-piece skeletal framework for the wing which included the leading and trailing edges. This assembly was machined to a contour which, after the application of an aluminum alloy skin, would result in the proper wing shape. The skin was then bonded to the core and to the framework under

pressure using a resin adhesive. In the fabrication of the body, sections of shoft sheet aluminum were formed to shape in a drop-hammer die, then fastened together and attached to the case. The resulting weight of the model was approximately 16.7 pounds, of which the wing weight was 9.1 pounds, the tail 0.7 pound, the fuselage 3.3 pounds and the case 3.6 pounds.

APPARATUS

The static-force and -moment characteristics were measured with a 4-inch-diameter, four-component strain-gage balance enclosed within the model body. The dynamic stability derivatives were measured on a special oscillation apparatus which is a single-degree-of-freedom oscillatory system, described in detail in reference 13. The model was mounted on crossed-flexure restraining springs which permitted rotation about one axis only. Various combinations of rolling, pitching, and yawing motions were obtained in this system by variations in the orientation of the axis of oscillation. The moments due to prescribed combinations of these motions were measured and separated into the various stability derivatives.

Oscillations were excited and maintained about the axis of rotation by a push-rod linkage to an electromagnetic shaker. The shaker was, in turn, excited by an electronic feedback network which automatically selected the natural frequency of the oscillating model and the desired amplitude of oscillation. The necessary strain-gage measurements were processed through an analog computing system which evaluated and recorded the amplitude and phase relationship of each oscillatory quantity.

TESTS

Tests were originally planned for a range of angles of attack from -8° to $+18^{\circ}$ for Mach numbers from 0.25 to 0.95. The design of the oscillation apparatus was such that it was necessary to limit static pitching moments to approximately ±300 inch-pounds for the oscillation tests. The split flaps on the wing were therefore provided as a trimming device to maintain the pitching moment within these limits at high Mach numbers. This resulted in an overlapping in angle of attack at low Mach numbers with the various flap angles.

Oscillation tests were first attempted at a Reynolds number of 2,750,000. It was found that buffet or random aerodynamic disturbances were encountered for Mach numbers above 0.90 at all angles of attack, and for angles of attack above 8° at lower Mach numbers. These disturances resulted in difficulty in maintaining a uniform sinusoidal

oscillation and probably imposed loads on the model in excess of the design loads. The Reynolds number for the tests was therefore reduced to 1,500,000 at all Mach numbers above 0.25 to reduce the dynamic pressure and the possibility of model failure. While this permitted testing at Mach numbers up to 0.95 at low angles of attack, it was found that, despite the reduction in dynamic pressure, buffeting of the model and erratic aerodynamic moments still prevented reliable measurements above an angle of attack of 8° at Mach numbers above approximately 0.85.

Data were taken for oscillation frequencies of approximately 4 and 8 cycles per second. The oscillation frequency varied somewhat from these nominal values, depending on the variations in mass and aerodynamic restoring moments appropriate to a particular configuration. More complete data were obtained at the higher frequency because the restoring springs for this frequency were stiffer and the model oscillation was easier to control. Throughout the tests, data were taken for four different oscillation amplitudes ranging from peak amplitudes of less than 1° to approximately 3.5°. The data presented in this report were taken for a peak oscillation amplitude of approximately 2°, but no significant variations from the values shown were found for the other amplitudes.

CORRECTIONS TO DATA

The drag coefficient and the angle of attack have been corrected by the method of reference 14 for the induced effects of the tunnel walls resulting from lift on the model. The following corrections were added to the measured values:

$$\Delta\alpha = 0.25\ C_L, \text{ deg}$$

$$\Delta C_D = 0.0043\ C_L^2$$

Induced effects of the tunnel walls on the pitching-moment coefficient were calculated and found to be negligible. The dynamic stability derivatives have not been corrected for tunnel-wall effects resulting from lift on the model.

Corrections were applied to the data to account for the constriction effects of the tunnel walls using the method of reference 15. At a Mach number of 0.94 this correction amounted to an increase of less than 2 percent in the measured values of Mach number and dynamic pressure.

The drag data have been adjusted to correspond to a base pressure equal to free-stream static pressure. The effect of interference between the model and sting on measured values of pitching-moment coefficient was assumed to be negligible on the basis of measurements with two different

sting diameters - the 4-inch sting used for the static tests and the 2-1/4-inch sting used for the dynamic tests.

Corrections to the measured values of the damping coefficients due to internal damping of the model and oscillation mechanism were determined from wind-off measurements of the damping with the tunnel evacuated. This correction would have changed the measured values of C_{l_p} and C_{n_r} less than 0.005 (and values of $C_{m_q} + C_{m_{\dot{\alpha}}}$ less than 0.015) and was therefore considered negligible.

A correction to account for interaction within the oscillator mechanism was applied to the values of C_{n_p}. This correction was about 6 percent of the measured damping of the oscillation reduced to coefficient form (see ref. 13), and amounted to approximately -0.02 through the range of Mach numbers and angles of attack. Other interactions were found to be negligible.

The effect of sting resonance on the dynamic stability derivatives was established from a number of additional tests with the sting guyed rigidly to the tunnel wall and was found to be negligible. The effects of aerodynamic resonance caused by the wind-tunnel walls similar to that discussed in reference 16 cannot be determined accurately in this case. The relation used in reference 6 yields a minimum wind-tunnel resonant frequency of 17 cycles per second. This frequency was for a Mach number of 0.95, with higher resonant frequencies at lower Mach numbers. Since the model oscillation frequency never exceeded 10 cycles per second, it is doubtful that aerodynamic resonance had any important effect on the data.

RESULTS

Results of wind-tunnel tests of the model and some estimates of the controls-fixed oscillatory response are presented in the figures listed in the following table. All moments are referred to an assumed center of gravity situated in the plane of symmetry at a point $0.30\bar{c}$ behind the leading edge of the mean aerodynamic chord and $0.03\bar{c}$ above the wing-chord plane.

Static longitudinal characteristics	Figure
Basic data	4
Effects of fences	5
Effects of Reynolds number	6
Effects of sideslip angle	7
Body alone characteristics	7
Effects of Mach number	8

Except where noted, the Reynolds number for the tests was 2,750,000 for a Mach number of 0.25 and 1,500,000 for the higher Mach numbers.

DISCUSSION

Static Longitudinal Stability Characteristics

The static longitudinal characteristics of the model with no fences and with flaps undeflected are similar to results from other sources on triangular-wing models. In particular, the abrupt forward shift of the center of pressure and the corresponding reduction of lift-curve slope for angles of attack between 10° and 12° at high subsonic Mach numbers are similar to those noted in references 17 and 18. This effect has been attributed to a loss of lift at the wing tips as the leading-edge vortex separates from the wing tip and moves inboard.

Effects of flaps.- Deflection of the split flaps diminished the severity of the moment and lift change noted above, but the flap effectiveness was also greatly reduced for angles of attack above approximately 10°

(fig. 4). This is an undesirable characteristic if, as in this case, the flaps are used as a pitch control, since a reduction in flap effectiveness could result in difficulty in recovering from a pitched-up attitude.

Effects of fences.- Chordwise fences at 65-percent semispan were found to be partially effective in relieving the adverse effects of flow separation at the wing tips. This fence configuration was found to be the most promising of a number of possible wing fixes in tests of a similar model at the NACA's Langley Aeronautical Laboratory. As shown in figure 5, the presence of the fences on the wing prevented the reversal in the slope of the pitching-moment curve, but there was no corresponding improvement in flap effectiveness at the higher lift coefficients.

Effects of sideslip angle.- Moderate sideslip was found to alter the angle of attack at which the abrupt pitching-moment change occurred (fig. 7(c)). This was probably the result of changes in wing loading with the changes in effective sweepback angle for the sideslipping wing. The connection between pitching moment and sideslip angle in this range is also significant because it indicates an inter-relation between the longitudinal and lateral-directional stability problems, which are often considered separately.

Longitudinal Stability Derivatives, C_{m_α} and $C_{m_q} + C_{m_{\dot{\alpha}}}$

Two longitudinal stability derivatives were measured, C_{m_α} and $C_{m_q} + C_{m_{\dot{\alpha}}}$. These two terms and the lift-curve slope are the aerodynamic derivatives of greatest importance in determining the short-period, stick-fixed longitudinal motion, as will be shown for a representative airplane later in this report.

The static longitudinal stability derivative, C_{m_α}.- Values of C_{m_α}, the rate of change of pitching-moment coefficient with angle of attack, obtained in the oscillation tests are compared in figure 9 with values from static tests. Although there is substantial agreement between the two sets of data, values of C_{m_α} obtained under oscillatory conditions were generally more positive at the lower Mach numbers than those obtained under static conditions. After careful consideration of the possible sources of error, it was concluded that these data accurately reflect either a reduction in C_{L_α} or a slight forward shift in the center of pressure in the oscillatory case which was nearly independent of angle of attack. A forward shift in the center of pressure was observed in the data presented in reference 19 for a two-dimensional wing, while a rearward shift was noted in reference 5 for a triangular wing having an aspect ratio of 4. In the present case the change in C_{m_α} is equivalent to a shift of the center of pressure of not more than 5 percent of the mean aerodynamic chord.

The damping-in-pitch derivative, $C_{m_q} + C_{m_{\dot{\alpha}}}$.- Damping in pitch has been the subject of intensive investigation from both the theoretical and experimental standpoint in recent years. The theoretical analyses in references 2, 20, and 21 approach the problem from different viewpoints, yet the final results are in general agreement (fig. 13). The derivation of C_{m_q} given in Appendix A of reference 20 can be simplified by introducing numerical constants for some of the variables which were found to change only slightly with changes in aspect ratio and Mach number. (In using ref. 20 it should be noted that there is a typographical error in eq. (A13), and, as stated in the subsequently issued errata sheet, a minus sign should be inserted between C_{m_b}/ϵ and $\Delta X_{cg}/\bar{c}$.) The differences in the final result due to this approximation were found to be within ±0.1 for the plan form considered in this report, and this increment was not considered significant. The effect of the body on the damping in pitch can also be assumed negligible (figs. 12 and 13). Thus simplified, the expression for a triangular wing becomes

$$C_{m_q} = -\frac{1.0}{\sqrt{1-M^2}} - 0.9C_{L_\alpha}\left(\frac{\Delta X_{cg}}{\bar{c}}\right) - 2C_{L_\alpha}\left(\frac{\Delta X_{cg}}{\bar{c}}\right)^2 \qquad (1)$$

where C_{L_α} and $(\Delta X_{cg}/\bar{c})$ are from static-force data. Values of C_{m_q} calculated from equation (1) are shown in figure 13 to account approximately for the magnitude and the variation with Mach number of the experimental values of $C_{m_q} + C_{m_{\dot{\alpha}}}$ up to a Mach number of 0.92. No theory is known to the authors which would predict the observed reduction in damping above this Mach number.

The first term in equation (1) was obtained in reference 20 by a spanwise integration of the section pitching moments resulting from the effective camber and twist caused by the pitching motion. It is approximately constant for triangular wings at low Mach numbers, but can be shown to vary with wing plan form from approximately 1.0 for a triangular wing to $\pi/4$ for an unswept wing having a taper ratio of 1.0. The spanwise integration of section characteristics, or "strip theory," is also believed to be particularly applicable because the pitching moments due to camber do not depend on lift; therefore, a trailing vortex system does not have to be considered and the effects of finite span will be greatly reduced.

The damping in pitch given by equation (1) does not include $C_{m_{\dot{\alpha}}}$, but the theoretical values from reference 21 include such a contribution and consider the effect of the oscillating wake downstream of the wing from which the effects of frequency are calculated. At low Mach numbers the damping in pitch is shown (ref. 21) to remain approximately constant with variations in frequency at the low reduced frequencies encountered in dynamic stability calculations. This conclusion may not be valid,

however, at high Mach numbers or high angles of attack where the rate of change of angle of attack may have more profound effects on the damping.

Most theoretical estimates result in constant values of $C_{m_q} + C_{m_{\dot{\alpha}}}$ with variations of angle of attack. This follows from the same type of assumptions that result in theoretically constant values of C_{L_α} and C_{m_α} with angle of attack. These assumptions are not completely valid, however, and the changes that occur in damping in pitch with angle of attack are difficult to predict theoretically. A trend, noted previously in reference 22, is apparent in the data of this report and may be of value in empirically estimating variations of damping in pitch with angle of attack. It may be noted in figures 9 through 12 that there is a correspondence between variations in C_{m_α} with angle of attack and variations of opposite sign in $C_{m_q} + C_{m_{\dot{\alpha}}}$. This correlation extends even to small variations that might otherwise be dismissed as experimental scatter.

Effects of Mach number.- Comparison of these data with other measurements of damping in pitch for wings with related plan forms indicates that the variations with Mach number obtained in this case agree with trends anticipated from other data. In particular, the sharply reduced values of damping in pitch for Mach numbers of 0.94 and 0.95 (fig. 13) correspond with similar data in references 5, 6, 10, and 20 for triangular wings having aspect ratios from 2 to 4.

Effects of fences.- For Mach numbers of 0.60 and less, the changes in C_{m_α} caused by the addition of chordwise fences (fig. 10) are similar to changes indicated from the static-force data (fig. 5). For Mach numbers of 0.85 and 0.94 the beneficial effects of fences were not assessed because of the limited test range of angles of attack.

Static Lateral-Directional Stability Characteristics

The static lateral-directional characteristics of the model indicate a region of poor static stability at high Mach numbers for certain angles of attack. A range of marginal lateral stability existed which corresponds with the range in which difficulties were encountered with the static longitudinal stability, and presumably these two effects have the same origin. In addition, the static directional stability was adversely affected by a reduction in tail effectiveness in the presence of the wing at high Mach numbers.

In this discussion of the static lateral characteristics it is inferred that the static stability derivatives C_{l_β}, C_{Y_β}, and C_{n_β} can be calculated from data on C_l, C_Y, and C_n at $\beta = 6^\circ$. This requires the assumptions that C_l, C_Y, and C_n are zero for zero sideslip and that

they vary linearly with sideslip angle. Wind-tunnel data were obtained for zero sideslip and, although not presented, confirm that the lateral forces and moments were zero for zero sideslip. Additional tests, however, revealed some deviations from linearity at the higher Mach numbers in C_l, C_Y, and C_n between sideslip angles of 0° and 6°. From the data presented in figure 15 it is apparent that at a Mach number of 0.94 the tail contribution to C_n had a highly nonlinear variation with sideslip angle and therefore estimates of C_{n_β} based on the increment of C_n between 0° and 6° might be considerably in error in this region when applied to small variations of sideslip angle.

Separate effects of body, wing, and vertical tail.- The principal forces on a sideslipping body represent a yawing couple which tends to rotate the body to a position at right angles to the direction of flight. The resulting yawing-moment coefficient C_n is seen to be nearly constant through the range of Mach numbers and angles of attack (figs. 14(a) through 14(e)).

The important effect of sideslipping the wing is to be found in the rolling-moment coefficient C_l, or the effective dihedral parameter C_{l_β}. The recognized reason for the positive dihedral effect (negative values of C_l at positive angles of attack in fig. 14) is that the panel of a sideslipping swept wing which is advancing into the air stream will carry more lift than the trailing panel. This results in a rolling moment which tends to lift the advancing wing and to reduce the sideslip at positive angles of attack. For Mach numbers of 0.80 and 0.90 (figs. 14(b) and (c)) and angles of attack from 10° to 14°, the rolling moment contributed by the wing appears to have been nearly opposite to that which would be expected from the above reasoning. Evidently a loss of lift occurred on the outboard portions of the advancing wing in this range, adversely affecting the rolling as well as the static longitudinal stability.

As shown in figure 14, the vertical tail is necessary to stabilize the wing-body combination for all flight conditions. The destabilizing effect of the body is such that any marked decrease in C_n contributed by the tail results in static directional instability (figs. 14(c), (d), and (e)). The wing is shown to have had considerable influence on the tail characteristics from a comparison of the data for the wing-body-tail combination with those for the body-tail combination (fig. 14). One expected effect of the wing would be an increase in the effective aspect ratio of the tail. However, another effect is apparent at the higher Mach numbers which could account for the loss of directional stability noted in the preceding paragraph. For Mach numbers of 0.90 and above, the tail contribution depended on its position in the wing flow field. This latter effect is most clearly shown at a Mach number of 0.94 (fig. 14(e)) where the C_Y of the tail in the presence of the wing was less than in the absence of the wing for angles of attack between 0° and 10°.

The range of poor static directional stability noted in figure 14 includes the angles of attack and Mach numbers where poor static longitudinal and lateral stability were encountered. This combination of effects could result in extremely undesirable static stability characteristics because of the interrelations among the various moments involved.

Effects of wing fences.- Addition of the chordwise fences, which was found to be partially effective in improving the static longitudinal stability (fig. 5), is shown in figure 14 to have resulted in satisfactory lateral stability throughout the range of subsonic Mach numbers and angles of attack over which the tests were conducted. Addition of the fences produced little improvement in the regions of poor directional stability.

Sideslip Derivatives, C_{Y_β}, C_{l_β}, and C_{n_β}

Values of C_{l_β} and C_{n_β} obtained from the oscillation tests are presented in figure 16 along with values of C_{Y_β}, C_{l_β}, and C_{n_β} from the static-force and moment data. Theoretical methods of estimating these derivatives are available but little reliance is placed on these methods in practice (see ref. 12). Interference between the various parts of an airplane and the large and unpredictable effects of viscosity at the higher angles of attack prevent accurate estimation based on theory. Since these derivatives can be obtained from static-force and moment data similar to those in the preceding section, conventional wind-tunnel force tests are considered essential in their determination. In the present case a comparison can be made between values of C_{l_β} and C_{n_β} obtained separately from the oscillation tests and from the static tests.

Rolling moment due to sideslip, C_{l_β}.- At low Mach numbers (fig. 16(a)) values of C_{l_β} obtained under oscillatory conditions were approximately linear with angle of attack and differ considerably at high angles of attack from values obtained in static-force tests. For example, at an angle of attack of 18°, C_{l_β} from the oscillation tests was approximately double that from the static tests. The linear variation with angle of attack would be expected from purely theoretical considerations (ref. 12), and this effect may therefore be an indication of a decrease in viscous or boundary-layer effects under oscillatory conditions.

Small negative and even positive values of C_{l_β} were measured at 10° angle of attack in the oscillation tests at the higher Mach numbers (figs. 16(b), (c), and (d)). This agrees with the static-force data in indicating a region of reduced static lateral stability but does not cover as broad a range of angles of attack.

Yawing moment due to sideslip, C_{n_β}.- As seen in figures 16 and 19, the values of C_{n_β} obtained under oscillatory conditions do not agree with the values from static tests as well as would be expected. Some Reynolds number effects are apparent in the data from the oscillation tests (fig. 18), an increase in Reynolds number from 1,500,000 to 2,750,000 generally resulting in better agreement with the static-test data. Also, as noted previously, the static-force data are based on an increment of 6° in sideslip angle. The static-force data shown in figure 15 for an angle of attack of 6° indicate that if an increment of sideslip angle of ±2° had been used, as in the oscillation tests, the static-force data would then more nearly correspond with those obtained under oscillatory conditions at the lower Reynolds number.

Separate effects of wing, vertical tail, and body.- The remarks on the effect of the separate model components discussed in connection with the static lateral-directional characteristics apply also to the results of the oscillation tests, with the exception that the effectiveness of the wing and tail was apparently increased in the oscillatory case. These differences are pointed out in the above discussion of C_{l_β} and C_{n_β}.

Effects of the fences.- As shown in figure 17, addition of the chordwise fences resulted in a more linear variation of C_{l_β} with angle of attack. The increment of C_{l_β} due to the fences for a Mach number of 0.25 was somewhat higher than the increment indicated from the static data (fig. 14(a)). Addition of the chordwise fences produced no change in the measured values of C_{n_β} within the range of angles of attack at which tests were conducted and these data have been omitted.

Lateral-Directional Rotary Derivatives, C_{l_p}, C_{n_p}, $C_{l_r}-C_{l_{\dot\beta}}$, and $C_{n_r}-C_{n_{\dot\beta}}$

The most serious problem in calculating the oscillatory stability of an airplane is in accurately evaluating the lateral-directional damping derivatives including the cross derivatives. Little reliance can be placed on purely theoretical estimates because of the difficulty of predicting the effects of angle of attack and interference between different parts of the airplane. On the other hand, measurement of the derivatives requires special techniques and apparatus. The current methods of estimating these derivatives, particularly the cross derivatives C_{n_p} and $C_{l_r}-C_{l_{\dot\beta}}$, are semiempirical. Wind-tunnel force data are used as a basis for correcting theoretical estimates for the approximate effects of viscosity and interference. Suggested procedures and a summary of various methods for computing these derivatives are presented in reference 12 and have been used in this report as a basis for comparing the experimental data with calculated values. In the cases where it was found that reference 12 had been

superseded by more modern methods or that more recent experimental data had become available, this has been indicated.

Damping in roll, C_{l_p}.- Experimental data (figs. 20(b), (c), and (d)) indicate a reduction in the damping in roll at high Mach numbers and at 10° angle of attack, which is attributed to flow irregularities at the wing tips. Except for the fact that these flow irregularities occurred at an angle of attack about 2° higher in the static test than in the oscillation test, the estimates of C_{l_p} based on the static data agree well with data from the oscillatory tests.

Yawing moment due to rolling velocity, C_{n_p}.- This derivative appears to be the most nearly negligible of all the lateral-directional rotary derivatives for an airplane of this type. From the theory of reference 12 the wing contribution to C_{n_p} would be expected to have large positive values at the higher angles of attack (fig. 20). Reference 4 is a more recent paper in which it is shown that for a wing of this plan form much better agreement with experiment can be obtained by an improvement in the previous method. Estimated values of C_{n_p} for the wing alone using calculated values of C_{l_p} and the method of reference 4 are shown for the present data also to agree satisfactorily with the experimental data.

Rolling moment due to yawing velocity, $C_{l_r}-C_{l_{\dot{\beta}}}$.- In previous estimates of dynamic stability, it has generally been the practice to assume that the rolling moment due to sideslip velocity, $C_{l_{\dot{\beta}}}$, was negligible. Since $C_{l_{\dot{\beta}}}$ cannot be separated from C_{l_r} in the case of the present experimental data, it is not possible to check the validity of this assumption. The estimated values of C_{l_r} in figure 20 are based on a semiempirical method (ref. 12) first presented in reference 23 in which force-test data on C_{l_β} were used to predict a deviation of C_{l_r} from the theoretical straight-line variation with angle of attack. When values of C_{l_β} from the static-force tests are used, there is considerable discrepancy between the estimated and experimental values (fig. 20). At low speeds (fig. 20(a)) the experimental data for $C_{l_r}-C_{l_{\dot{\beta}}}$ appear to approach a theoretical straight-line variation with angle of attack in a manner similar to that noted previously in connection with C_{l_β}. Furthermore, the variation of C_{l_r} with C_L or α estimated from purely theoretical considerations (fig. 13 of ref. 12) is shown to agree approximately with experiment in figure 20(a). However, because of the lack of agreement between estimated and experimental values of C_{l_β} (C_{l_β} from either static or dynamic tests), this is not the variation that would be obtained using

the method of reference 23, and experimental values of C_{l_β}. This suggests that the theory for the variation of C_{l_r} with C_L is valid within its limits, but that it may not be desirable to apply the empirical correction to the theory indicated in reference 23.

From the limited data at high Mach numbers and high angles of attack, it appears that $C_{l_r}-C_{l_{\dot{\beta}}}$ is violently affected by the flow irregularities at the wing tips. Data have been included for an angle of attack of 10° at 0.80 Mach number (fig. 20(c)) which indicated a value of this derivative of +0.8. It is important to note here that since all the rolling-moment derivatives, C_{l_β}, C_{l_p}, and $C_{l_r}-C_{l_{\dot{\beta}}}$, are particularly sensitive to asymmetry in the lift on the wings, any abrupt changes in loading with angle of attack on either wing panel would be expected to affect these derivatives.

Damping in yaw, $C_{n_r}-C_{n_{\dot{\beta}}}$.- In the past the yawing moment due to sideslipping velocity has usually been neglected and the damping in yaw computed as the yawing moment due to yawing velocity, C_{n_r}. Estimates of C_{n_r} from the method of reference 12 are generally about half as large as the experimental values at the lower Mach numbers and angles of attack, and the largest discrepancy is in the contribution of the tail. This discrepancy can be accounted for by noting that, because of the short tail length compared with the root chord of the tail, certain terms which are neglected in reference 12 assume considerable importance. As the tail length is shortened, estimation of C_{n_r} becomes analogous to that for C_{m_q}. The yawing velocity introduces changes in loading which move the effective center of pressure of the tail rearward and result in higher values of C_{n_r} than the method of reference 12 indicates.

The equation given in reference 12 for the damping in yaw of the tail is

$$C_{n_{r_{tail}}} = 2\left(\frac{l}{b}\right)^2 C_{Y_{\beta_{tail}}} \tag{2}$$

where the tail length l is the distance between the center of pressure of the tail and the moment center of the airplane measured parallel to the longitudinal stability axis. Where this distance is calculated from force-test data, the damping of the tail becomes

$$C_{n_{r_{tail}}} = 2\frac{\left(C_{n_{\beta_{tail}}}\right)^2}{C_{Y_{\beta_{tail}}}} \tag{3}$$

A simplified form of the equation for the damping in pitch of a triangular wing was shown to be (eq. (1)).

$$C_{m_q} = -\frac{1.0}{\sqrt{1-M^2}} - 0.9C_{L_\alpha}\left(\frac{\Delta X_{cg}}{\bar{c}}\right) - 2C_{L_\alpha}\left(\frac{\Delta X_{cg}}{\bar{c}}\right)^2 \qquad (1)$$

Comparison of equations (1) and (2) reveals that the expression for $C_{n_{r_{tail}}}$ (eq. (2)) corresponds to the last term of the equation for C_{m_q}, and that a more accurate result would be obtained by including the additional terms similar to those in equation (1). The equation for $C_{n_{r_{tail}}}$ then becomes, for a triangular vertical tail,

$$C_{n_{r_{tail}}} = -\frac{1.0}{\sqrt{1-M^2}}\frac{S_t}{S}\left(\frac{\bar{c}_t}{b}\right)^2 + 0.9C_{Y_{\beta_{tail}}}\left(\frac{\bar{c}_t}{b}\right)\left(\frac{l}{b}\right) + 2C_{Y_{\beta_{tail}}}\left(\frac{l}{b}\right)^2 \qquad (4)$$

Equation (4) illustrates the relative importance of tail chord $\bar{c}_t$ and tail length l. In a form in which force-test data could be used to compute effective tail length, equation (4) becomes

$$C_{n_{r_{tail}}} = -\frac{1.0}{\sqrt{1-M^2}}\frac{S_t}{S}\left(\frac{\bar{c}_t}{b}\right)^2 - 0.9\left(\frac{\bar{c}_t}{b}\right)C_{n_{\beta_{tail}}} + 2\frac{\left(C_{n_{\beta_{tail}}}\right)^2}{C_{Y_{\beta_{tail}}}} \qquad (5)$$

The additional terms in equation (5) amount to approximately -0.06 for $M = 0$, using $\bar{c}_t$ based on a projection of the tail to the fuselage center line. This approximately accounts for the difference between the experimental data and the theory of reference 12 for low speeds (fig. 20(a)).

There was a sharp decrease in tail contribution to the damping in yaw at high Mach numbers (figs. 20(g), (h), and 23). Although no positive values of $C_{n_r}-C_{n_{\dot{\beta}}}$ were measured, it is evident that at the highest Mach number the trend was toward a further reduction in damping with increasing Mach number. This observed variation of damping in yaw with Mach number is similar to that observed previously in damping in pitch (fig. 13).

Separate effects of body, wing, and vertical tail.- The body contribution to the lateral-velocity derivatives is normally small (ref. 12). Experimental data were obtained only for the damping in yaw of the body alone. This derivative, $C_{n_r}-C_{n_{\dot{\beta}}}$, was found to be positive, or destabilizing, for angles of attack above approximately 12° (fig. 20). Similar

effects at moderate angles of attack have been observed previously for bodies with flattened upper and lower surfaces (ref. 24). When the wings are added to the body, however, the combination becomes dynamically stable and the damping in yaw increases at the higher angles of attack in the manner indicated by the theory for the wing-body combination.

Since the wing and tail had the same plan form, and since the damping in roll is proportional to the area of the lifting surface and the square of a lever arm, the relative contribution of the wing and tail should be roughly proportional to the fourth power of their linear dimensions. On this basis, the contribution of the tail should be approximately 8 percent of the wing damping in roll, where the tail is assumed to extend to the body center line. This is approximately the order of magnitude indicated in the experimental data (fig. 20).

At high angles of attack, the wing is of chief importance in the determination of the rolling moment due to yawing, $C_{l_r}-C_{l_\beta}$. In addition, the tail is subjected to two effects which diminish its effectiveness; one of these is the blanketing effect of the body, and the other is a shortening of the tail height due to inclination of the model longitudinal axis.

Effects of fences.- In figure 21 it is shown that the addition of wing fences resulted in a more nearly linear variation of $C_{l_r}-C_{l_\beta}$ with angle of attack for Mach numbers of 0.25 and 0.60 and near 10° angle of attack. Data were not taken at high Mach numbers in this range of angles of attack, but it appears from a study of the static-force data (figs. 5 and 14) that a change similar to that shown in figs. 21(a) and (b) would be expected at higher Mach numbers.

Effects of Reynolds number.- For the Reynolds numbers at which oscillation tests were conducted (1,500,000 and 2,750,000) there were no large effects of Reynolds number on the lateral rotary derivatives (fig. 22). It will be recalled, however, from the discussion of C_{n_β} and figure 18 that there was a change in the tail contribution to C_{n_β} in this range of Reynolds number. No effects of Reynolds number on the contribution of the wing were apparent in these data or in the longitudinal characteristics (figs. 6 and 11).

Effects of oscillation frequency.- The effects of frequency were found to be small from additional tests conducted at a frequency of approximately 4 cycles per second, roughly half the oscillation frequency at which most of the oscillation data were obtained. The combination of changes in Mach number and oscillation frequency made available a range of reduced frequencies $\omega b/2V$, from approximately 0.003 at the high Mach numbers to 0.26 at low speeds. Experimental data for three representative Mach

numbers are shown in figure 18 for the sideslip derivatives and in figure 22 for the rotary derivatives.

It will be noted that in figure 22 the data on the cross derivatives have been presented as the combined derivative term $C_{n_p} + \left(C_{l_r} - C_{l_{\dot{\beta}}}\right)$. This form was considered justifiable because of the lack of apparent frequency effects in the range investigated, and resulted in considerable simplification in the test procedure.

Effects of oscillation amplitude.- All the experimental data presented in this report were taken for a peak oscillation amplitude of approximately 2°. The range of the tests, however, included peak oscillation amplitudes from less than 1° to approximately 3.5° to establish the effects of oscillation amplitude (see ref. 13). Particular attention was directed to the type of low-amplitude instability in pitch at high Mach numbers noted in reference 6 but no similar effects were found in the present investigation.

Dynamic-Stability Estimates

In order to provide more perspective in the evaluation of the dynamic stability of this particular configuration, the data in the foregoing figures have been applied to estimates of the dynamic motions for a representative airplane geometrically similar to the model. Values of the period and time to damp of the short-period longitudinal and the lateral-directional oscillations have been calculated. The longitudinal characteristics have then been compared with the Air Force and Navy flying qualities requirements (ref. 25) defining the relation between the period and damping which is considered satisfactory from the standpoint of dynamic stability. These criteria of dynamic stability do not necessarily imply that unsafe or divergent motions will result if the criteria are not satisfied, but are merely rough indications as to whether the airplane will be able to execute satisfactorily its expected maneuvers in this range.

A wing area of 650 square feet and an airplane weight of 23,000 pounds has been assumed in the calculations. Additional assumed mass and geometric data are listed in table II. The airplane was considered to be in level flight at the start of the motion with no movement of the control surfaces during the oscillation.

Dynamic longitudinal stability.- The method used in the estimation of the period and damping of the short-period longitudinal oscillation is given in the appendix, and the results of the calculations are presented in figure 24. On the basis of figure 24 it appears that the dynamic stability is satisfactory for level flight between the Mach numbers of 0.25

and 0.94. For Mach numbers between 0.92 and 0.94, the strongest contributing factor in the increase in time to damp is the decrease in damping in pitch in this range (fig. 13). The extremely low negative or even positive values of damping-in-pitch coefficient do not result in similarly lightly damped or divergent motions in the stick-fixed, longitudinal oscillation because of the additional damping contributed by C_{L_α}. (See Appendix A, eq. (A7).)

A number of other aerodynamic derivatives enter into the estimation of the longitudinal oscillation (see appendix), but the effects of these additional terms can be shown to be small and in many cases entirely negligible. Variations in $C_{L_{\dot{\alpha}}}$ and C_{L_q} through a range of values from 0 to 4 (typical for this configuration) resulted in changes in period and time to damp of the order of 1 to 2 percent. Independent measurement of C_{m_q} or $C_{m_{\dot{\alpha}}}$ does not appear to be necessary for the conditions represented in figure 24 since the term $C_{m_q} + C_{m_{\dot{\alpha}}}$ is important when computing the time to damp, but some changes are produced in the period of the oscillation by the relative contribution of C_{m_q} and $C_{m_{\dot{\alpha}}}$. If the measured damping is assumed to be entirely due to $C_{m_{\dot{\alpha}}}$, the estimated period of the oscillation for this airplane will be about 10 percent higher than if the damping is assumed to be entirely due to C_{m_q} (from Appendix A, eq. (A8)).

Dynamic lateral stability.- The period and damping of the lateral-directional oscillation, calculated by the method of reference 12, are presented in figure 25. It is important to note that the period and damping of the lateral-directional mode of oscillation is not always a sufficient indication of whether the dynamic motion of an airplane following various types of disturbances will be satisfactory. The flying qualities requirements (ref. 25) have recently been changed to take note of this, and calculations of the time histories of the motions are becoming more popular. The results presented in figure 25, however, indicate that for Mach numbers above 0.85 the damping of the lateral oscillation becomes markedly less at altitude.

For level flight the angles of attack of 10° and 12° are encountered only at high altitudes and low Mach numbers. The differences in oscillation characteristics between 30,000 and 40,000 feet at a Mach number of 0.60 (fig. 25) represent the effect of increasing the angle of attack from 7° to 10°, the point where the previously noted flow separation at the wing tips occurred. Although no large effects are indicated in figure 25, these calculations should be interpreted with considerable caution in this angle-of-attack region because of the possibly large effects of nonlinearities or other deviations from the assumed conditions.

Derivatives other than those included in the data of this report are encountered in the calculation of the lateral-directional motions of a rigid airplane, the most important of which are C_{Y_r} and C_{Y_p}. Estimates

[redacted]

of these derivatives revealed that for the present configuration, their effect was small and could be neglected. The equations in reference 12 do not consider the derivatives due to sideslipping velocity, and therefore the measured values of $C_{n_r}-C_{n_{\dot{\beta}}}$ and $C_{l_r}-C_{l_{\dot{\beta}}}$ have been used in the equations in place of C_{n_r} and C_{l_r}. This is, however, believed to be the most accurate way to account for the possible effects of sideslipping velocity in the absence of independent measurements of $C_{l_{\dot{\beta}}}$ and $C_{n_{\dot{\beta}}}$.

SUMMARY OF RESULTS

From the results of wind-tunnel measurements of the static-force characteristics and the dynamic rotary stability derivatives for a triangular-wing airplane model having a triangular vertical tail, the following observations may be made:

1. For Mach numbers above 0.60 and angles of attack of 10° and higher, the static longitudinal stability characteristics were found to be undesirable. A chordwise fence was partially successful in improving the longitudinal characteristics in this range.

2. The static lateral stability was found to be marginal for the same test conditions that resulted in undesirable static longitudinal characteristics. In addition, some of the data indicate a decrease in effectiveness of the vertical tail at high Mach numbers at certain positive angles of attack with a consequent reduction and, in some instances, loss of directional stability.

3. Measured values of the damping-in-pitch derivative, $C_{m_q} + C_{m_{\dot{\alpha}}}$, were in approximate agreement with current methods of estimating this coefficient up to a Mach number of 0.92. A sharp reduction in damping was noted above this Mach number which agrees with trends indicated by other experimental data.

4. The damping-in-roll derivative, C_{l_p}, was found to be negative and in fair agreement with theory through the Mach number range.

5. The yawing-moment-due-to-rolling derivative, C_{n_p}, was found to be small and could be estimated approximately with an existing semiempirical method.

6. Values of the damping-in-yaw derivative, $C_{n_r}-C_{n_{\dot{\beta}}}$, estimated by a current approximate method were found to agree with experiment at low speeds when a modification was made to account properly for the contribution of the vertical tail. At Mach numbers of 0.94 and 0.95 the damping

in yaw was reduced from that at 0.92 and lower Mach numbers in a manner similar to that observed with damping in pitch.

7. The rolling-moment-due-to-yawing derivative, $C_{l_r}-C_{l_{\dot{\beta}}}$, was in generally poor agreement with theory for both the wing and the tail contribution. In addition, limited data at high Mach numbers and high angles of attack indicate that this derivative is violently affected by the flow irregularities which also result in the reduced static stability.

8. Differences were noted in some cases between values of the derivatives, C_{m_α}, C_{l_β}, and C_{n_β}, under oscillatory conditions and those from the static data.

Ames Aeronautical Laboratory,
National Advisory Committee for Aeronautics,
Moffett Field, Calif., Jan. 28, 1955.

APPENDIX A

PERIOD AND TIME TO DAMP OF THE LONGITUDINAL OSCILLATION

The equations for the short-period stick-fixed longitudinal motion and their solution have been presented in a number of publications, but not in a form which is readily applicable to the calculation of the period and time to damp to one-half amplitude. The equations of motion (A1) and (A2) are identical to those in reference 20, wherein it is assumed that changes in aircraft forward speed are negligible and that the longitudinal motion is a small-amplitude disturbance from equilibrium. The motion is defined approximately by two linear differential equations describing pitching about the y axis and translation along the z axis.

$$\frac{1}{2}\rho V^2 S\left[\frac{\bar{c}}{2V}\left(C_{L_{\dot{\alpha}}}\dot{\alpha}+C_{L_q}q\right)+C_{L_\alpha}(\Delta\alpha)\right]=mV(q-\dot{\alpha}) \tag{A1}$$

$$\frac{1}{2}\rho V^2 S\bar{c}\left[\frac{\bar{c}}{2V}\left(C_{m_{\dot{\alpha}}}\dot{\alpha}+C_{m_q}q\right)+C_{m_\alpha}(\Delta\alpha)\right]=I_{\dot{q}} \tag{A2}$$

where m is the mass of the airplane; I is the mass moment of inertia about the y axis; and $\Delta\alpha$ is an incremental change in angle of attack.

With the substitutions $\tau=\frac{m}{\rho VS}$, $K=\frac{2I}{\rho V^2 S\bar{c}}$, and by use of the operator $D=\frac{d}{dt}$, the above equations become,

$$\left[\left(\frac{\bar{c}}{2V}C_{L_{\dot{\alpha}}}+2\tau\right)D+C_{L_\alpha}\right]\Delta\alpha+\left(\frac{\bar{c}}{2V}C_{L_q}-2\tau\right)q=0 \tag{A3}$$

$$\left(\frac{\bar{c}}{2V}C_{m_{\dot{\alpha}}}D+C_{m_\alpha}\right)\Delta\alpha+\left(\frac{\bar{c}}{2V}C_{m_q}-KD\right)q=0 \tag{A4}$$

The solution is of the form

$$\Delta\alpha,q=(\text{const.})e^{\lambda t}$$

where λ is a root of the characteristic equation of the system, given by

$$A\lambda^2+B\lambda+C=0 \tag{A5}$$

and

$$A = -K\left(\frac{\bar{c}}{2V} C_{L_{\dot{\alpha}}} + 2\tau\right)$$

$$B = \left(\frac{\bar{c}}{2V}\right)^2 \left(C_{m_q} C_{L_{\dot{\alpha}}} - C_{m_{\dot{\alpha}}} C_{L_q}\right) + 2\tau \frac{\bar{c}}{2V} \left(C_{m_q} + C_{m_{\dot{\alpha}}}\right) - KC_{L_\alpha}$$

$$C = \frac{\bar{c}}{2V} \left(C_{m_q} C_{L_\alpha} - C_{m_\alpha} C_{L_q}\right) + 2\tau C_{m_\alpha}$$

Thus,

$$\lambda_1, \lambda_2 = \frac{-B \pm \sqrt{B^2 - 4AC}}{2A} \tag{A6}$$

For an oscillatory system, $4AC > B^2$ and the roots are complex conjugates. The logarithmic decrement of the oscillation becomes $-\frac{B}{2A}$, and the time to damp to one-half amplitude becomes

$$T_{1/2} = \left(\frac{2A}{B}\right) \ln 2 = 1.386 \frac{A}{B} \tag{A7}$$

The period of the oscillation is derived from the imaginary part of the root as

$$P = \frac{4\pi A}{\sqrt{4AC - B^2}} = \frac{2\pi}{\sqrt{\frac{C}{A} - \frac{B^2}{4A^2}}} \tag{A8}$$

REFERENCES

1. Toll, Thomas A., and Queijo, M. J.: Approximate Relations and Charts for Low-Speed Stability Derivatives of Swept Wings. NACA TN 1581, 1948.

2. Sacks, Alvin H.: Aerodynamic Forces, Moments, and Stability Derivatives for Slender Bodies of General Cross Section. NACA TN 3283, 1954.

3. Bird, John D., and Jaquet, Byron M.: A Study of the Use of Experimental Stability Derivatives in the Calculation of the Lateral Disturbed Motions of a Swept-Wing Airplane and Comparison With Flight Results. NACA Rep. 1031, 1951.

4. Wiggins, James W.: Wind-Tunnel Investigation at High Subsonic Speeds to Determine the Rolling Derivatives of Two Wing-Fuselage Combinations Having Triangular Wings, Including a Semiempirical Method of Estimating the Rolling Derivatives. NACA RM L53L18a, 1954.

5. Tobak, Murray: Damping in Pitch of Low-Aspect-Ratio Wings at Subsonic and Supersonic Speeds. NACA RM A52L04a, 1953.

6. Beam, Benjamin H.: The Effects of Oscillation Amplitude and Frequency on the Experimental Damping in Pitch of a Triangular Wing Having an Aspect Ratio of 4. NACA RM A52G07, 1952.

7. Triplett, William C., and Brown, Stuart C.: Lateral and Directional Dynamic-Response Characteristics of a 35° Swept-Wing Airplane as Determined from Flight Measurements. NACA RM A52I17, 1952.

8. Donegan, James J., and Pearson, Henry A.: Matrix Method of Determining the Longitudinal-Stability Coefficients and Frequency Response of an Aircraft from Transient Flight Data. NACA Rep. 1070, 1952.

9. Donegan, James J., Robinson, Samuel W., Jr., and Gates, Ordway B. Jr.: Determination of Lateral-Stability Derivatives and Transfer-Function Coefficients From Frequency-Response Data for Lateral Motions. NACA TN 3083, 1954.

10. D'Aiutolo, Charles T.: Low-Amplitude Damping-in-Pitch Characteristics of Tailless Delta-Wing-Body Combinations at Mach Numbers from 0.80 to 1.35 as Obtained With Rocket-Powered Models. NACA RM L54D29, 1954.

11. Milliken, W. F., Jr.: Dynamic Stability and Control Research. Cornell Aeronautical Laboratory Rep. CAL-39, Buffalo, 1951.

12. Campbell, John P. and McKinney, Marion O.: Summary of Methods for Calculating Dynamic Lateral Stability and Response and for Estimating Lateral Stability Derivatives. NACA Rep. 1098, 1952.

13. Beam, Benjamin H.: A Wind-Tunnel Test Technique for Measuring the Dynamic Rotary Stability Derivatives Including the Cross Derivatives at High Mach Numbers. NACA TN 3347, 1955.

14. Glauert, H.: The Elements of Aerofoil and Airscrew Theory. The University Press, Cambridge, England, 1926, ch. XIV.

15. Herriot, John G.: Blockage Corrections for Three-Dimensional-Flow Closed-Throat Wind Tunnels With Consideration of the Effect of Compressibility. NACA Rep. 995, 1950. (Formerly NACA RM A7B28)

16. Runyan, Harry L., Woolston, Donald S., and Rainey, A. Gerald: A Theoretical and Experimental Study of Wind-Tunnel-Wall Effects on Oscillating Air Forces for Two Dimensional Subsonic Compressible Flow. NACA RM L52I17a, 1953.

17. Wiggins, James W.: Wind-Tunnel Investigation at High Subsonic Speeds of the Static Longitudinal and Static Lateral Stability Characteristics of a Wing-Fuselage Combination Having a Triangular Wing of Aspect Ratio 2.31 and an NACA 65A003 Airfoil. NACA RM L53G09a, 1953.

18. Smith, Donald W., and Heitmeyer, John C.: Lift, Drag, and Pitching Moment of Low-Aspect-Ratio Wings at Subsonic and Supersonic Speeds - Plane Triangular Wing of Aspect Ratio 2 with NACA 0005-63 Section. NACA RM A50K21, 1951.

19. Wyss, John A., and Herrera, Raymond: Effects of Angle of Attack and Airfoil Profile on the Two-Dimensional Flutter Derivatives for Airfoils Oscillating in Pitch at High Subsonic Speeds. NACA RM A54H12, 1954.

20. Tobak, Murray, Reese, David E., Jr., and Beam, Benjamin H.: Experimental Damping in Pitch of 45° Triangular Wings. NACA RM A50J26, 1950.

21. Lehrian, Doris E.: Calculation of Stability Derivatives for Oscillating Wings. British ARC 15,695 - 0.1045, S. & C. 2750, 1953.

22. Kemp, William B., Jr., and Becht, Robert E.: Damping-in-Pitch Characteristics at High Subsonic and Transonic Speeds of Four 35° Sweptback Wings. NACA RM L53G29a, 1953.

23. Campbell, John P., and Goodman, Alex: A Semi-empirical Method for Estimating the Rolling Moment Due to Yawing of Airplanes. NACA TN 1984, 1949.

24. Johnson, Joseph L.: Damping in Yaw and Static Directional Stability of a Canard Airplane Model and of Several Models Having Fuselages of Relatively Flat Cross Section. NACA RM L50H30a, 1950.

25. Anon.: Flying Qualities of Piloted Airplanes. U. S. Air Force Spec. MIL-F-8785(ASG), Sept. 1, 1954.

TABLE I.- MODEL DIMENSIONS

Wing (Basic plan form, leading and trailing edges extending to vertex and to plane of symmetry)	
Span, b, ft	2.86
Area, S, sq ft	3.72
Mean aerodynamic chord, $\bar{c}$, ft	1.74
Aspect ratio	2.20
Leading-edge sweep, deg	60
True taper ratio (with cropped tips)	0.03
Incidence, deg	0
Dihedral, deg	0
Airfoil section	NACA 0004-65
Vertical location (chord plane below moment center), ft	0.05
Vertical Tail (Basic triangle projected to body center line)	
Span, ft	0.91
Area, S_t, sq ft	0.71
Exposed area above body, sq ft	0.37
Mean aerodynamic chord, $\bar{c}_t$, ft	1.05
Aspect ratio	1.16
Airfoil section	NACA 0004-65
Length, l (moment center to 0.35 $\bar{c}_t$), ft	0.60
Flap	
Area (total), sq ft	0.39
Length (moment center to hinge line), ft	1.00
Body	
Length, ft	3.67
Base area, sq ft	0.12
Moment Center (on body center line)	
Horizontal location (aft of leading edge of m. a. c.)	0.30$\bar{c}$

TABLE II.- ASSUMED GEOMETRIC AND MASS DATA FOR REPRESENTATIVE AIRPLANE

Geometric data	
Model scale (wing area 650 sq ft)	0.075
Mass data	
Weight, lb	23,000
I_{x_o}, slug-ft^2	13,566
I_{y_o}, slug-ft^2	89,357
I_{z_o}, slug-ft^2	99,695
ϵ, deg	1.75

where: I_{x_o}, I_{y_o}, I_{z_o} moments of inertia about the principal axes

ϵ inclination of the principal axes to the body axes (positive principal longitudinal axis below wing chord line)

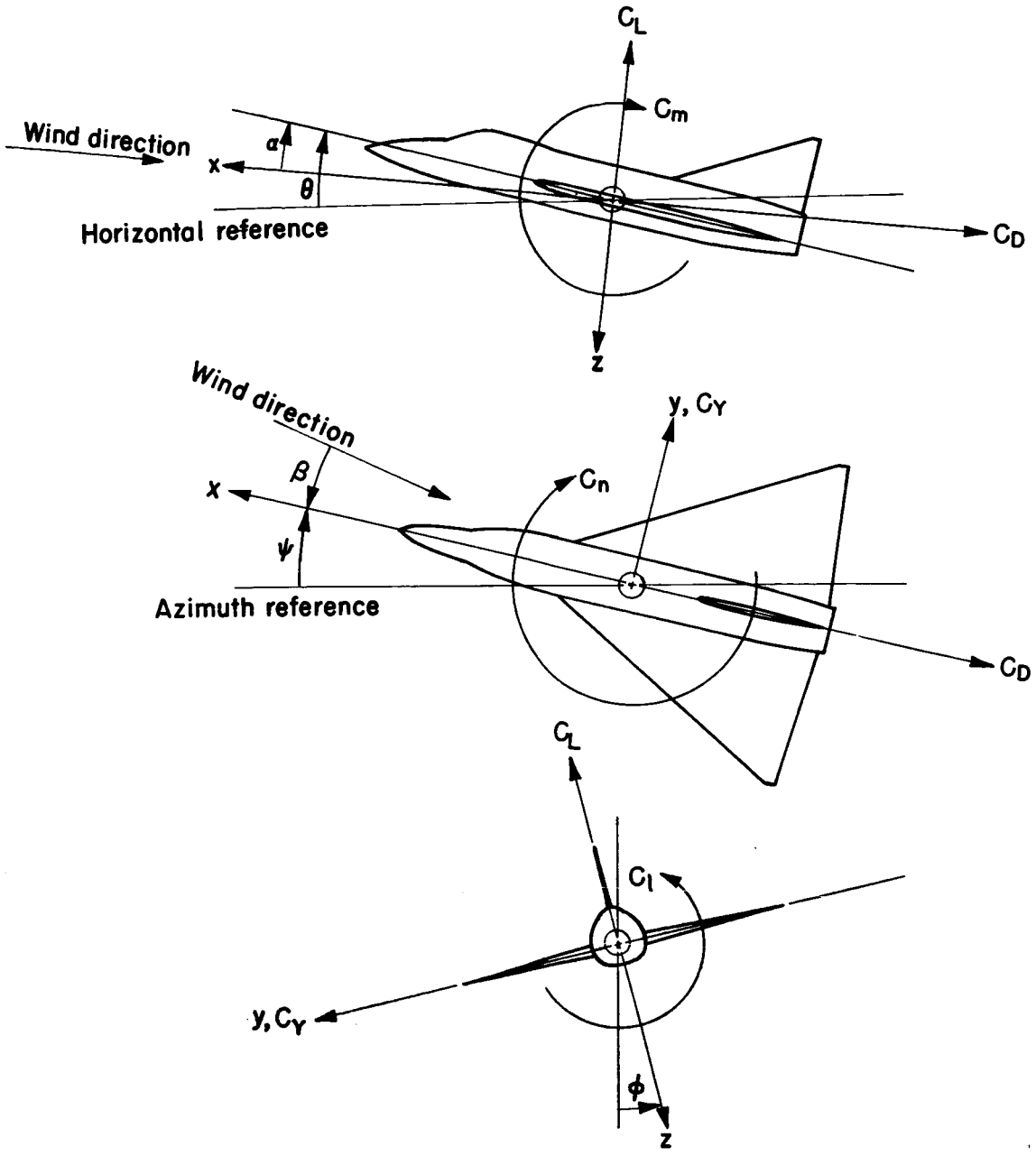

Figure 1.- The stability system of axes is an orthogonal system of axes having its origin at the center of gravity, the z axis in the plane of symmetry and perpendicular to the relative wind, the x axis in the plane of symmetry and perpendicular to the z axis, and the y axis perpendicular to the plane of symmetry. Arrows indicate the positive directions of forces and moments.

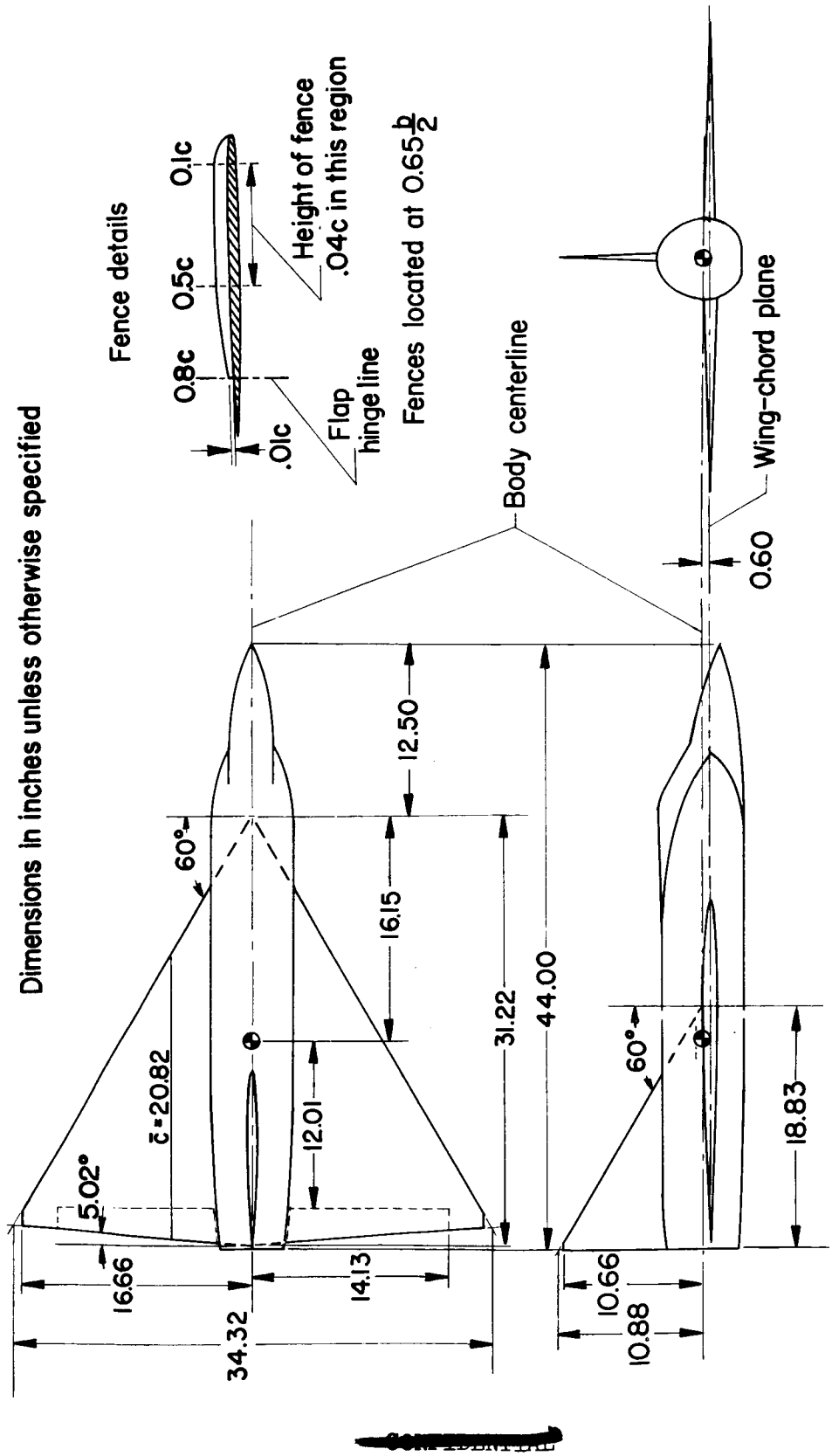

Figure 2.- Three-view drawing of the model.

A-18500.1

(a) View of the model in the wind tunnel.

Figure 3.- Photographs of the model mounted on the oscillation apparatus.

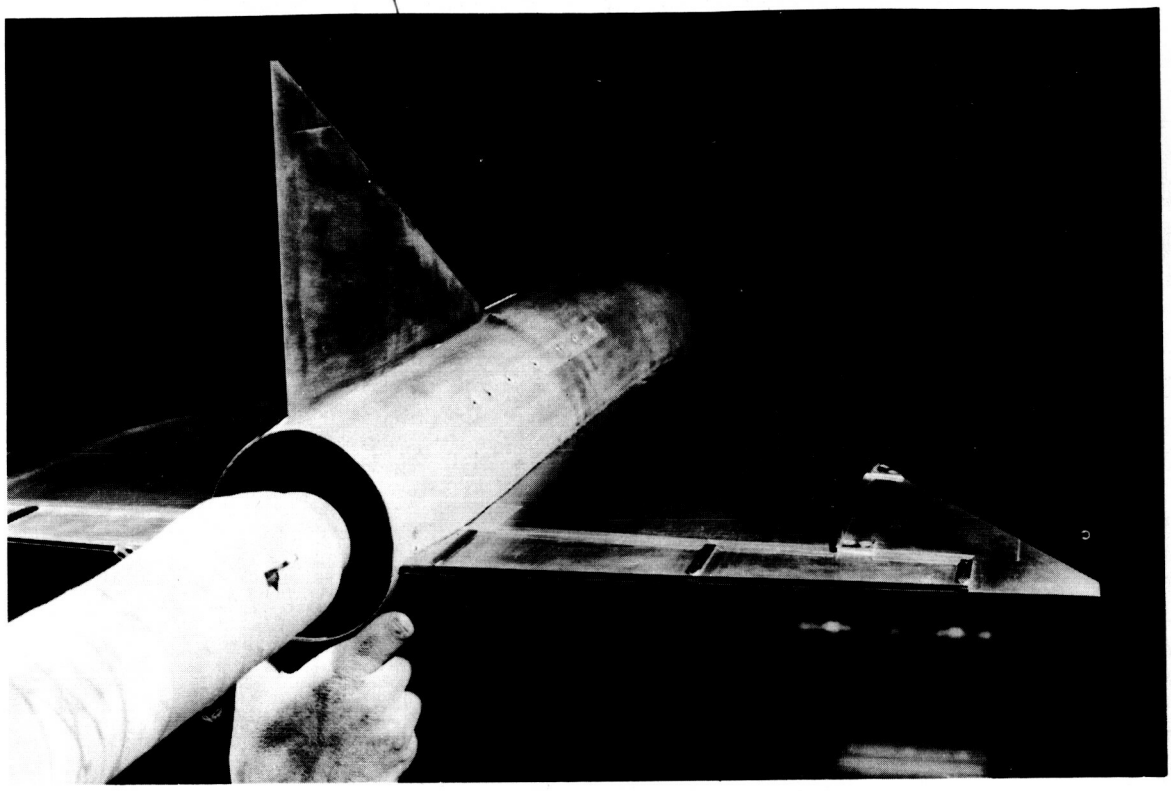

A-19099

(b) Rear view showing the flaps and fences.

Figure 3.- Concluded.

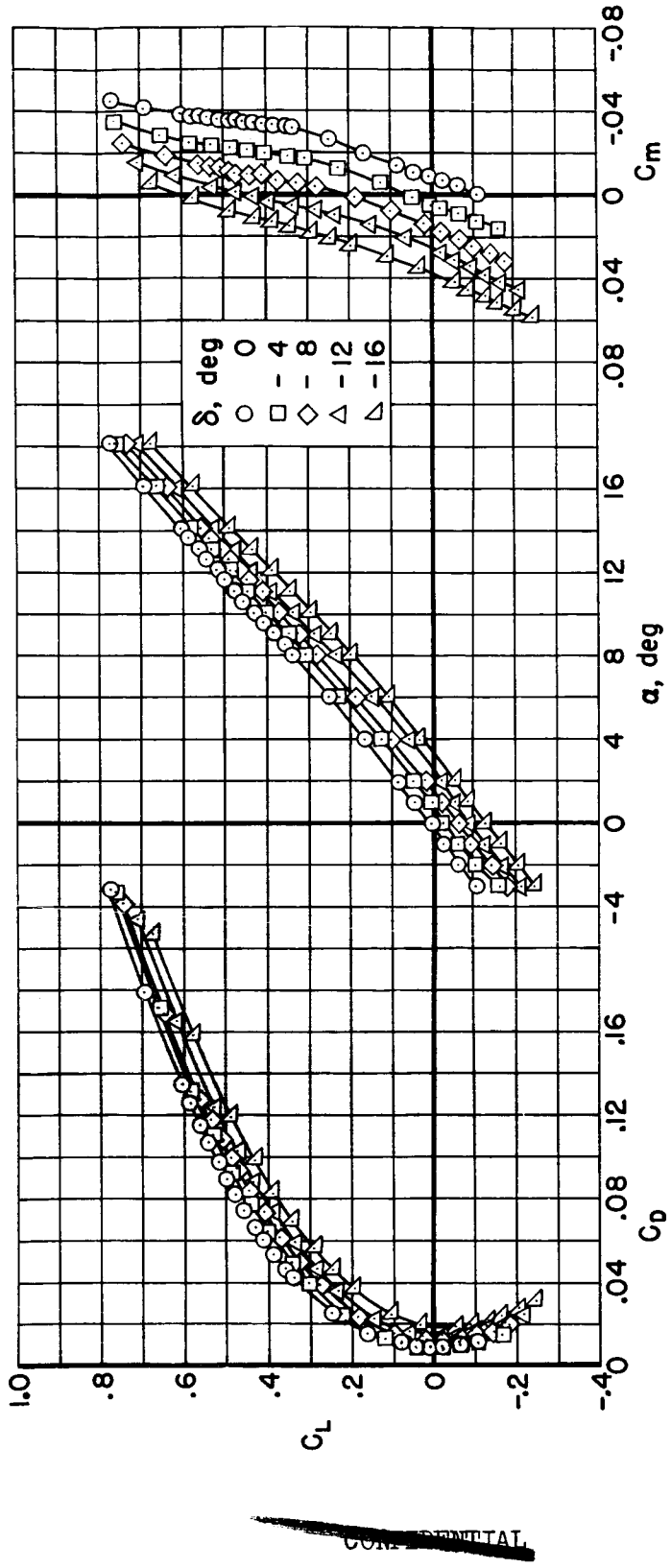

(a) M = 0.25

Figure 4.- The static longitudinal aerodynamic characteristics.

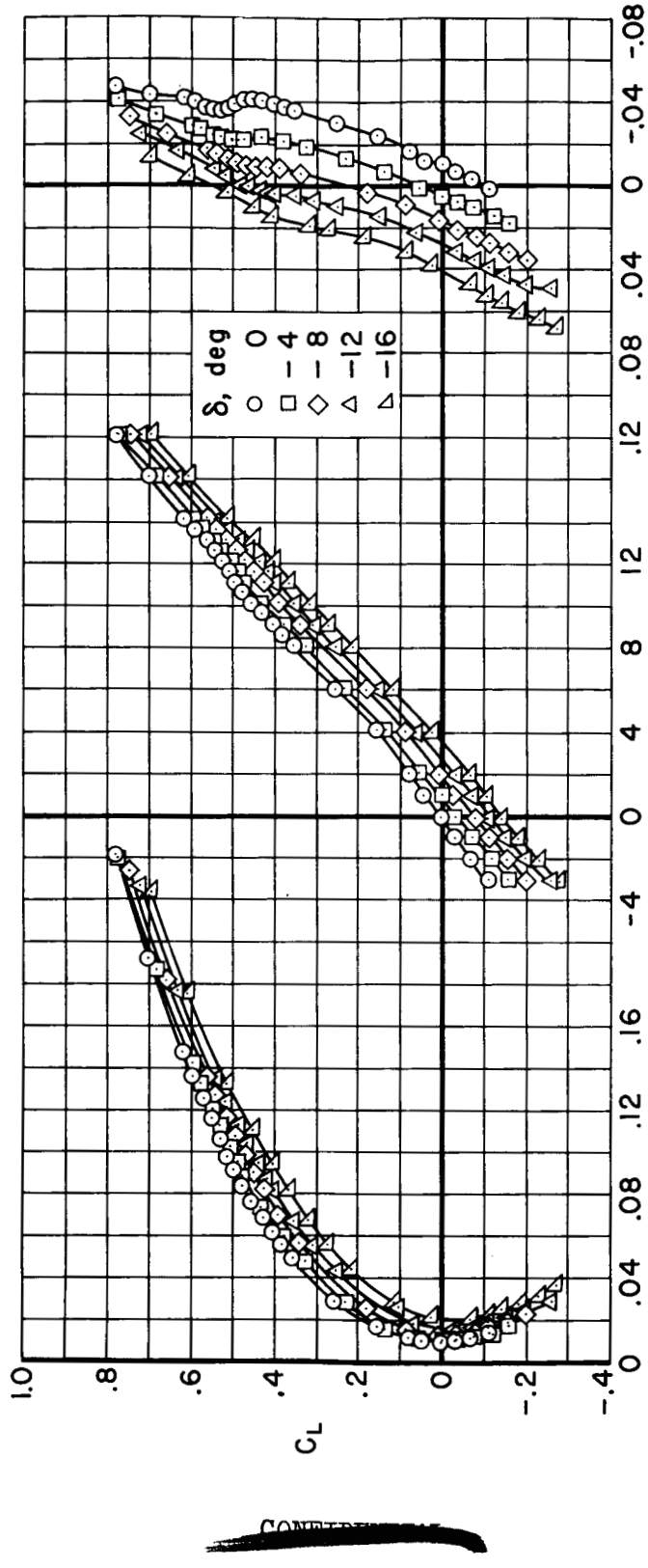

(b) M = 0.60

Figure 4.- Continued.

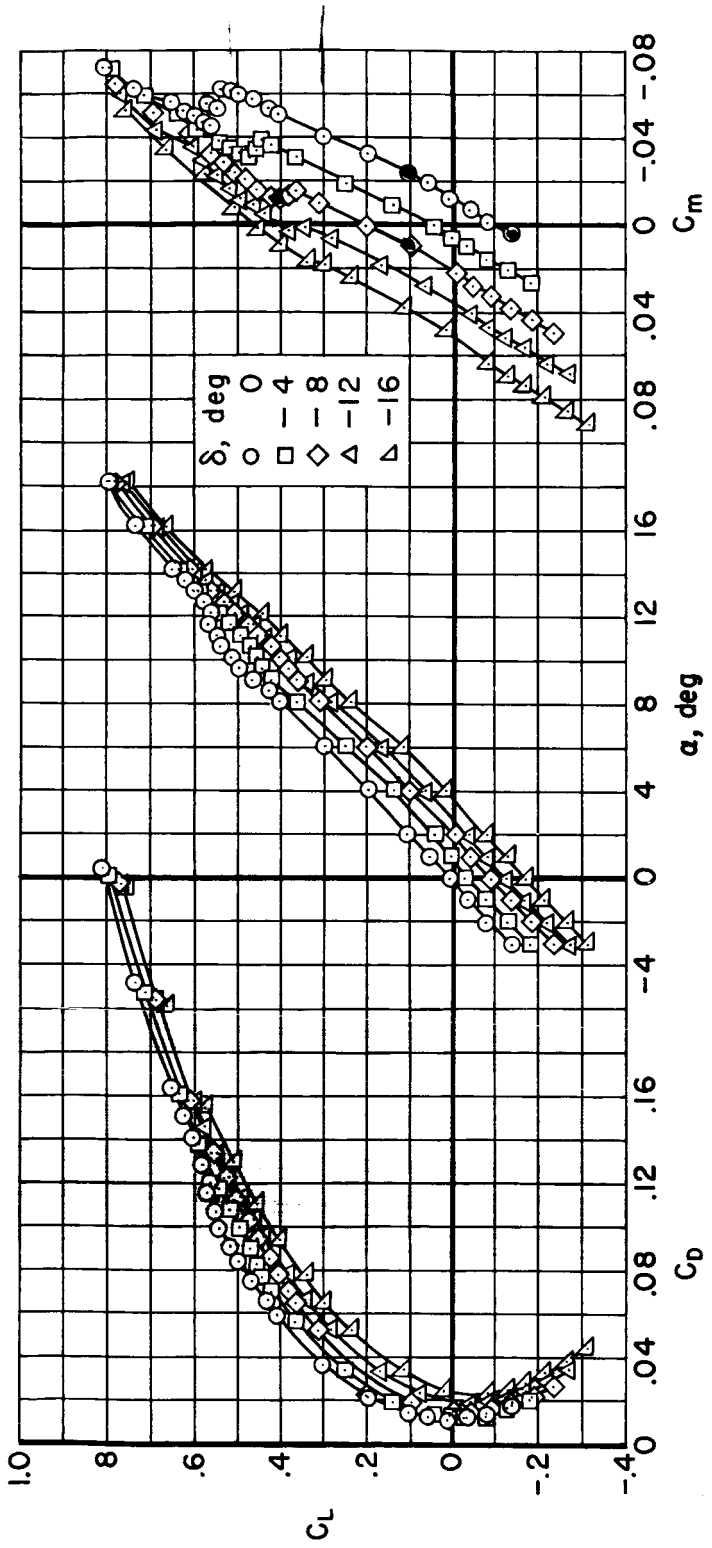

(c) M = 0.85

Figure 4.- Continued.

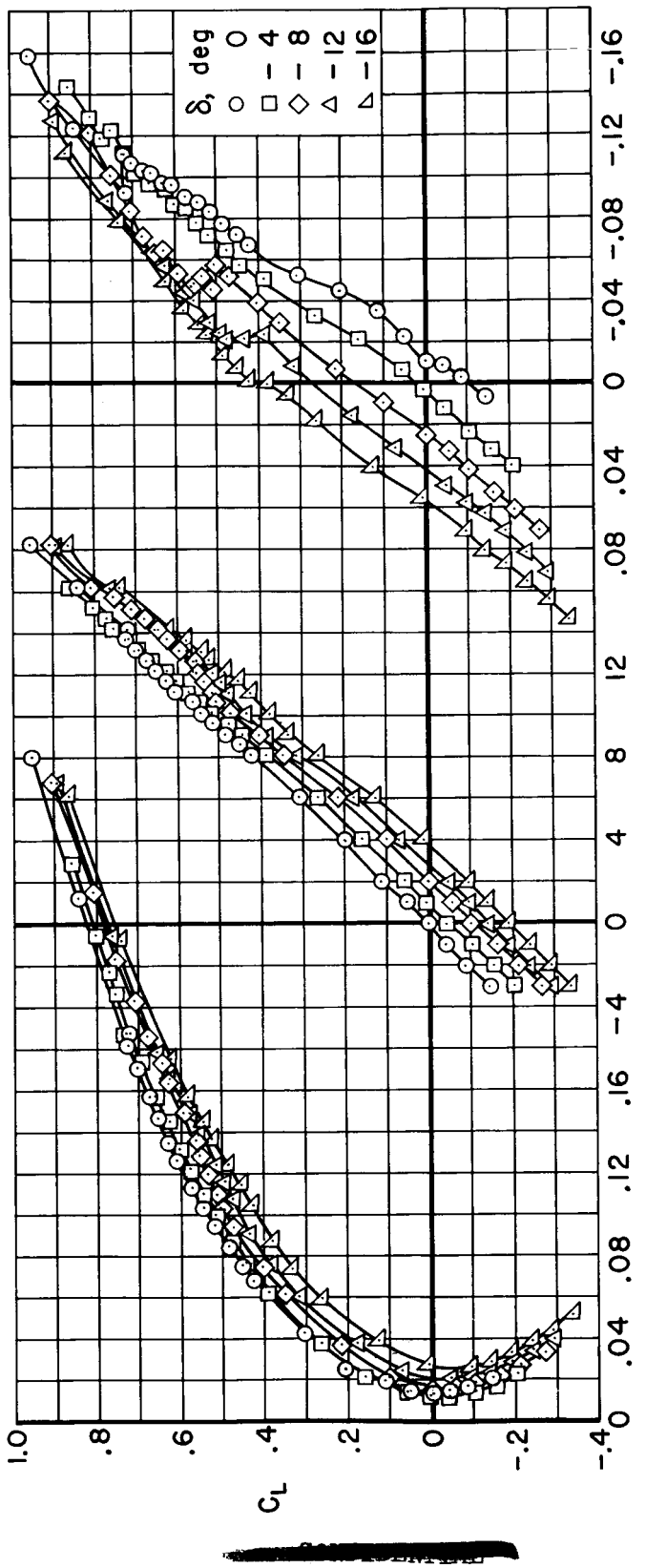

(d) M = 0.92

Figure 4.- Continued.

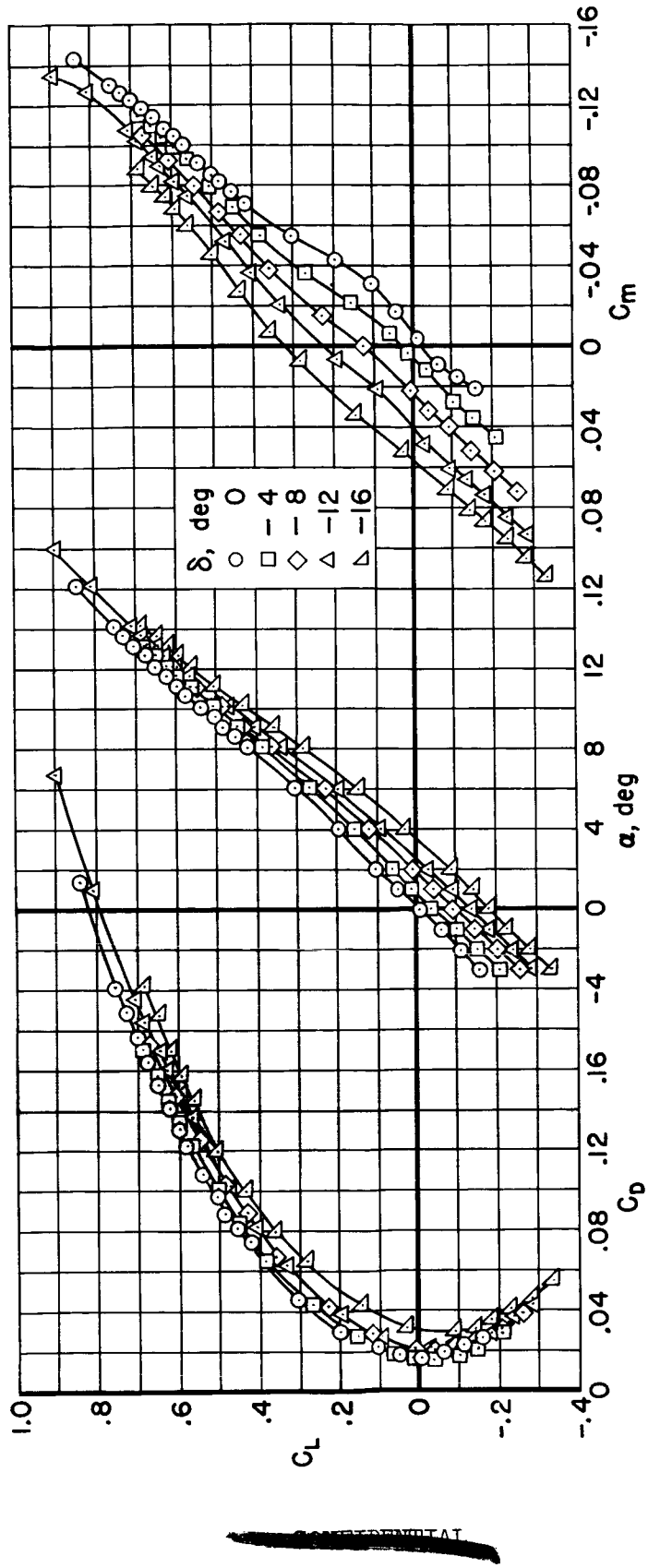

(e) M = 0.94

Figure 4.- Concluded.

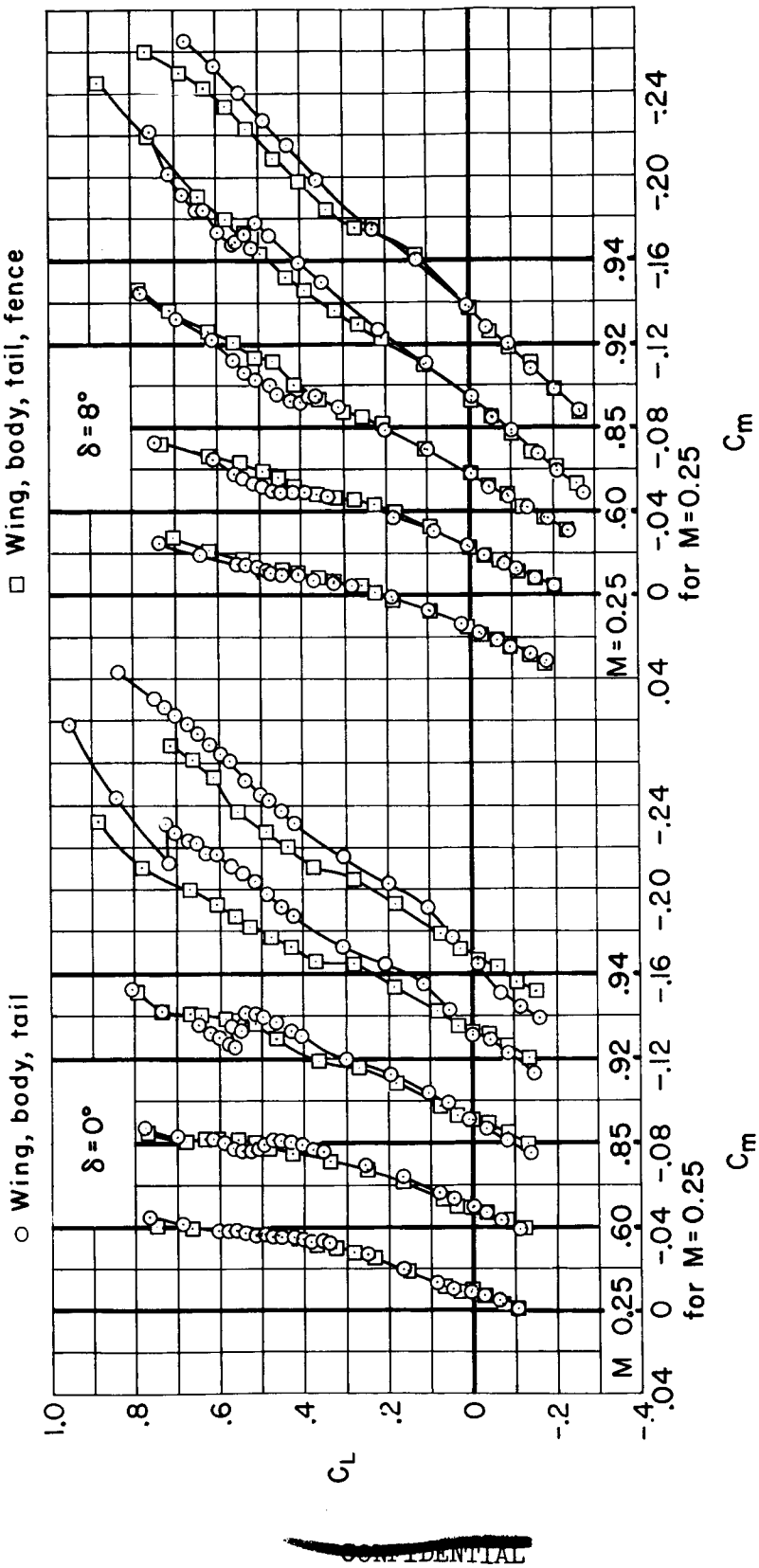

Figure 5.- The effect of chordwise fences on the static pitching-moment coefficient.

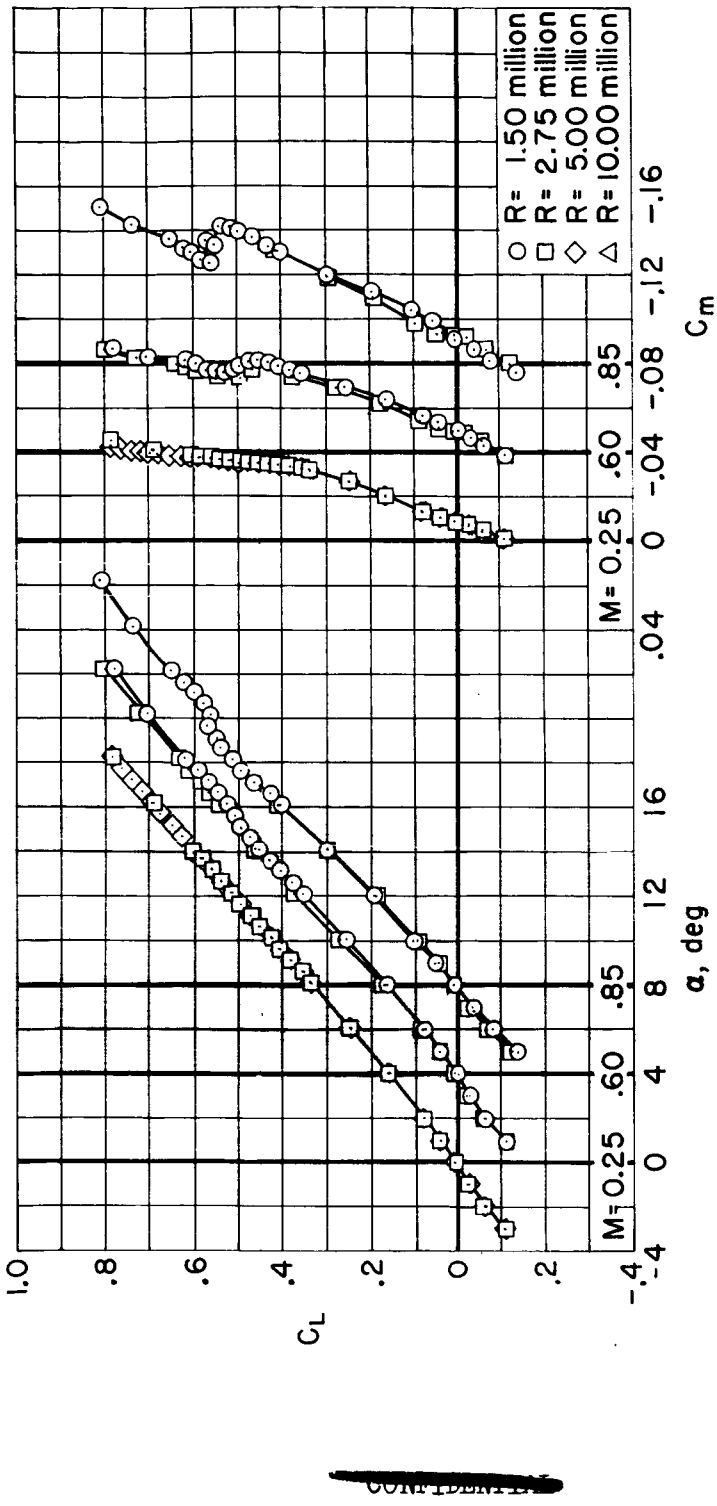

Figure 6.- The effect of Reynolds number on the lift and pitching-moment coefficients; $\delta = 0^{\circ}$.

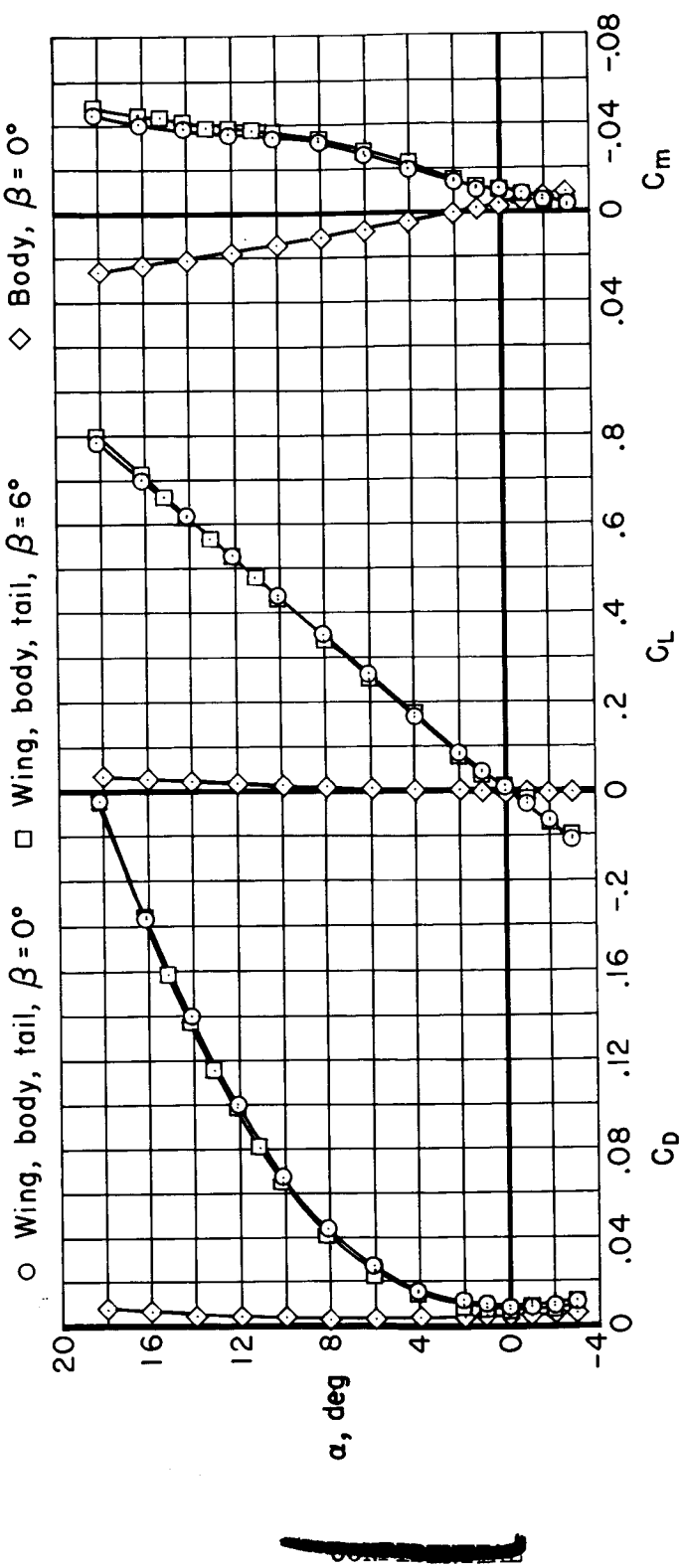

(a) M = 0.25

Figure 7.- The static longitudinal characteristics of the body, and the effects of sideslip on the longitudinal characteristics of the complete model; $\delta = 0^{\circ}$.

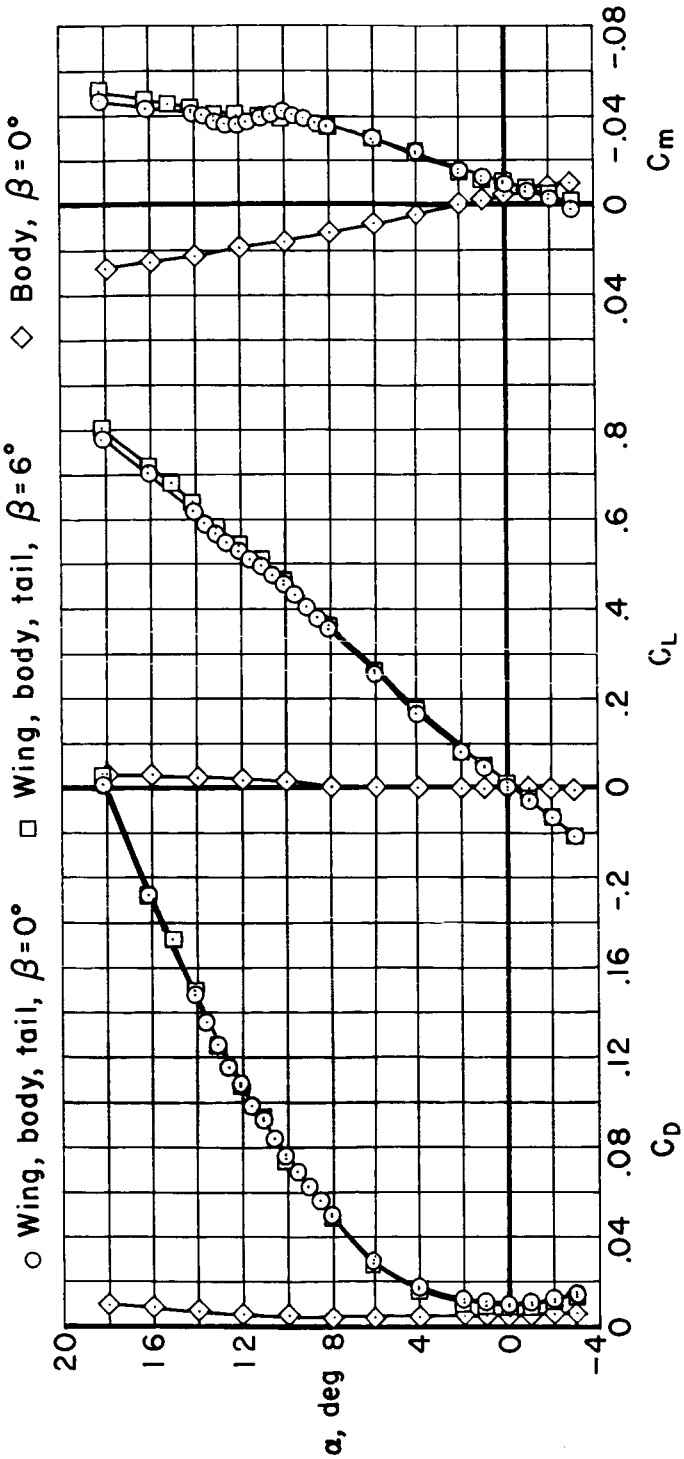

(b) M = 0.60

Figure 7.- Continued.

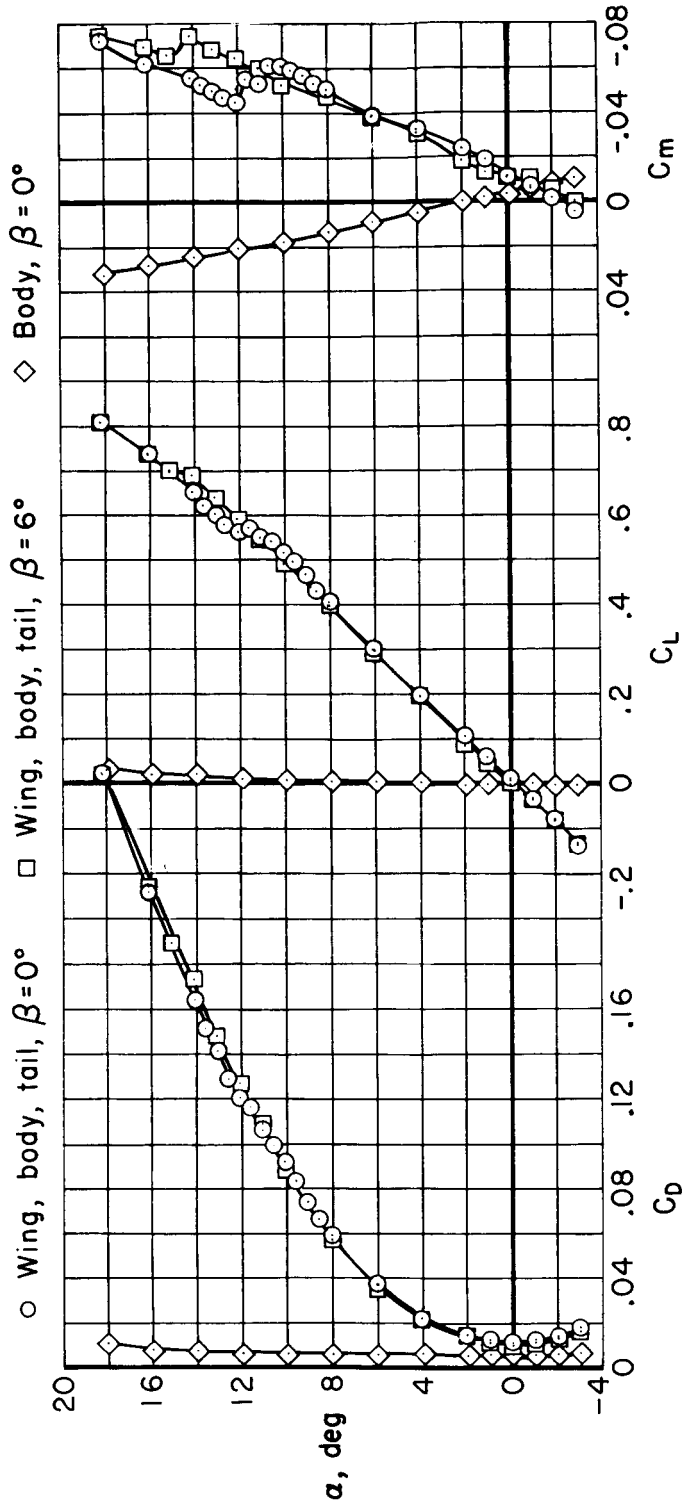

(c) M = 0.85

Figure 7.- Continued.

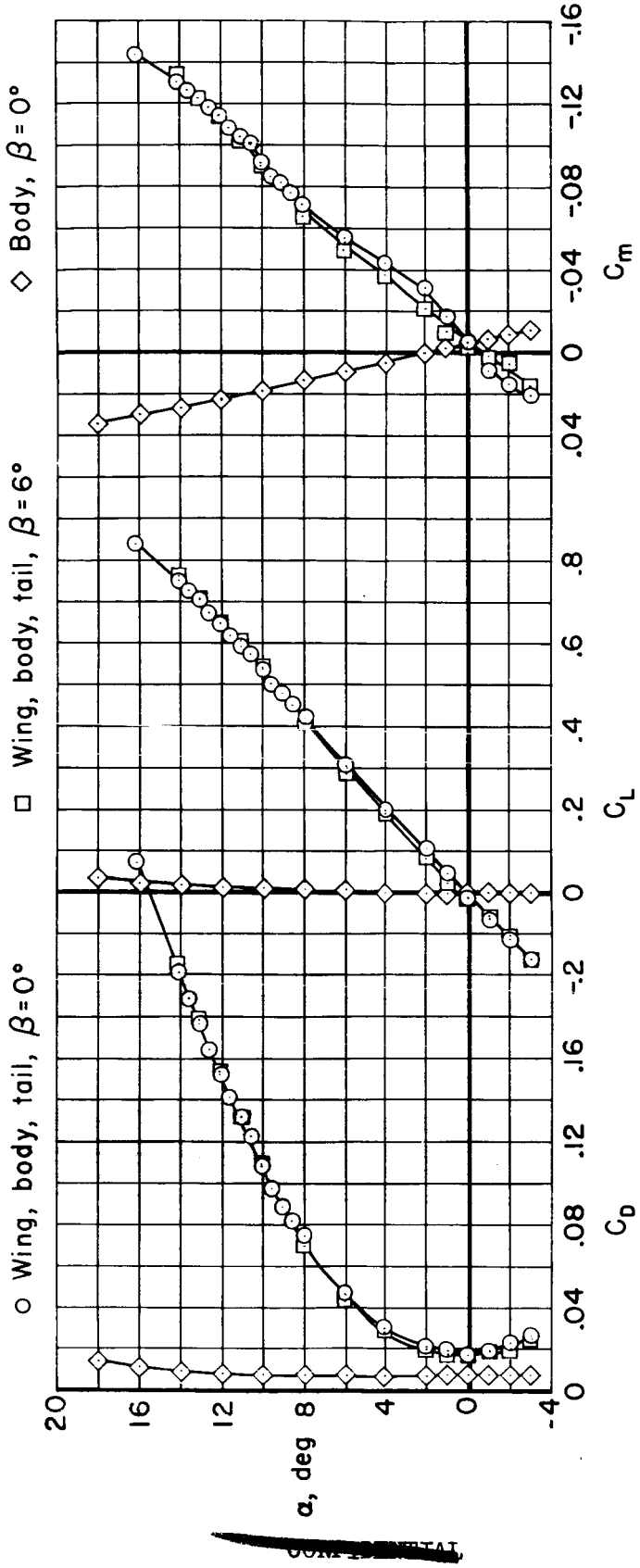

(d) M = 0.94

Figure 7.- Concluded.

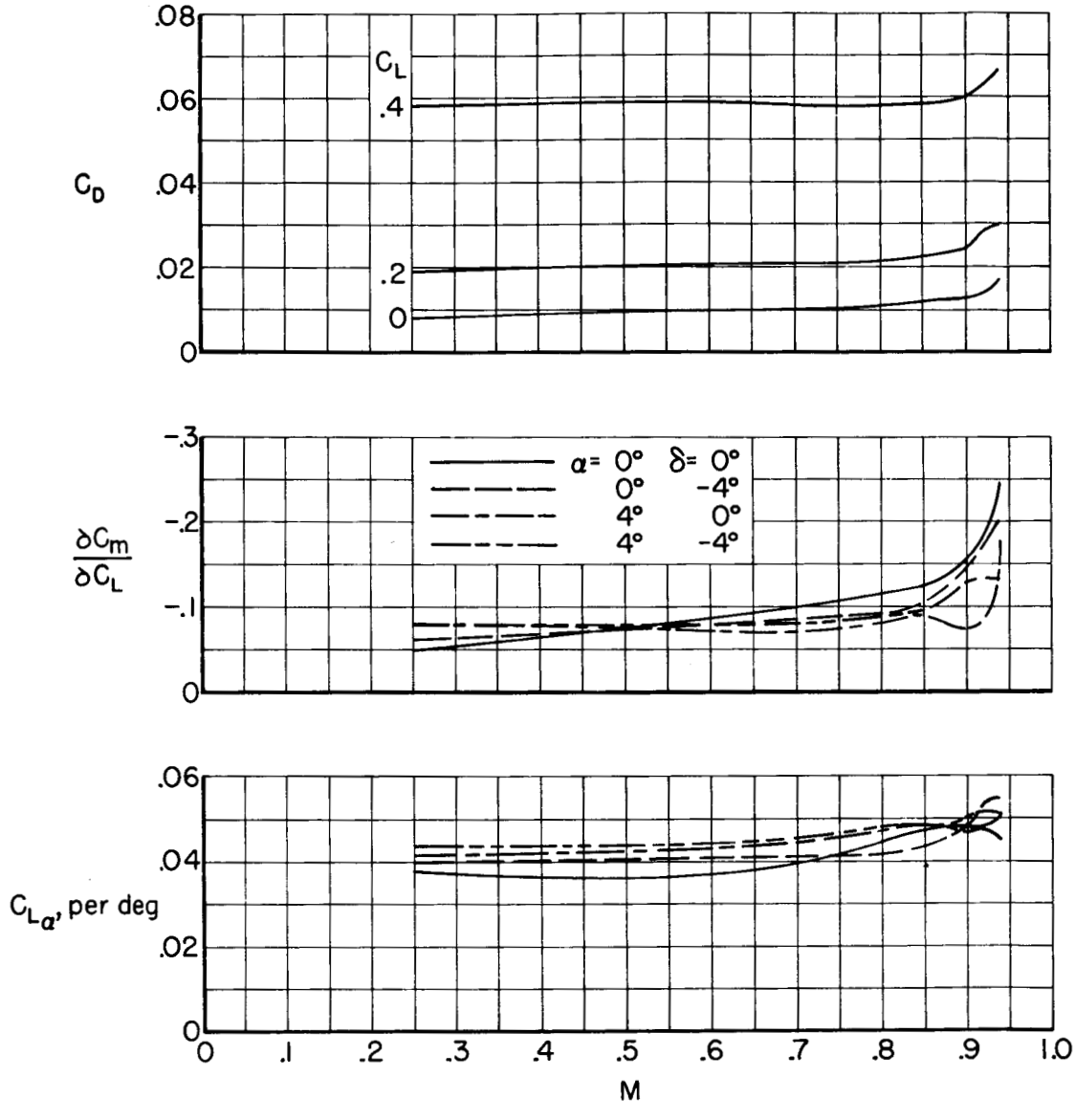

(a) C_D, $\frac{\partial C_m}{\partial C_L}$, C_{L_α}

Figure 8.- The variation with Mach number of the static longitudinal stability and control parameters.

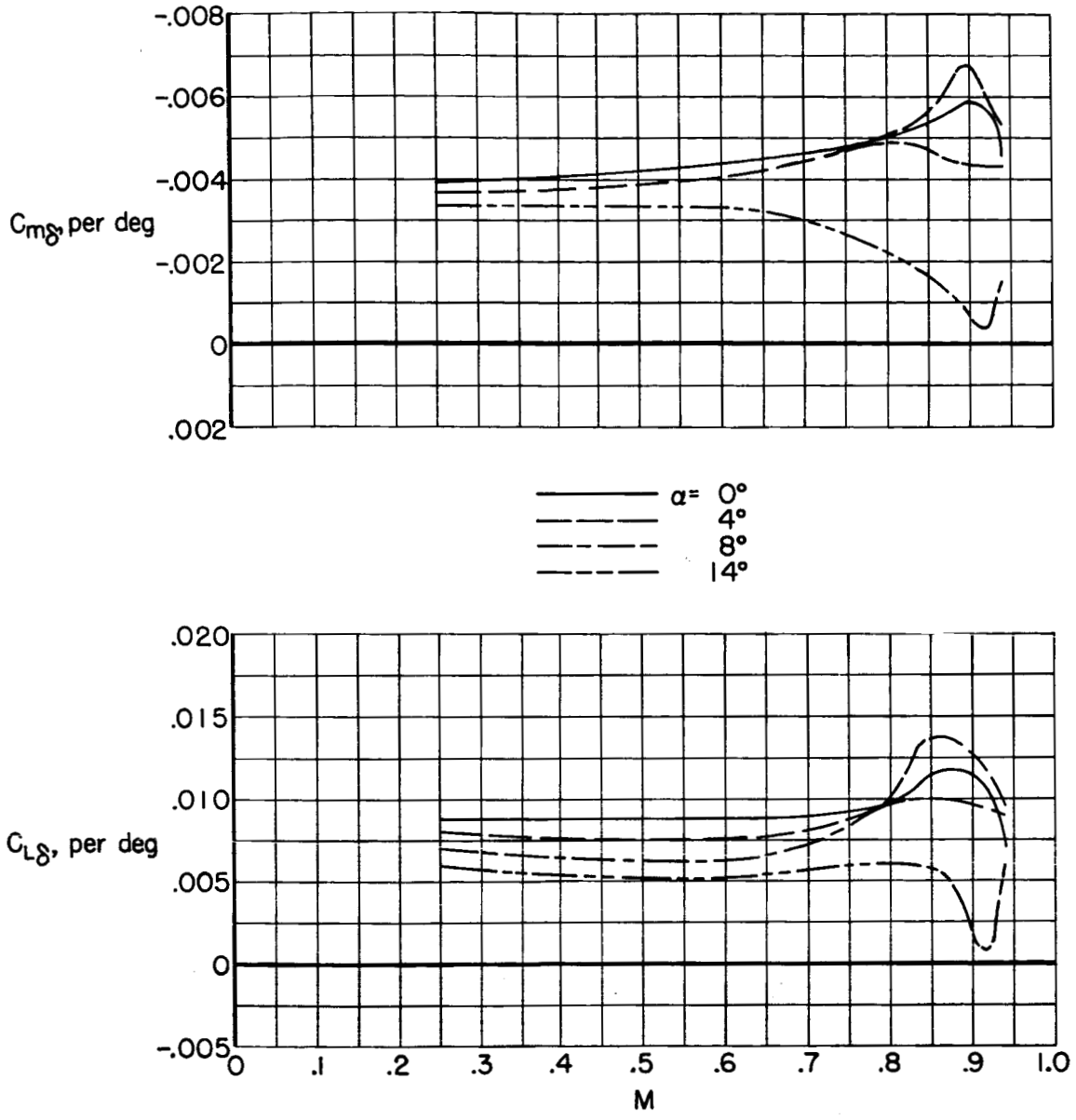

(b) C_{m_δ}, C_{L_δ}

Figure 8.- Concluded.

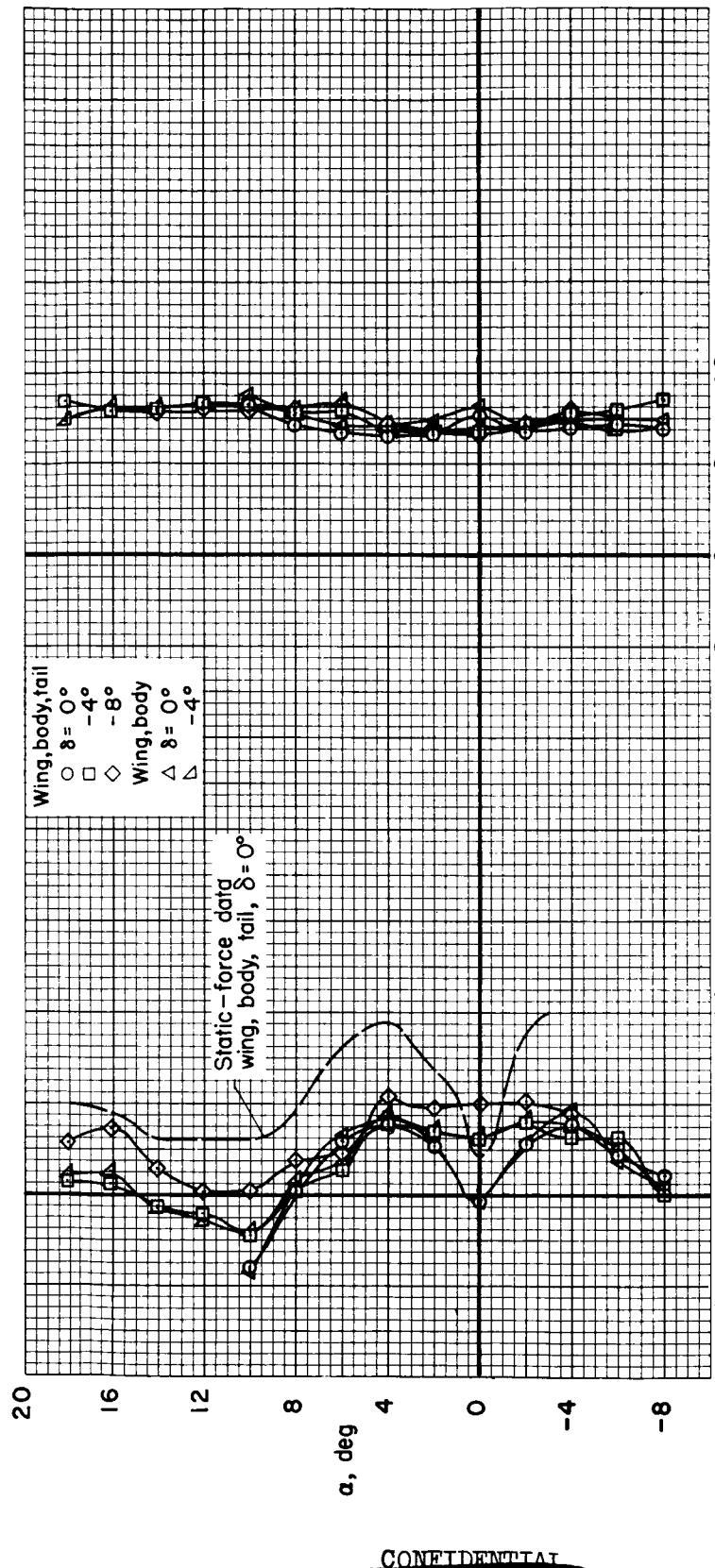

(a) M = 0.25

Figure 9.- The dynamic longitudinal stability derivatives from oscillation tests; f = approximately 8 cycles per second.

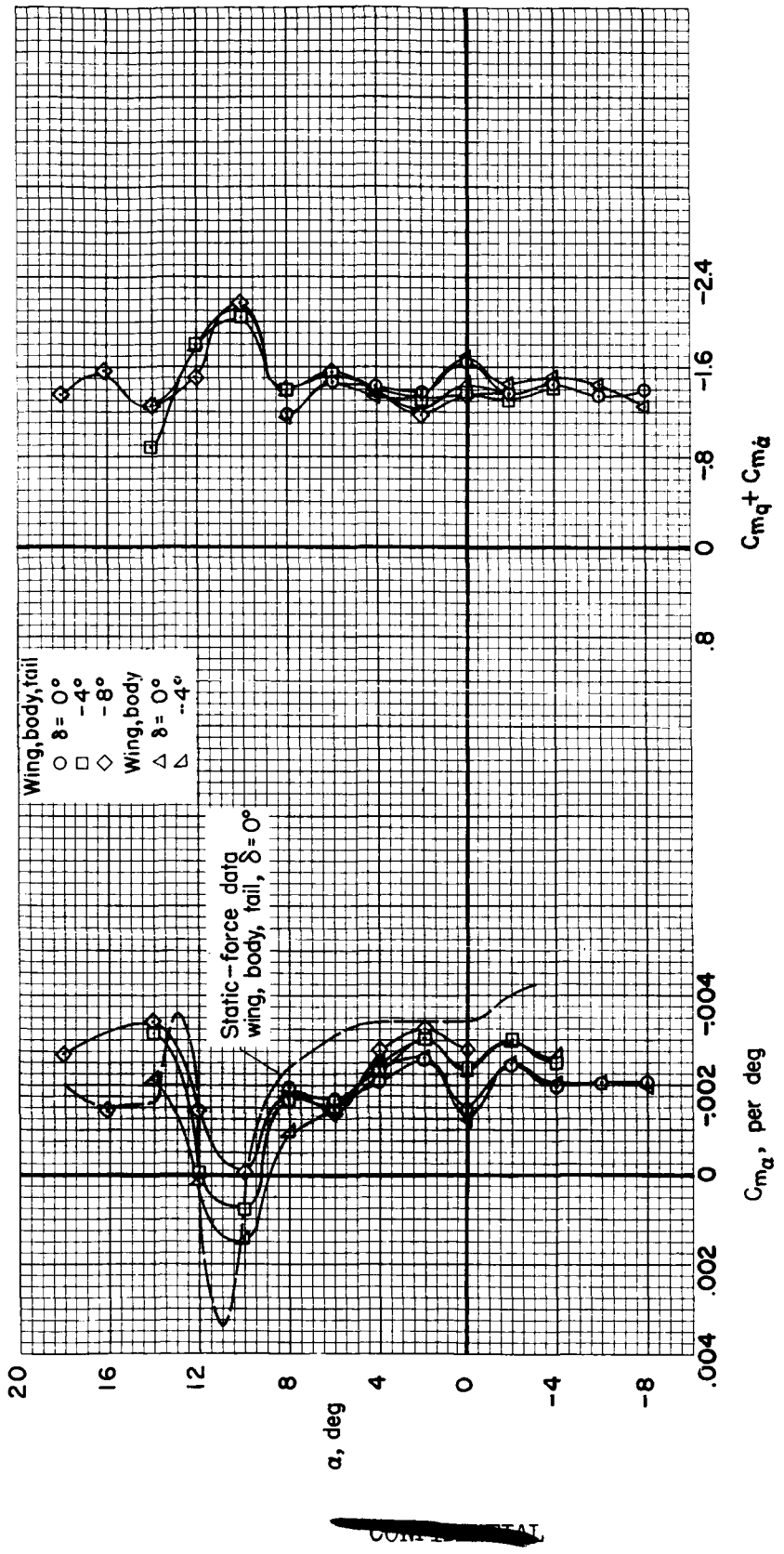

(b) M = 0.60

Figure 9.- Continued.

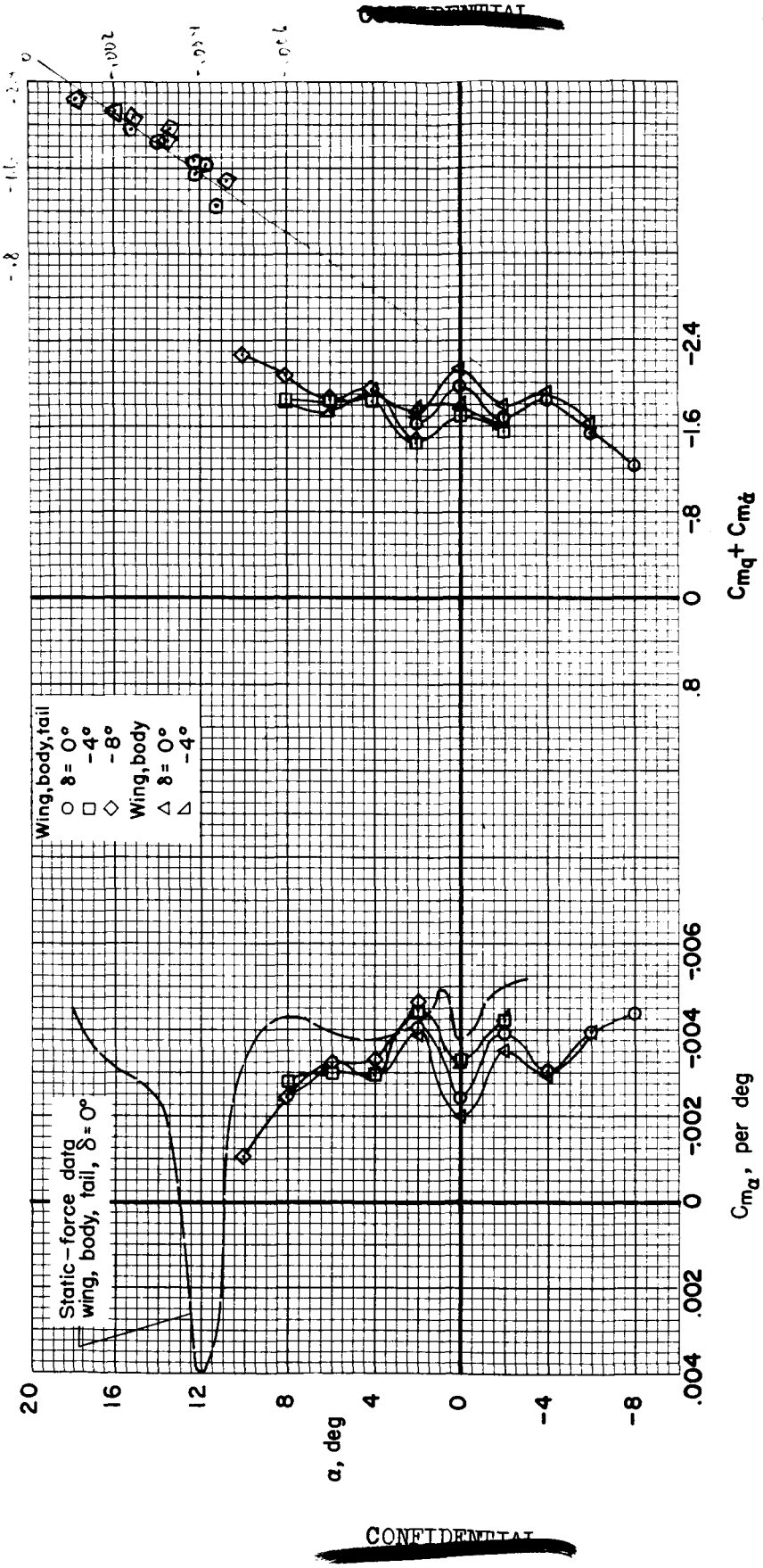

(c) M = 0.80

Figure 9.- Continued.

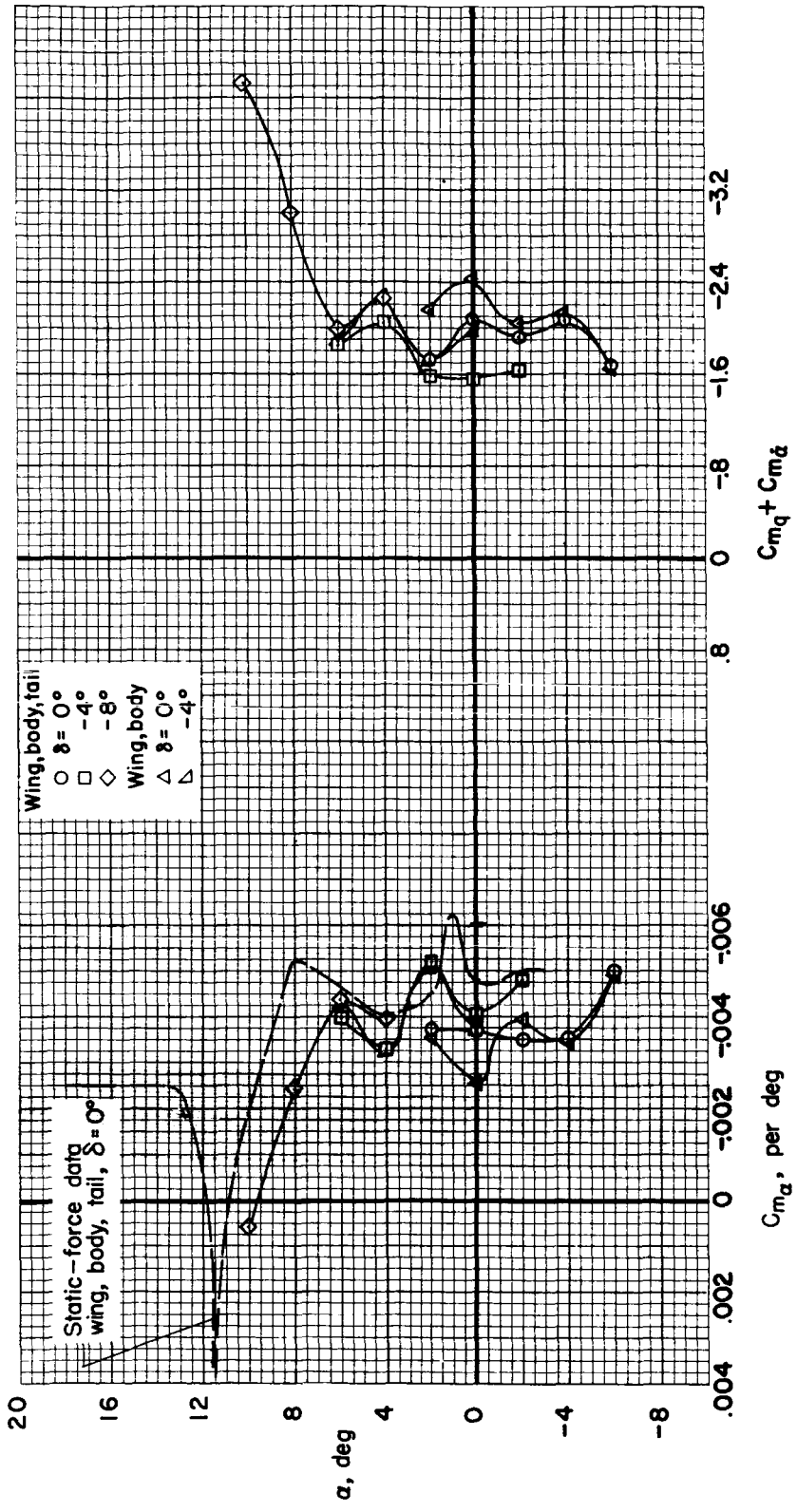

(d) M = 0.85

Figure 9.- Continued.

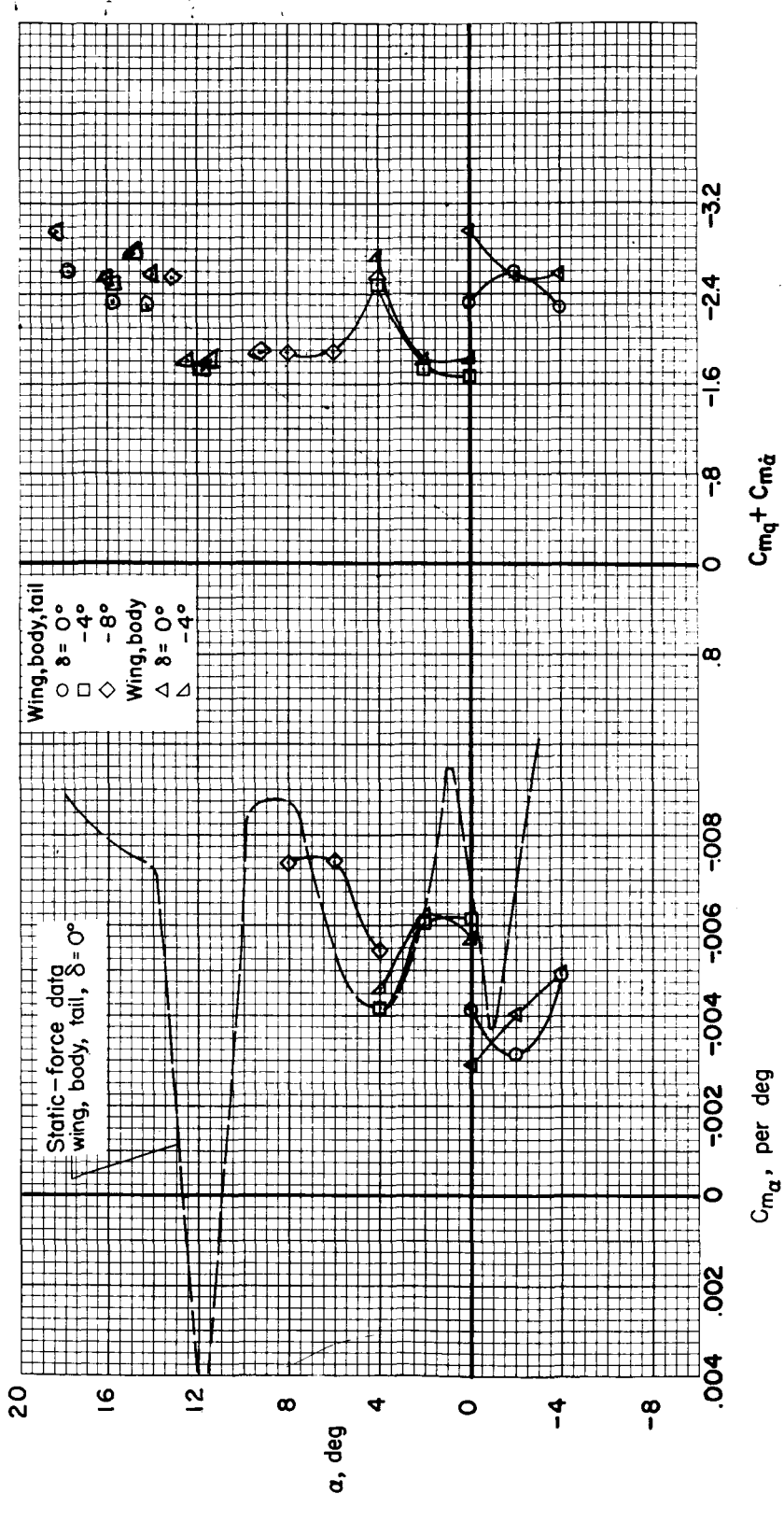

(e) M = 0.90

Figure 9.- Continued.

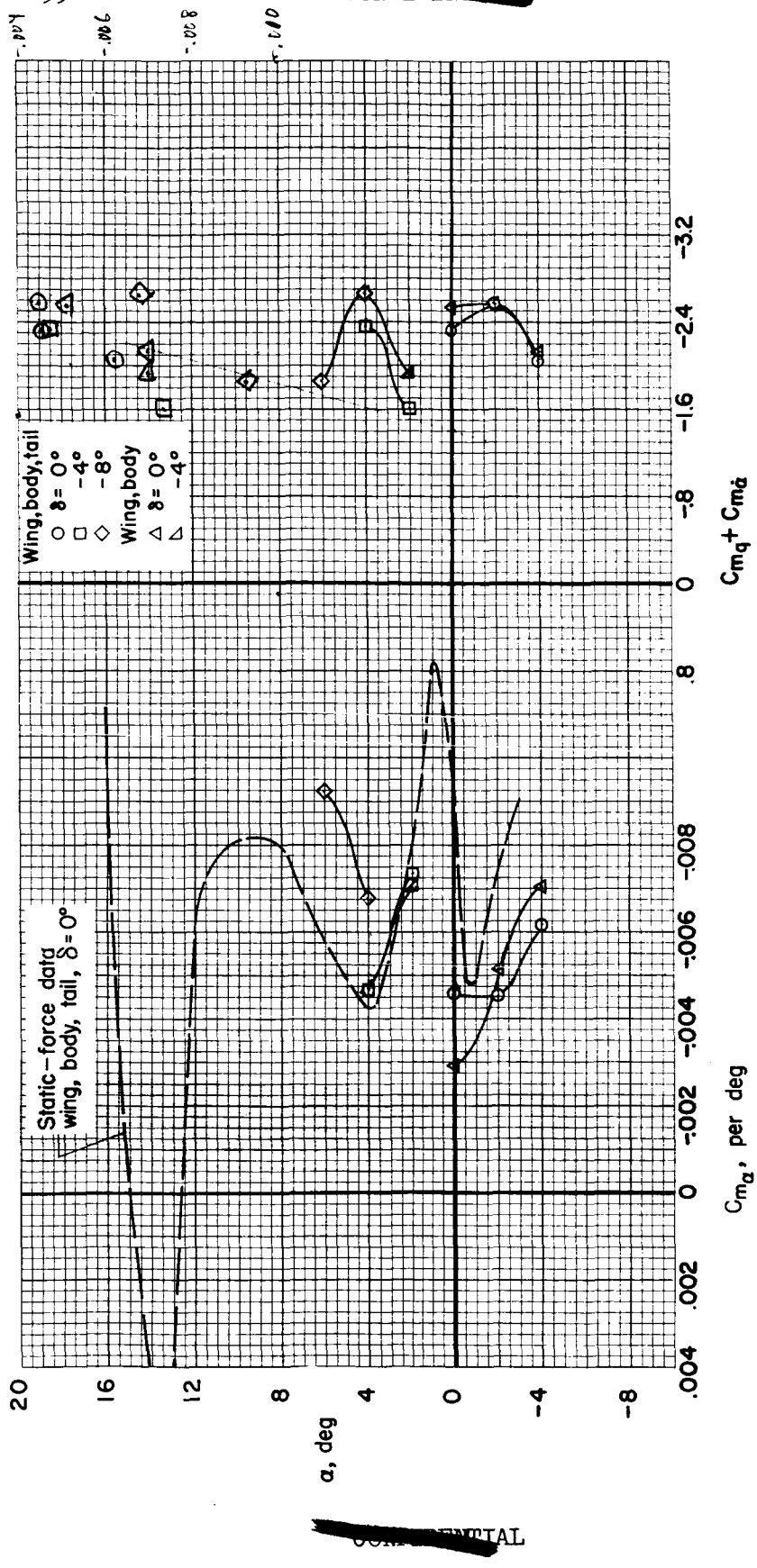

(f) M = 0.92

Figure 9.- Continued.

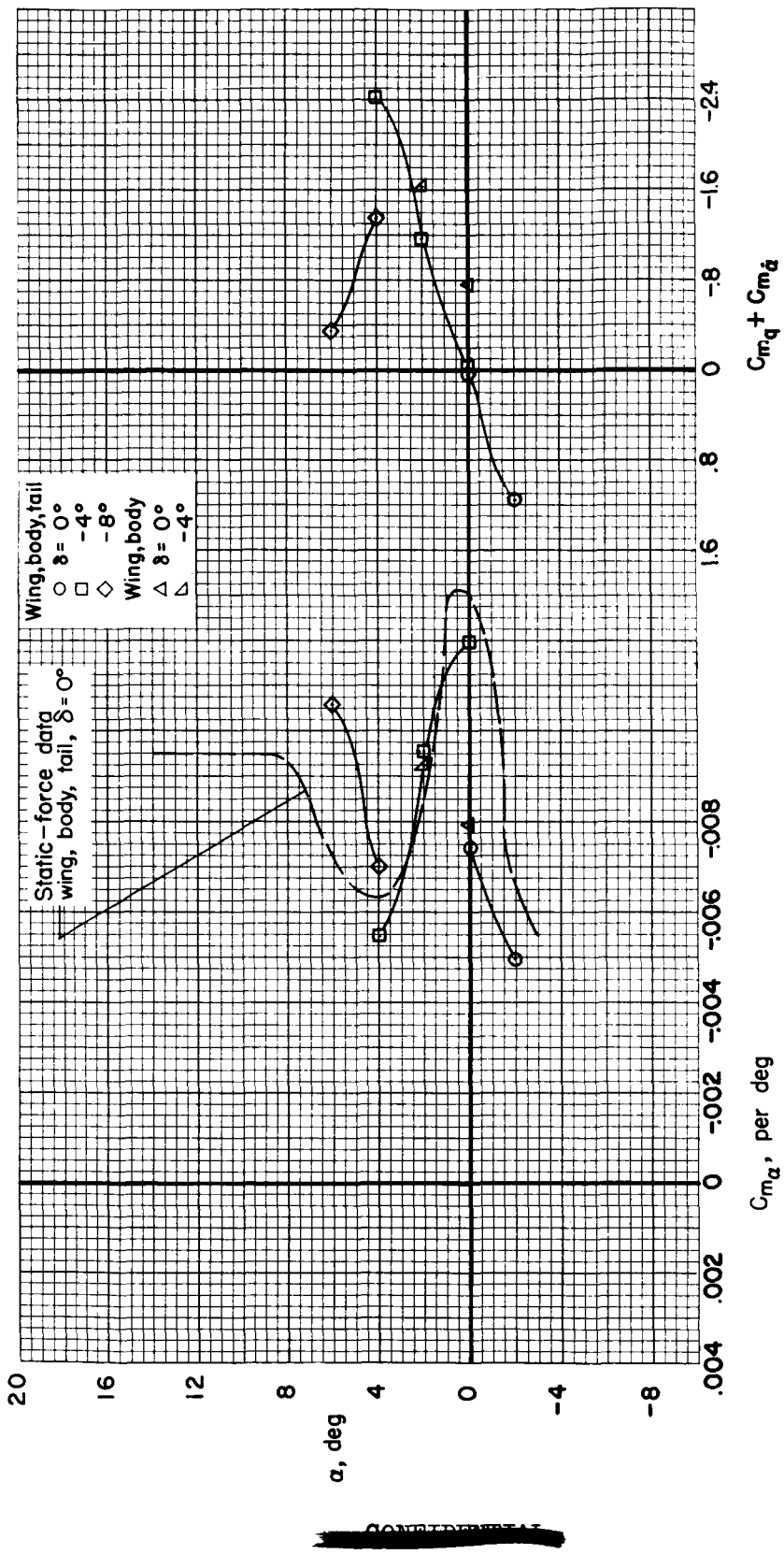

(g) M = 0.94

Figure 9.- Continued.

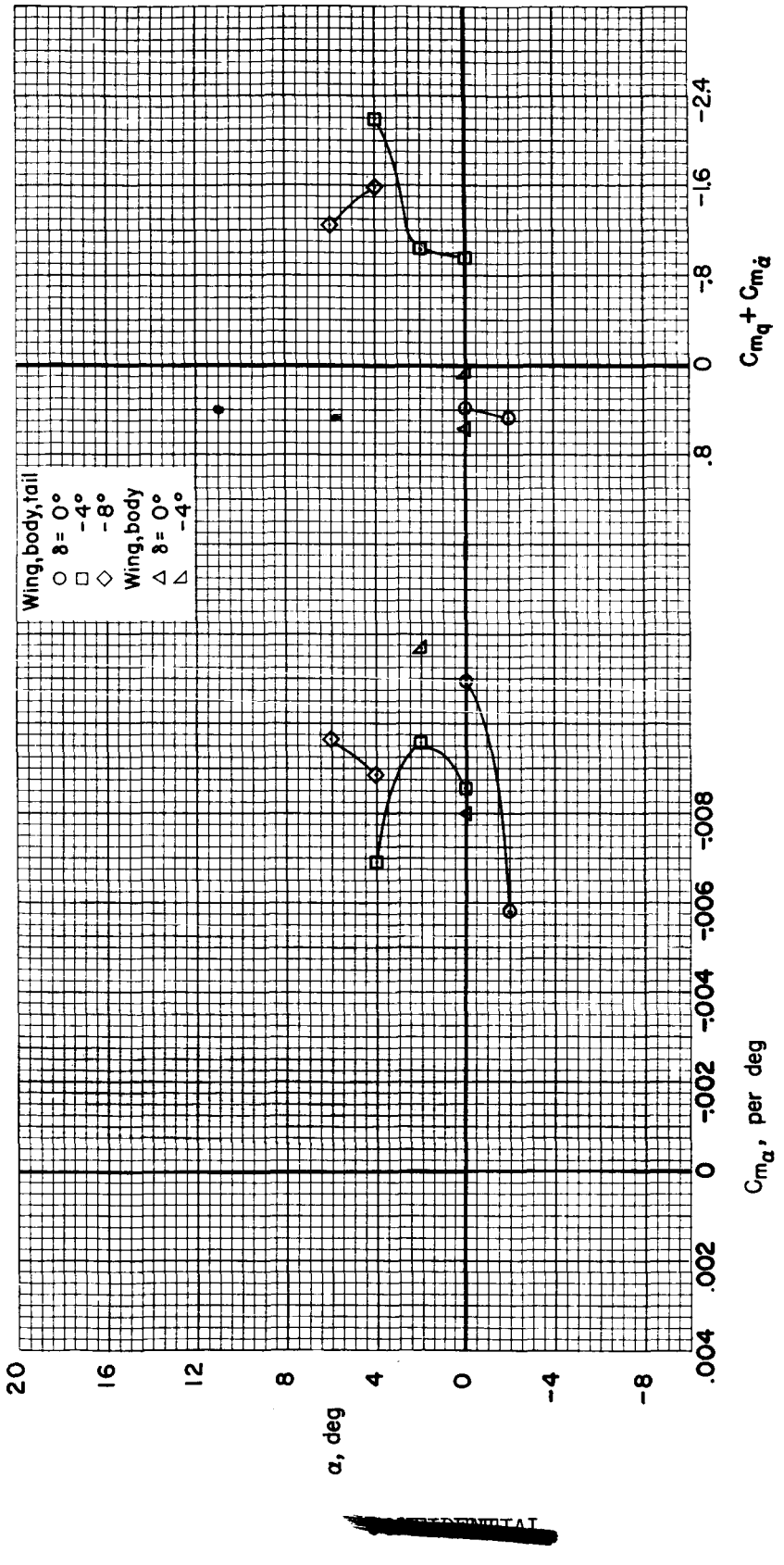

(h) M = 0.95

Figure 9.- Concluded.

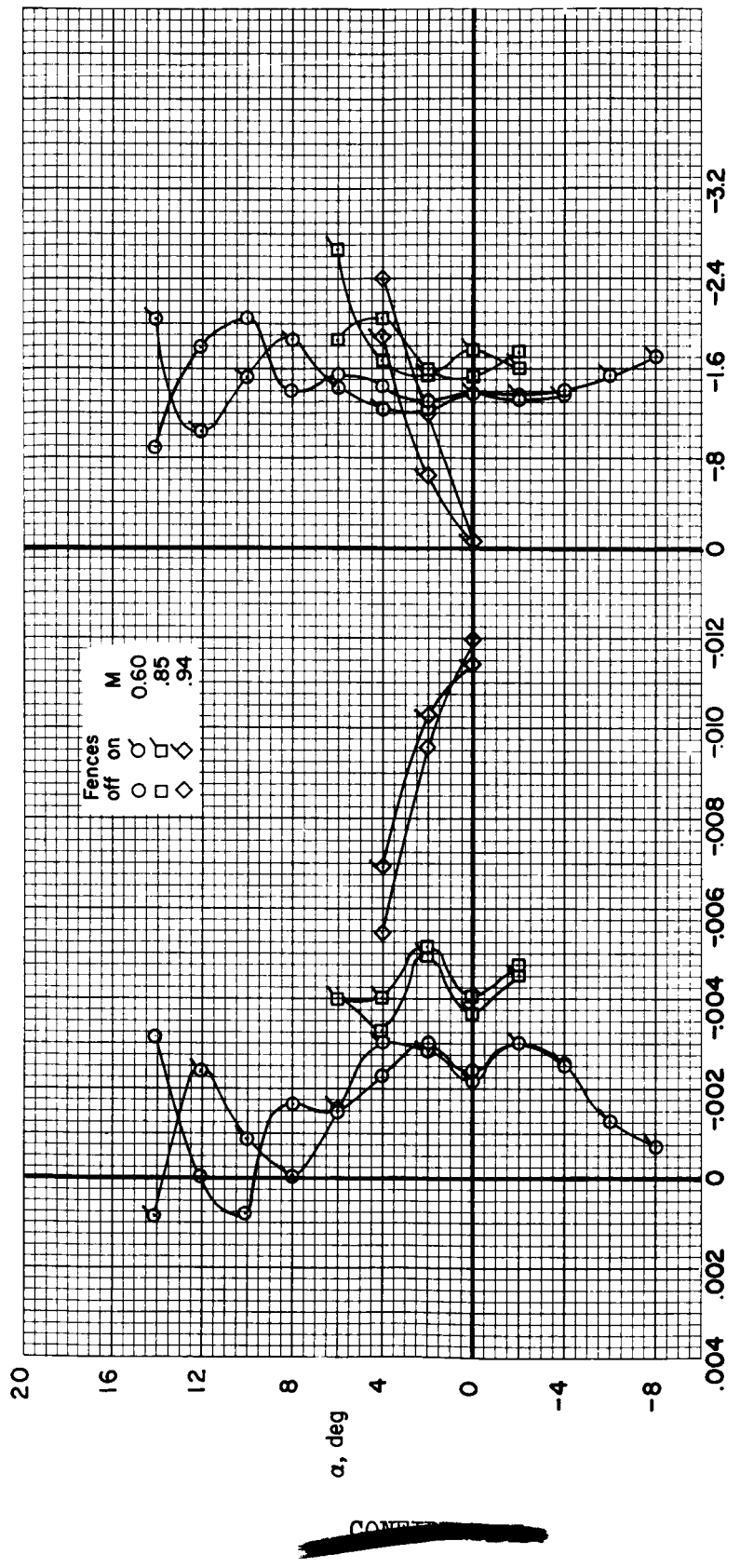

Figure 10.- The effect of chordwise fences on the dynamic longitudinal stability derivatives, C_{m_α} and $C_{m_q} + C_{m_{\dot{\alpha}}}$; f = approximately 8 cycles per second; $\delta = -4^\circ$.

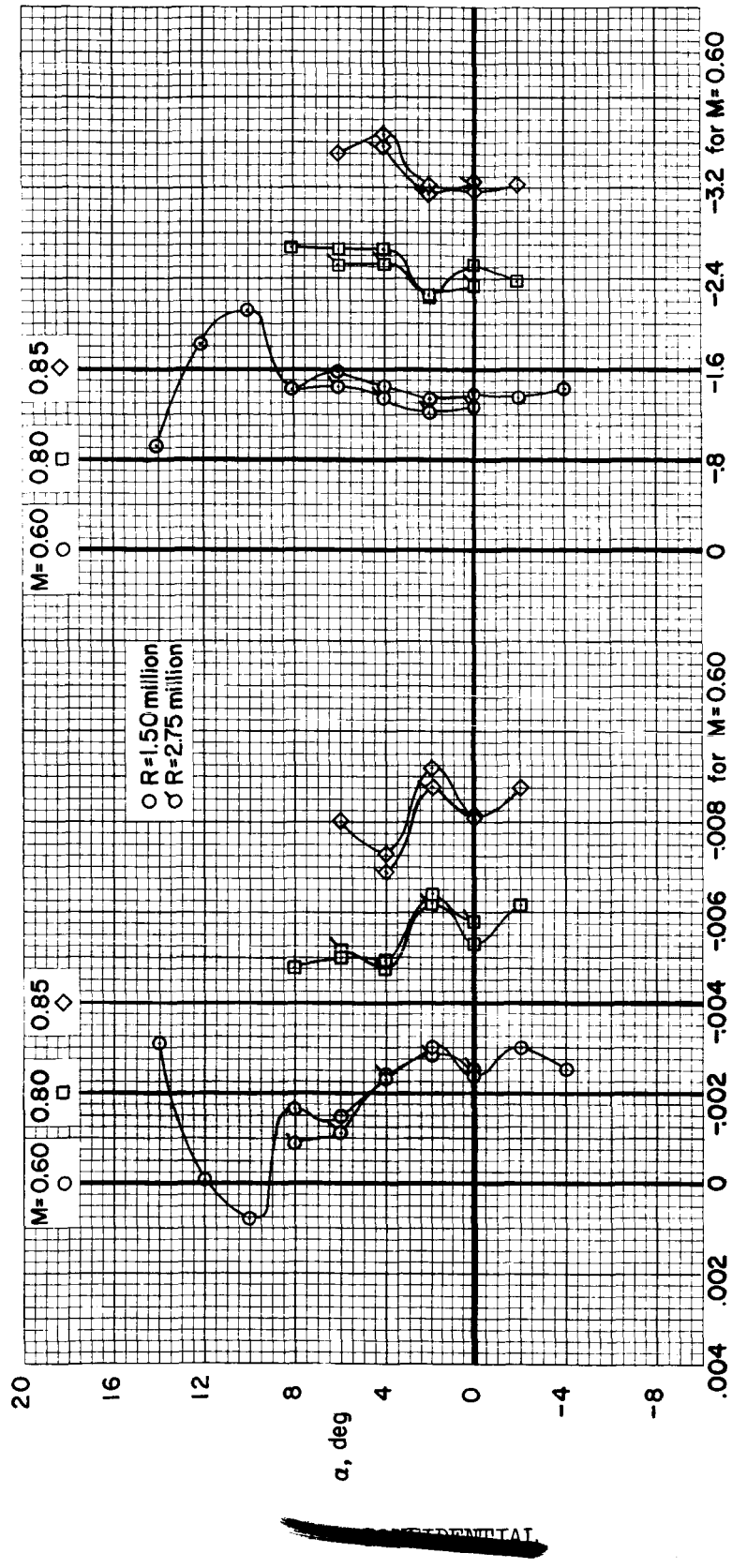

Figure 11.- The effect of Reynolds number on the dynamic longitudinal stability derivatives, C_{m_α} and $C_{m_q} + C_{m_{\dot{\alpha}}}$; f = approximately 8 cycles per second; $\delta = -4^\circ$.

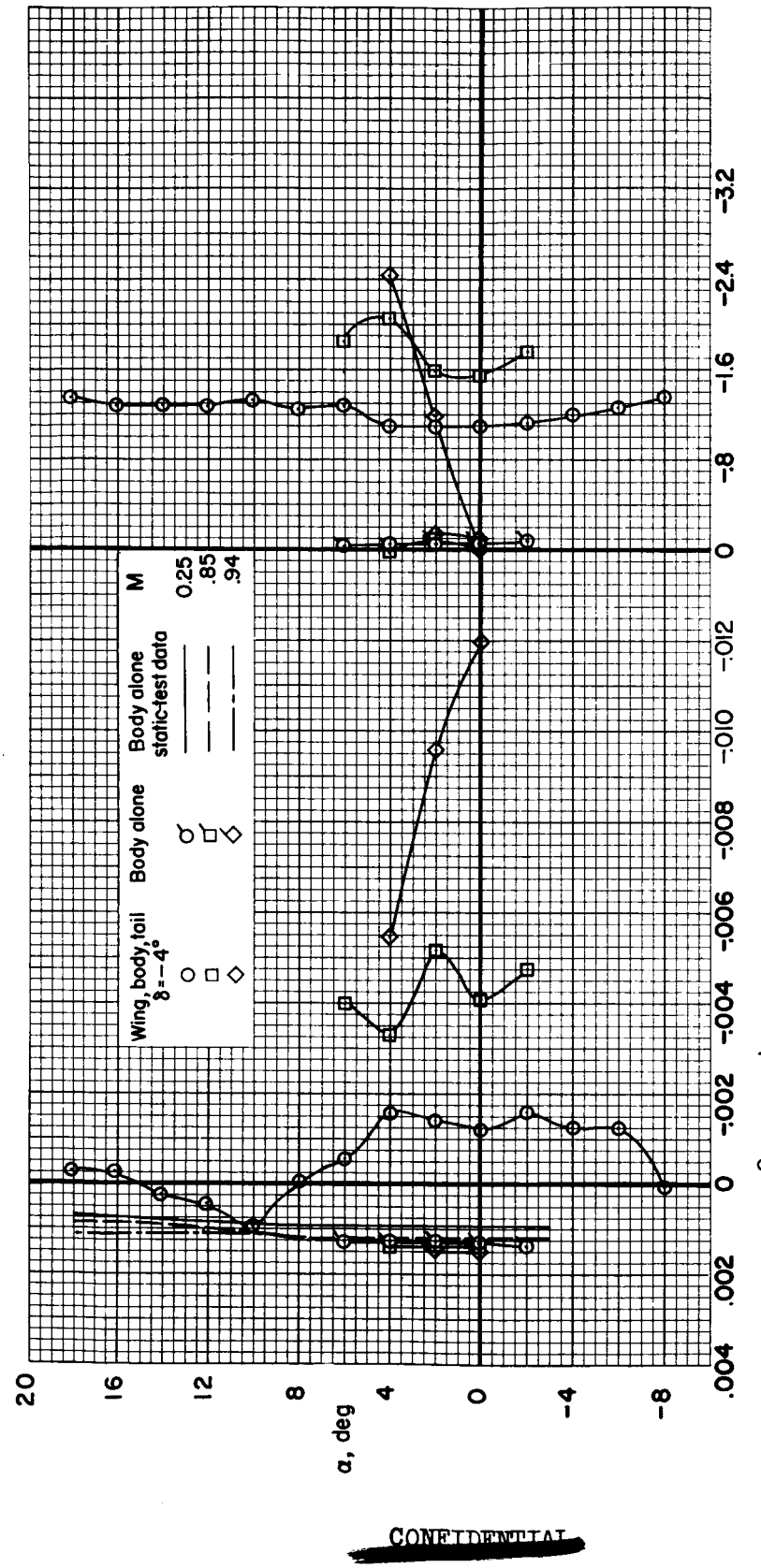

Figure 12.- The dynamic longitudinal stability derivatives for the body alone; f = approximately 4 cycles per second.

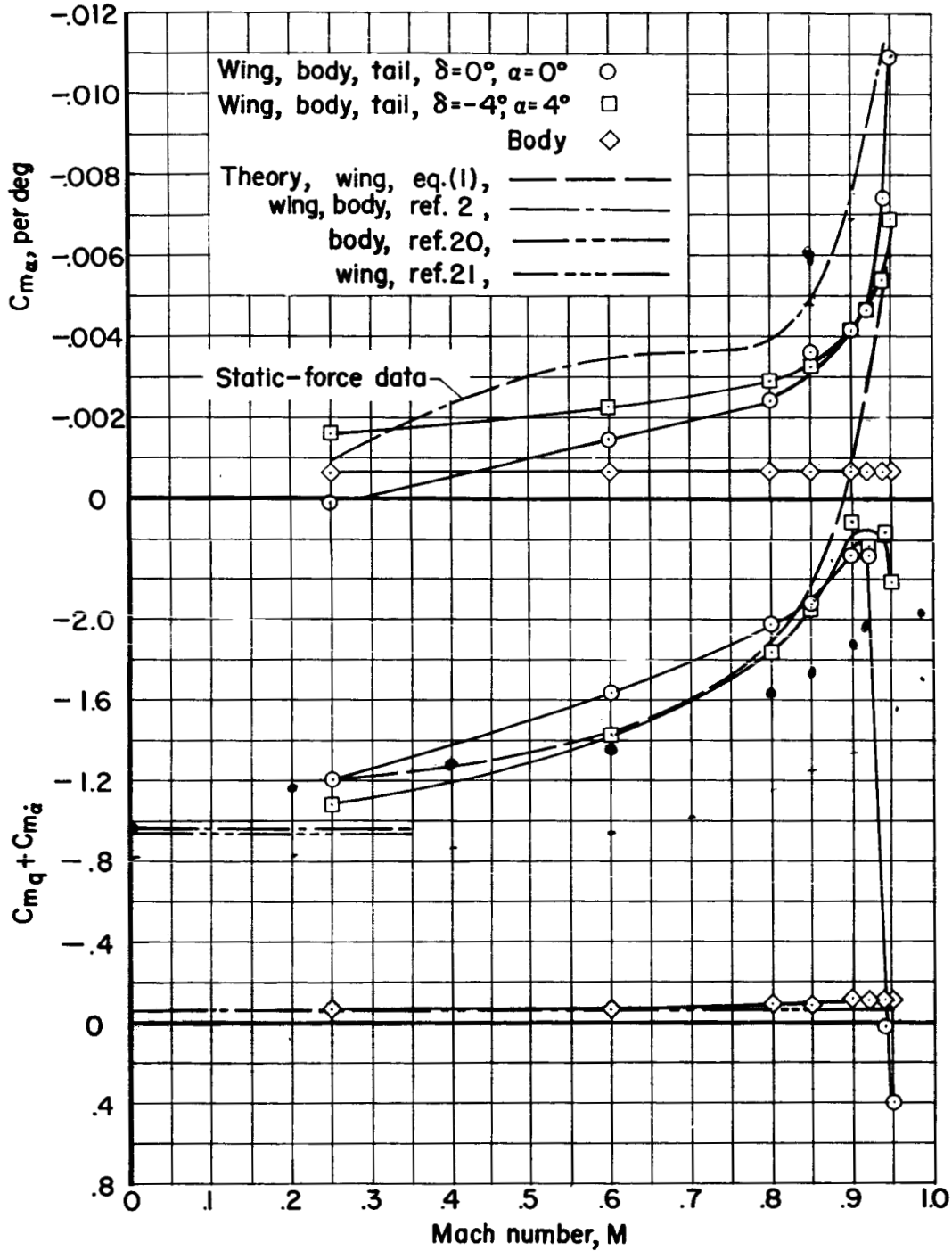

Figure 13.- The variation with Mach number of the dynamic longitudinal stability derivatives, C_{m_α} and $C_{m_q} + C_{m_{\dot\alpha}}$; f = approximately 8 cycles per second.

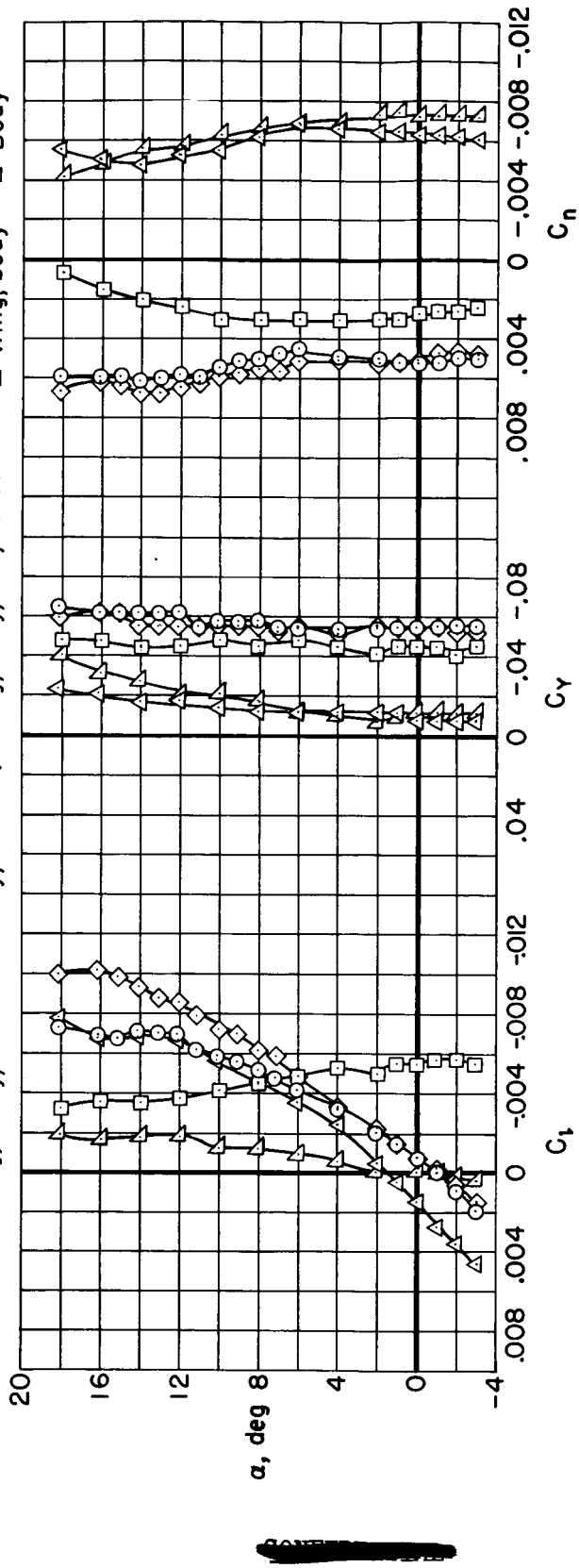

(a) M = 0.25; $\beta = 6^\circ$

Figure 14.- The static rolling-moment, side-force, and yawing-moment coefficients for a constant sideslip angle.

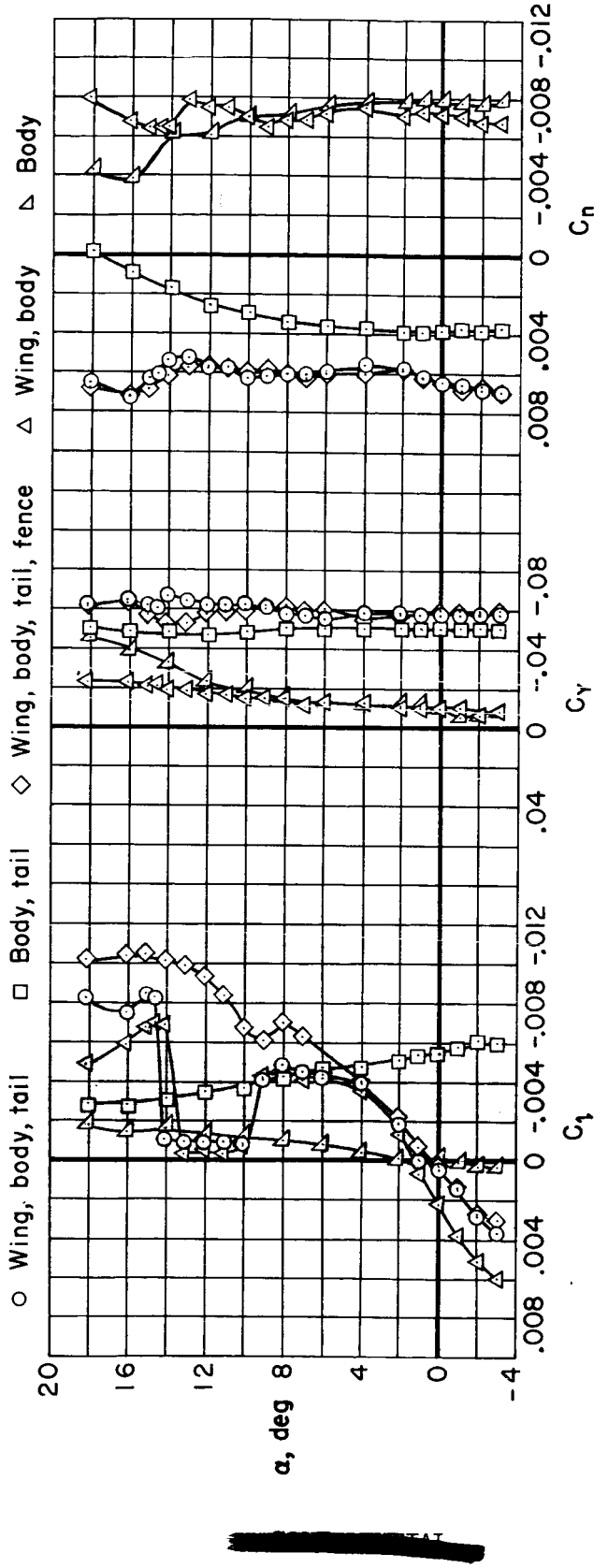

(b) M = 0.80; β = 6°

Figure 14.- Continued.

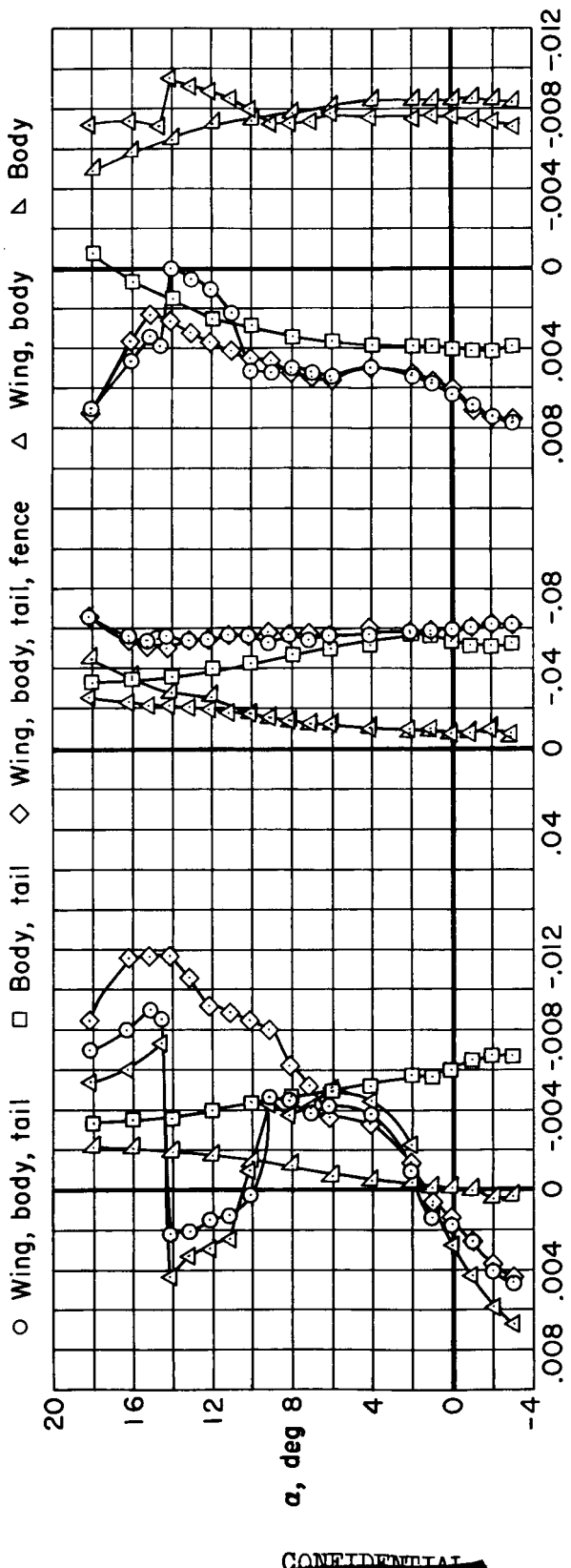

(c) M = 0.90; $\beta = 6^\circ$

Figure 14.- Continued.

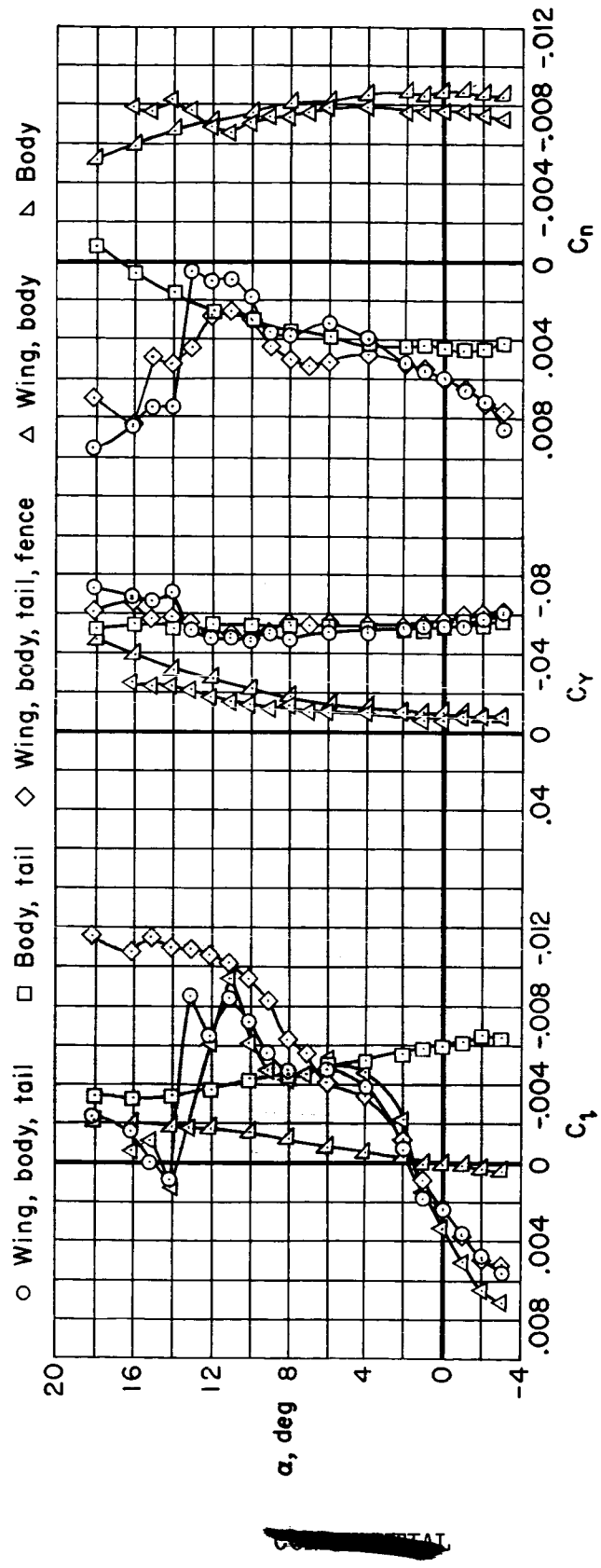

(d) M = 0.92; β = 6°

Figure 14.- Continued.

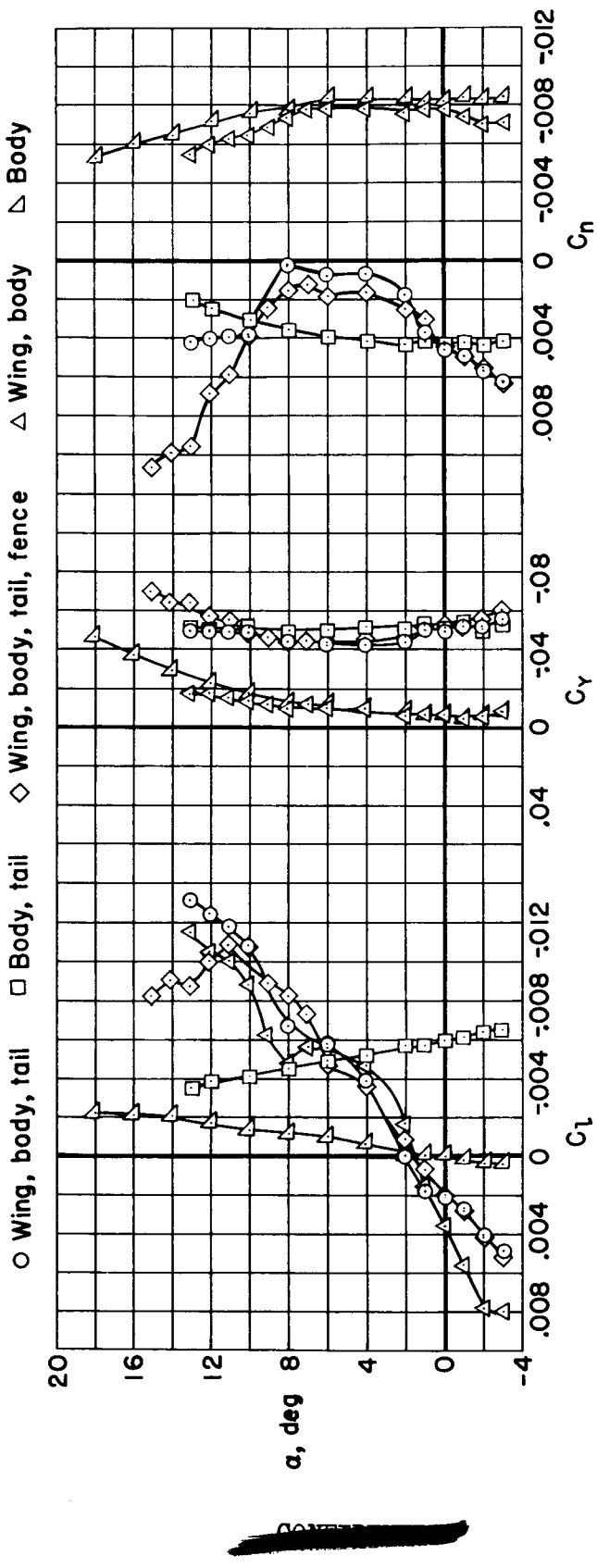

(e) M = 0.94; β = 6°

Figure 14.- Concluded.

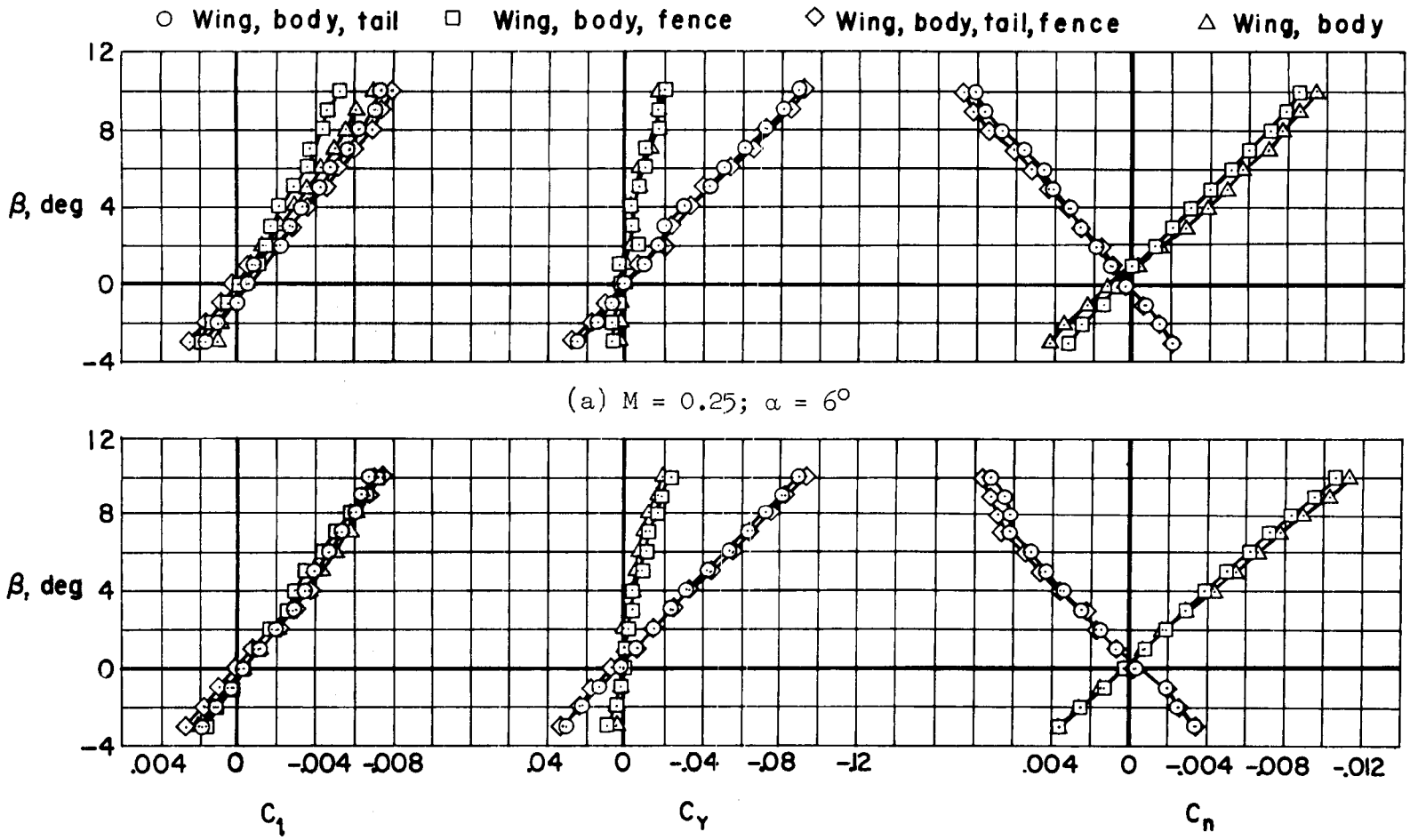

(a) M = 0.25; $\alpha = 6^\circ$

(b) M = 0.80; $\alpha = 6^\circ$

Figure 15.- The effect of sideslip angle on the static lateral-directional characteristics at a constant angle of attack.

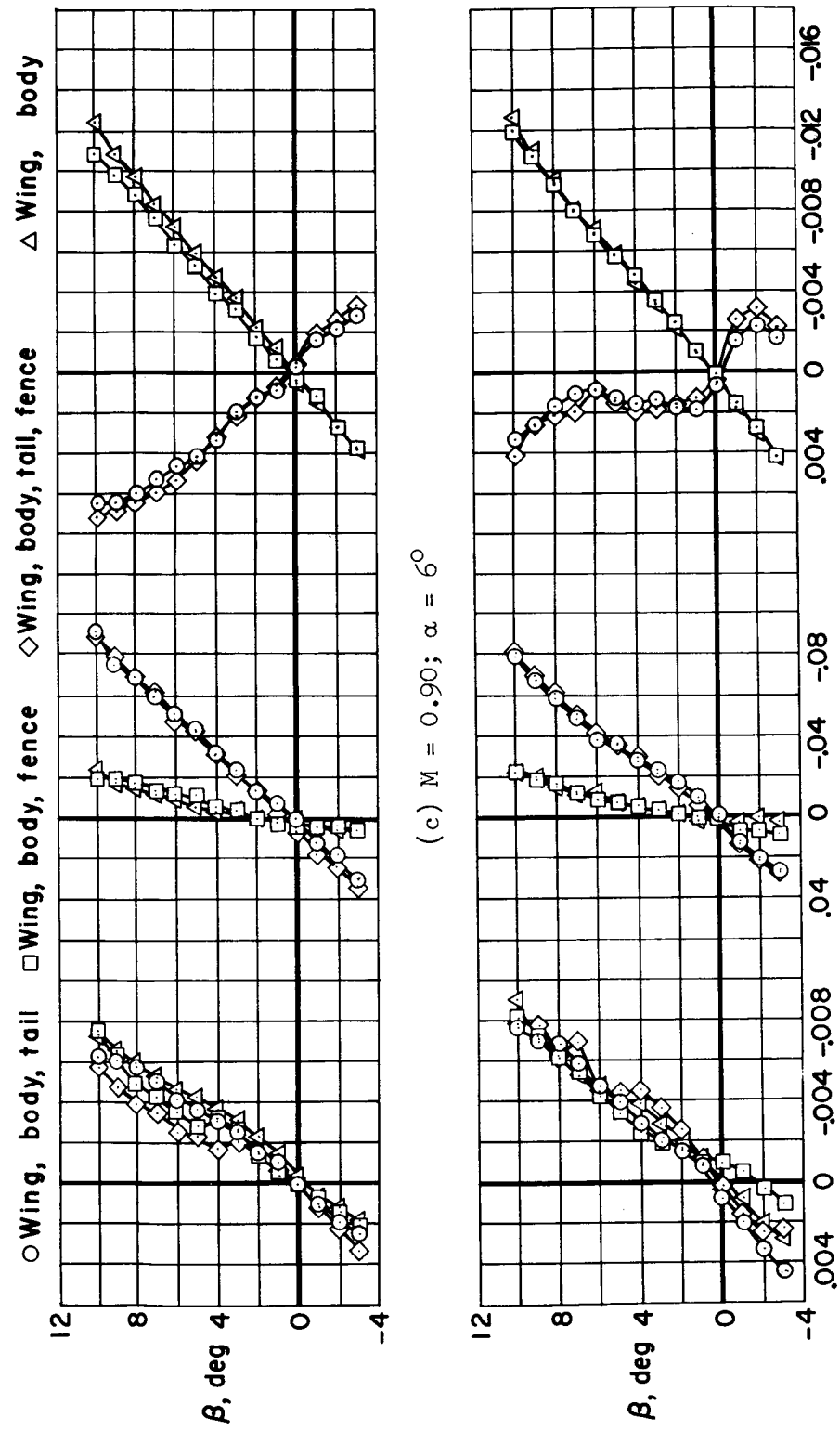

(c) M = 0.90; $\alpha = 6^\circ$

(d) M = 0.94; $\alpha = 6^\circ$

Figure 15.- Concluded.

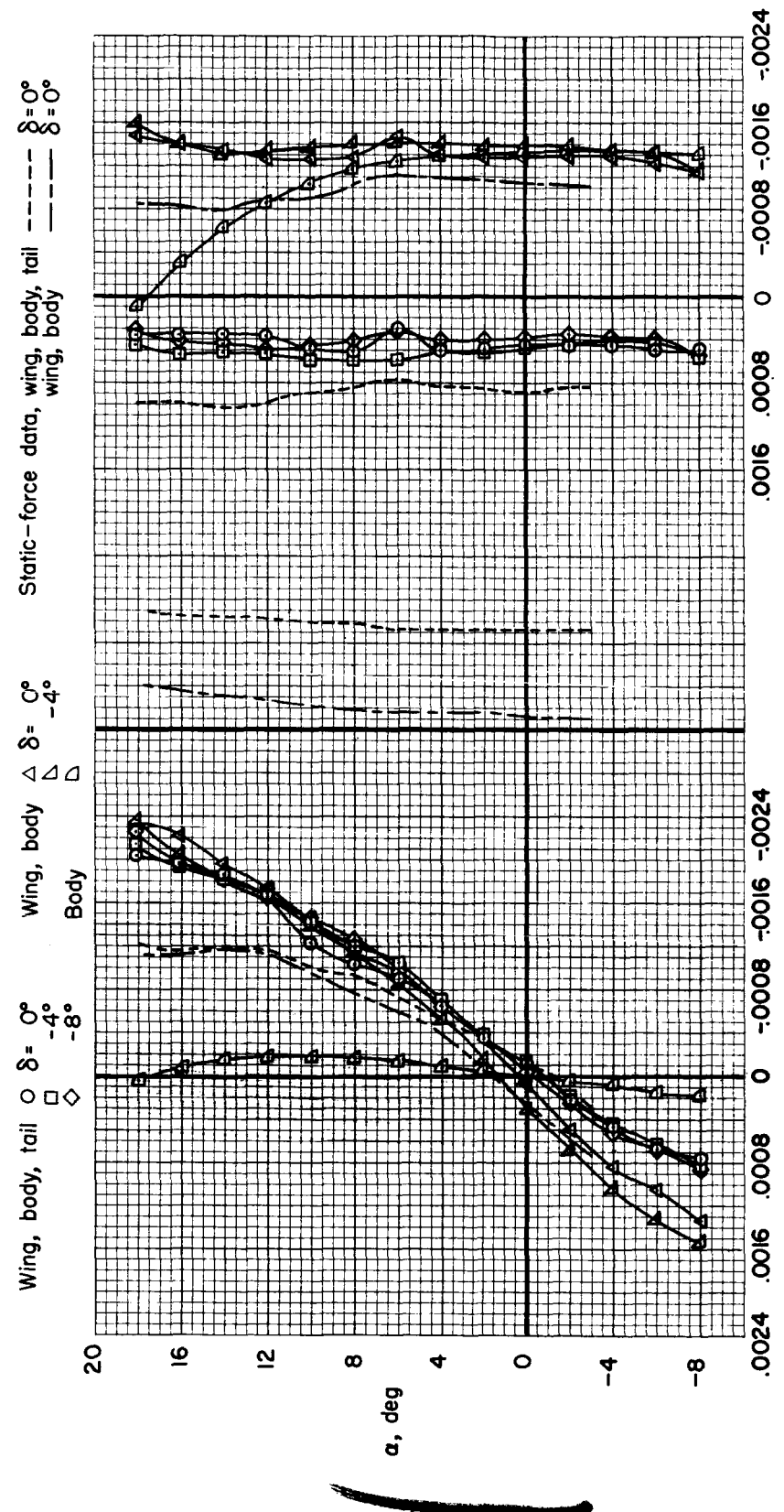

(a) M = 0.25

Figure 16.- The sideslip derivatives from oscillation tests; f = approximately 8 cycles per second.

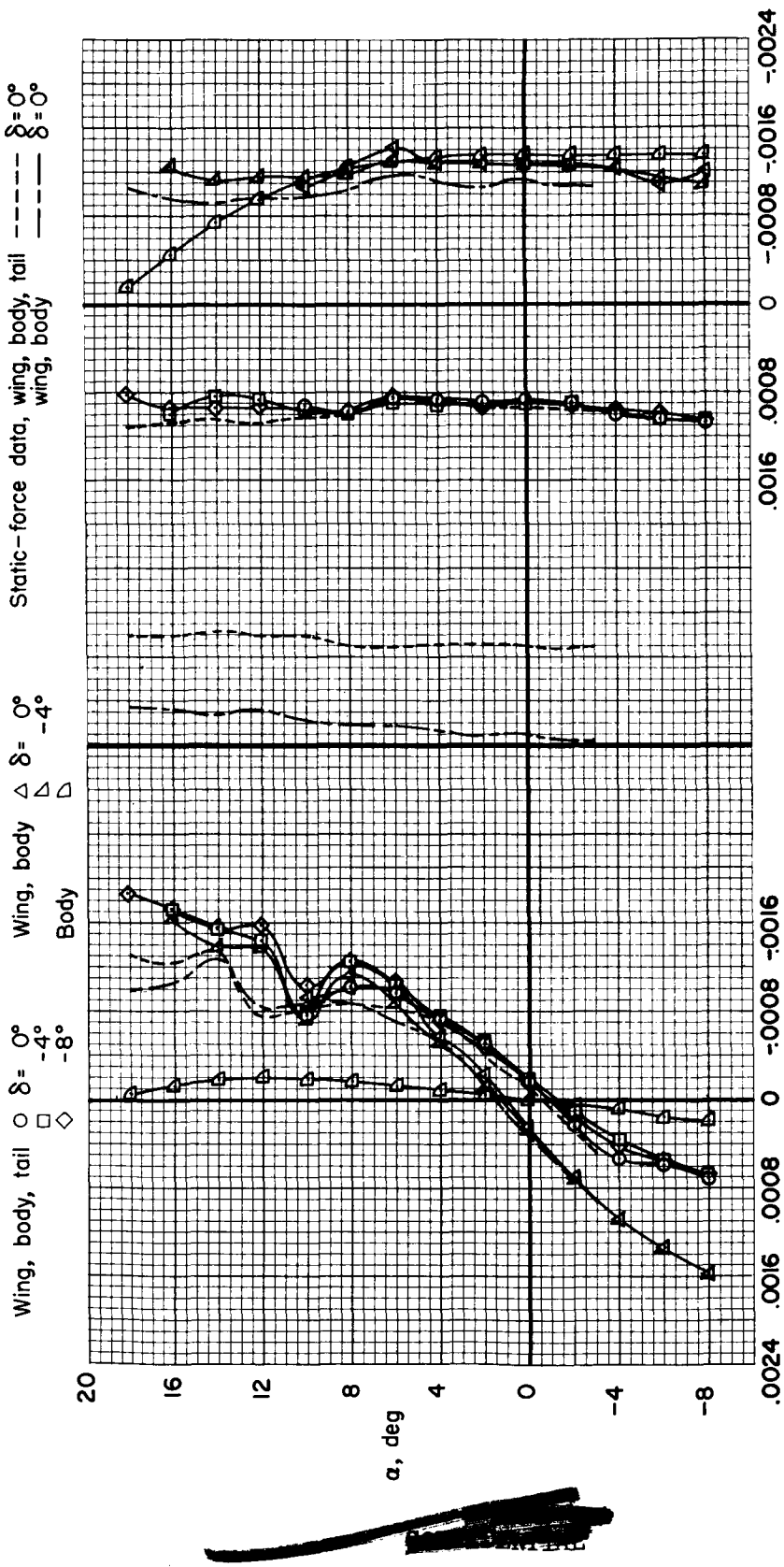

(b) M = 0.60

Figure 16.- Continued.

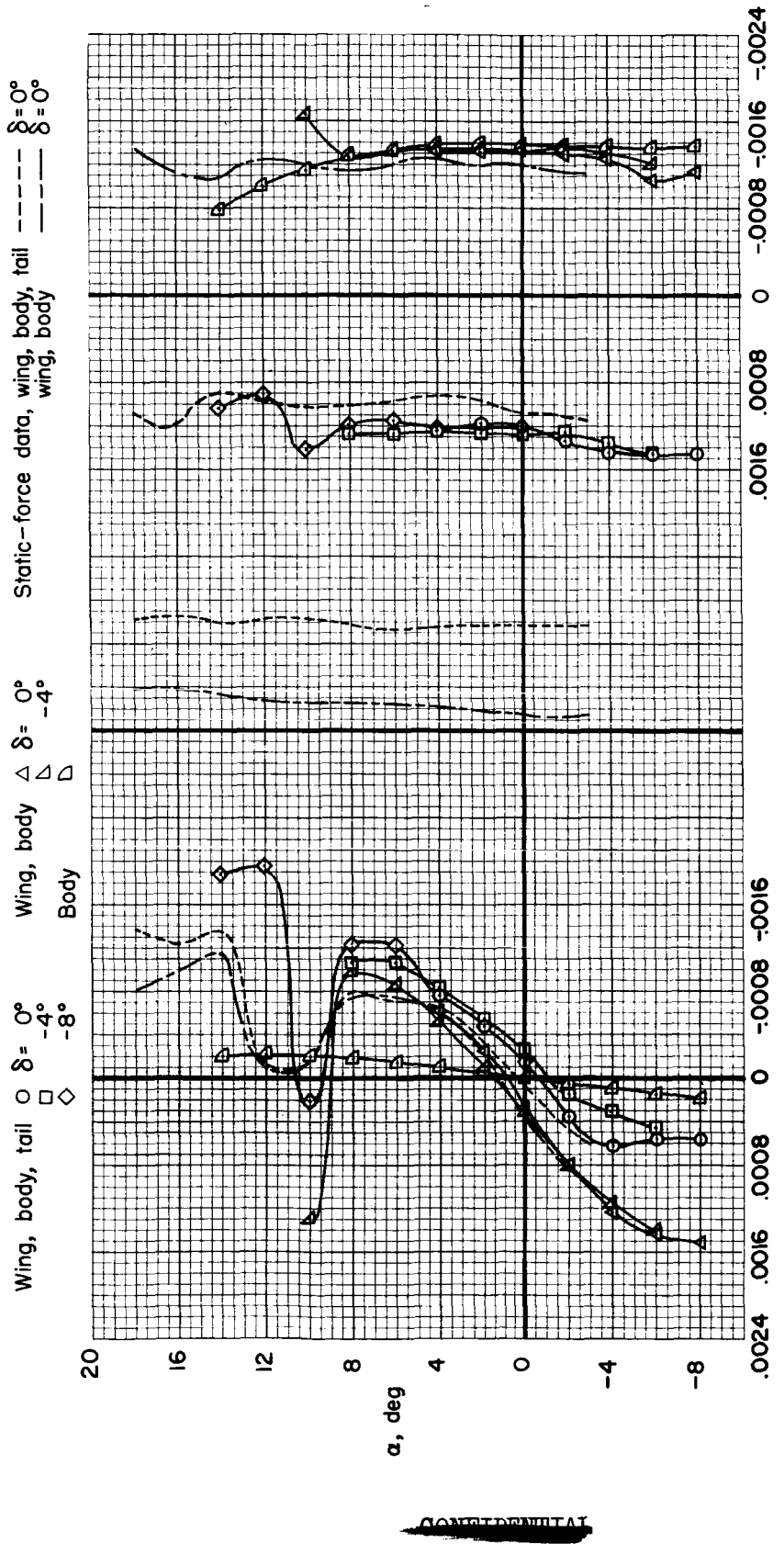

(c) M = 0.80

Figure 16.- Continued.

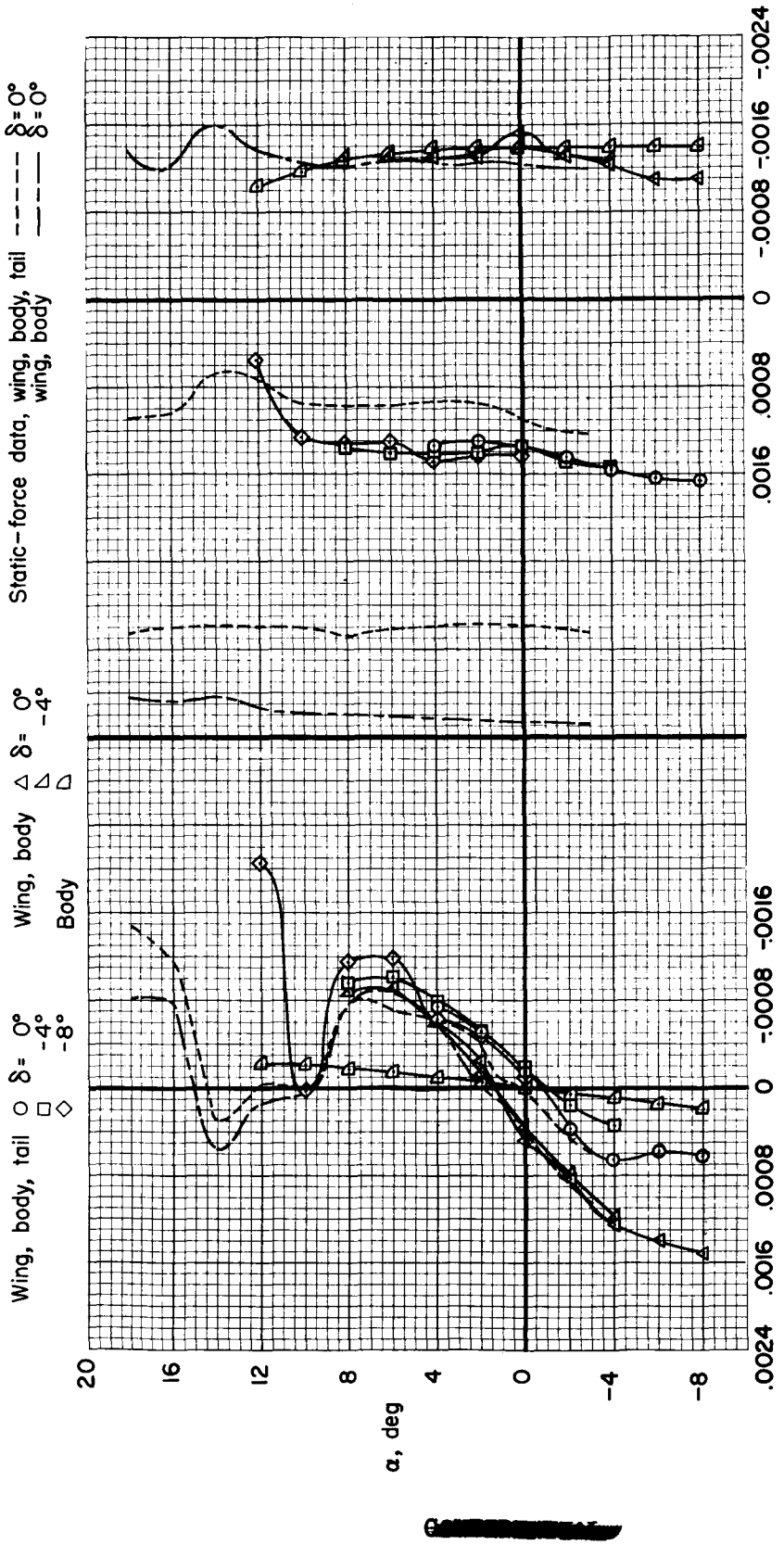

(d) M = 0.85

Figure 16.- Continued.

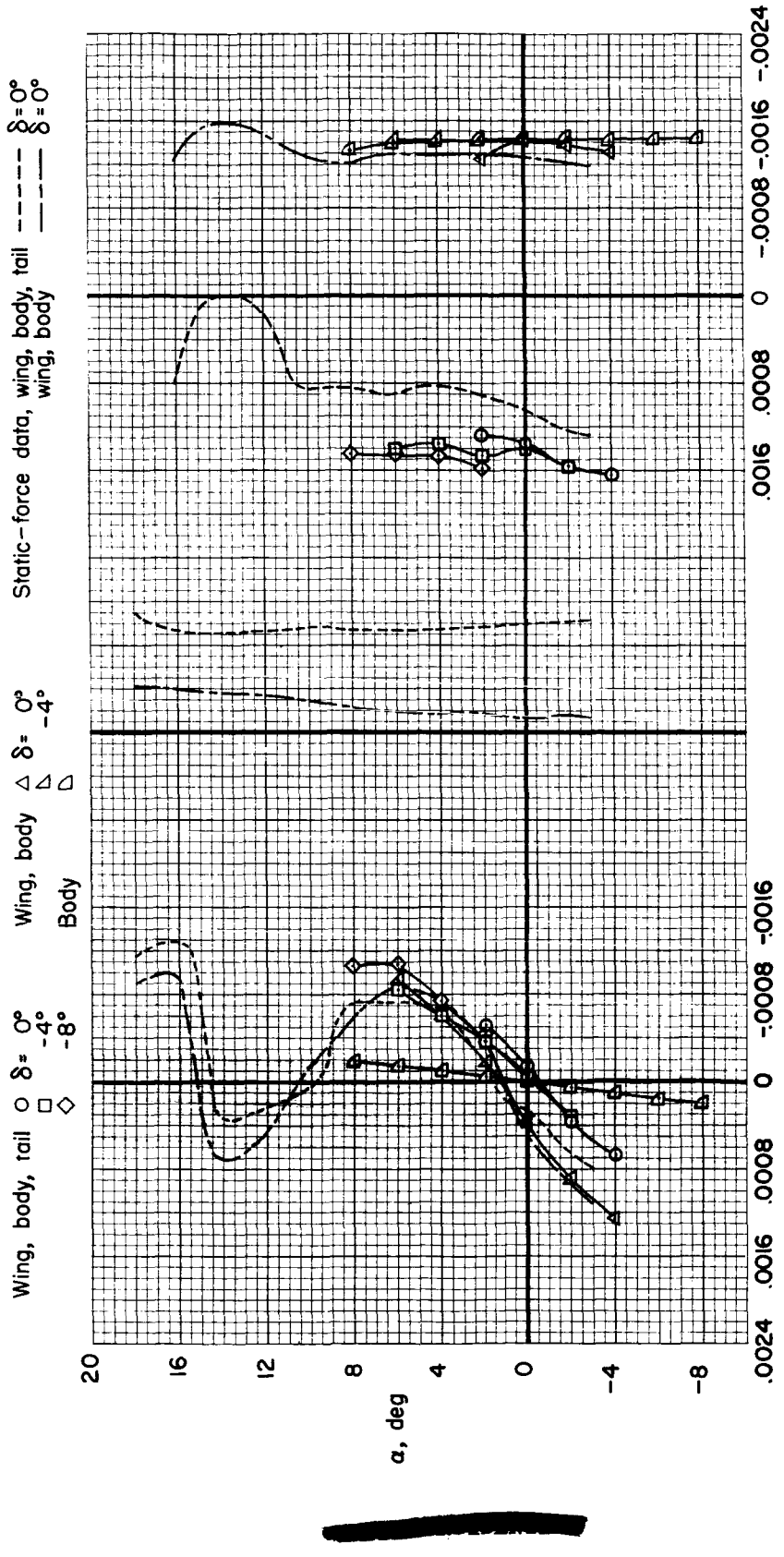

(e) M = 0.90

Figure 16.- Continued.

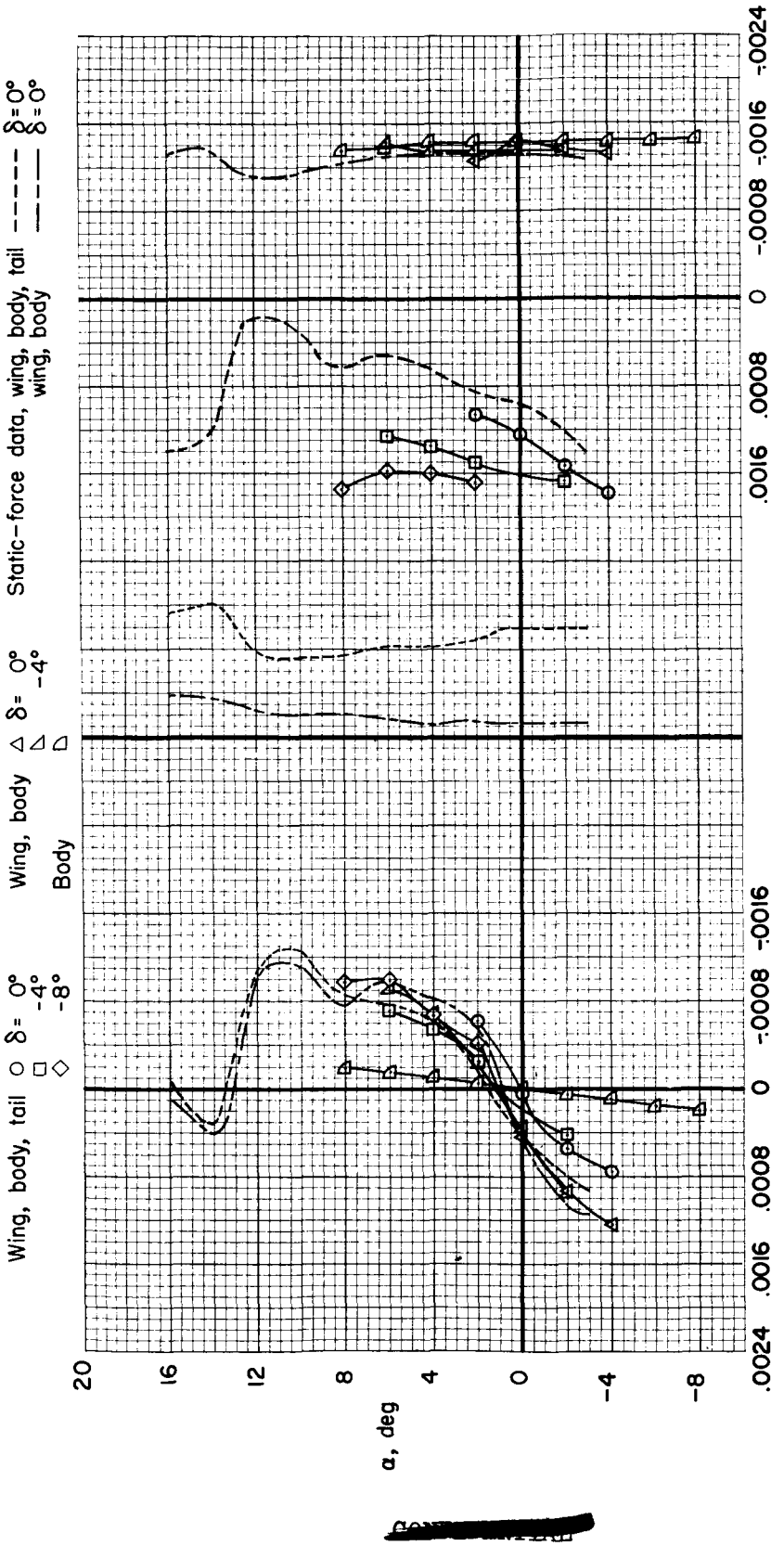

(f) M = 0.92

Figure 16.- Continued.

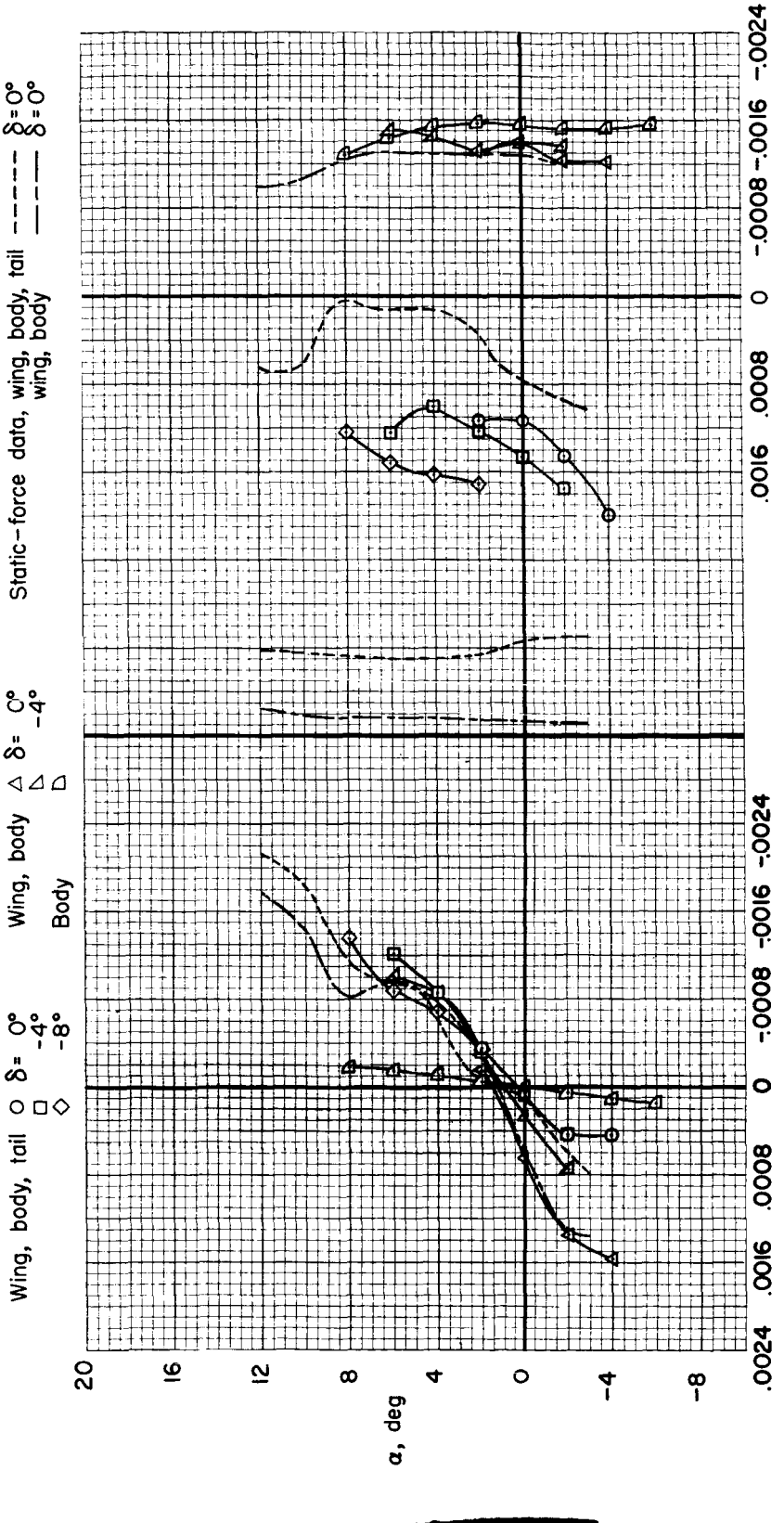

(g) M = 0.94

Figure 16.- Continued.

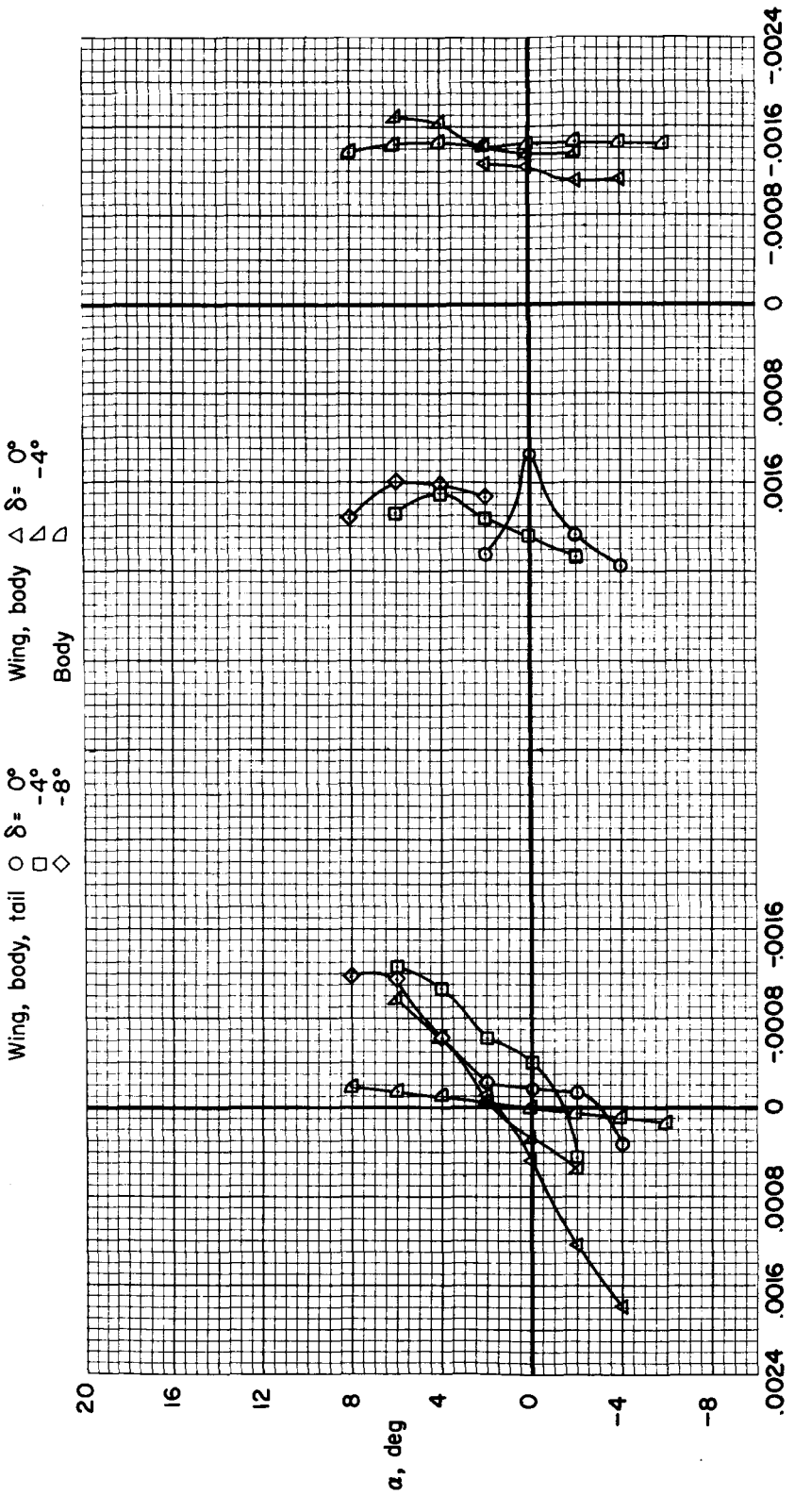

(h) M = 0.95

Figure 16.- Concluded.

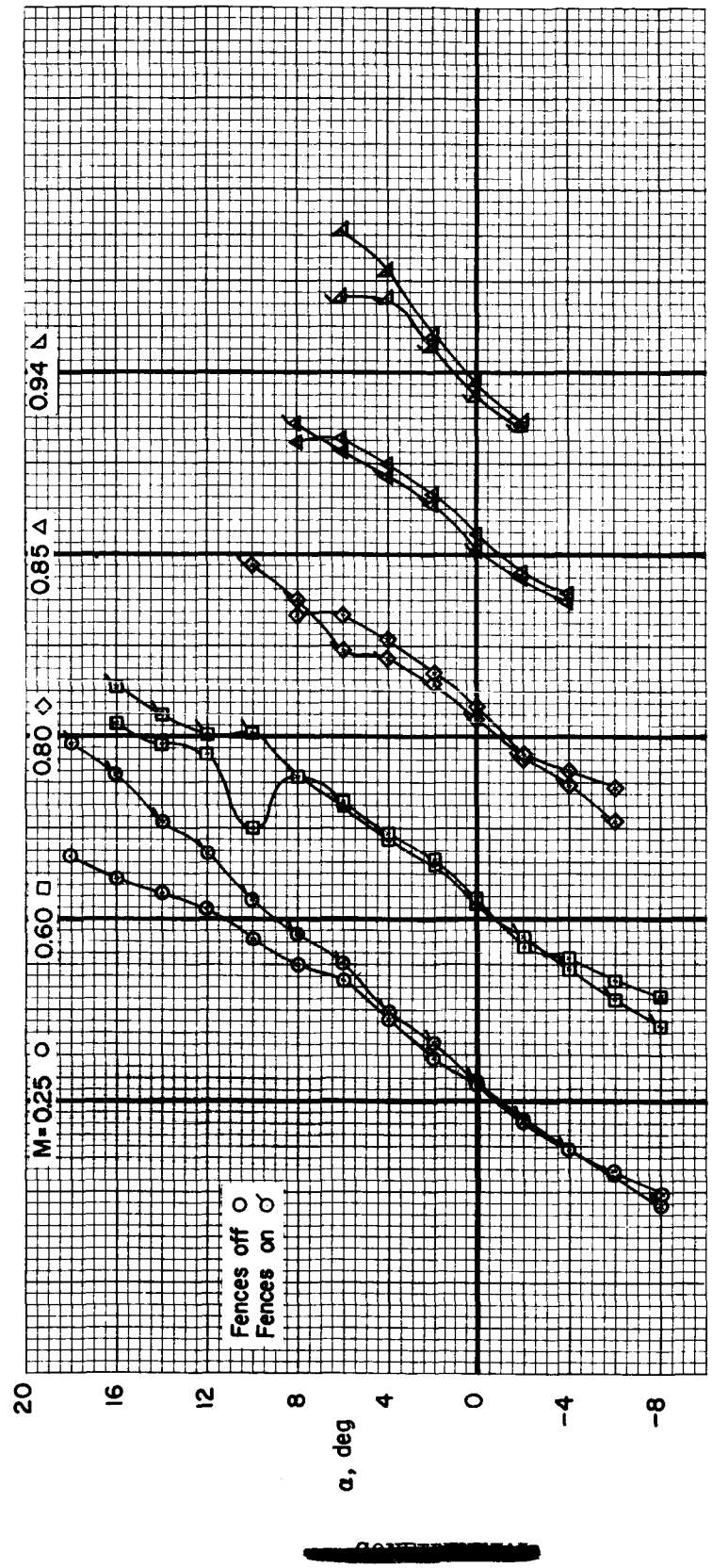

Figure 17.- The effect of chordwise fences on the rolling-moment-due-to-sideslip derivative C_{l_β} from oscillation tests; f = approximately 8 cycles per second.

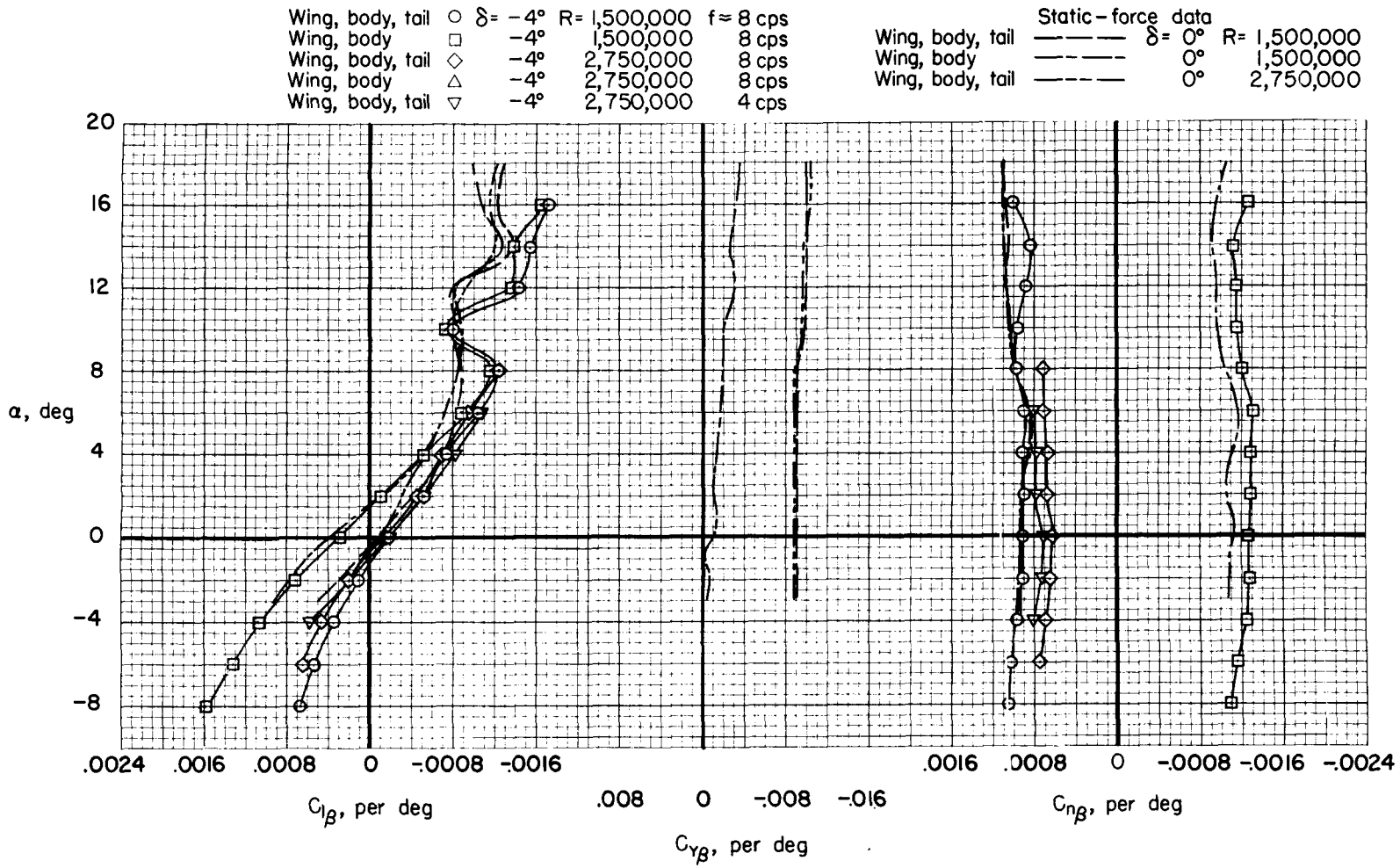

(a) M = 0.60

Figure 18.- The effect of Reynolds number and frequency of oscillation on the sideslip derivatives.

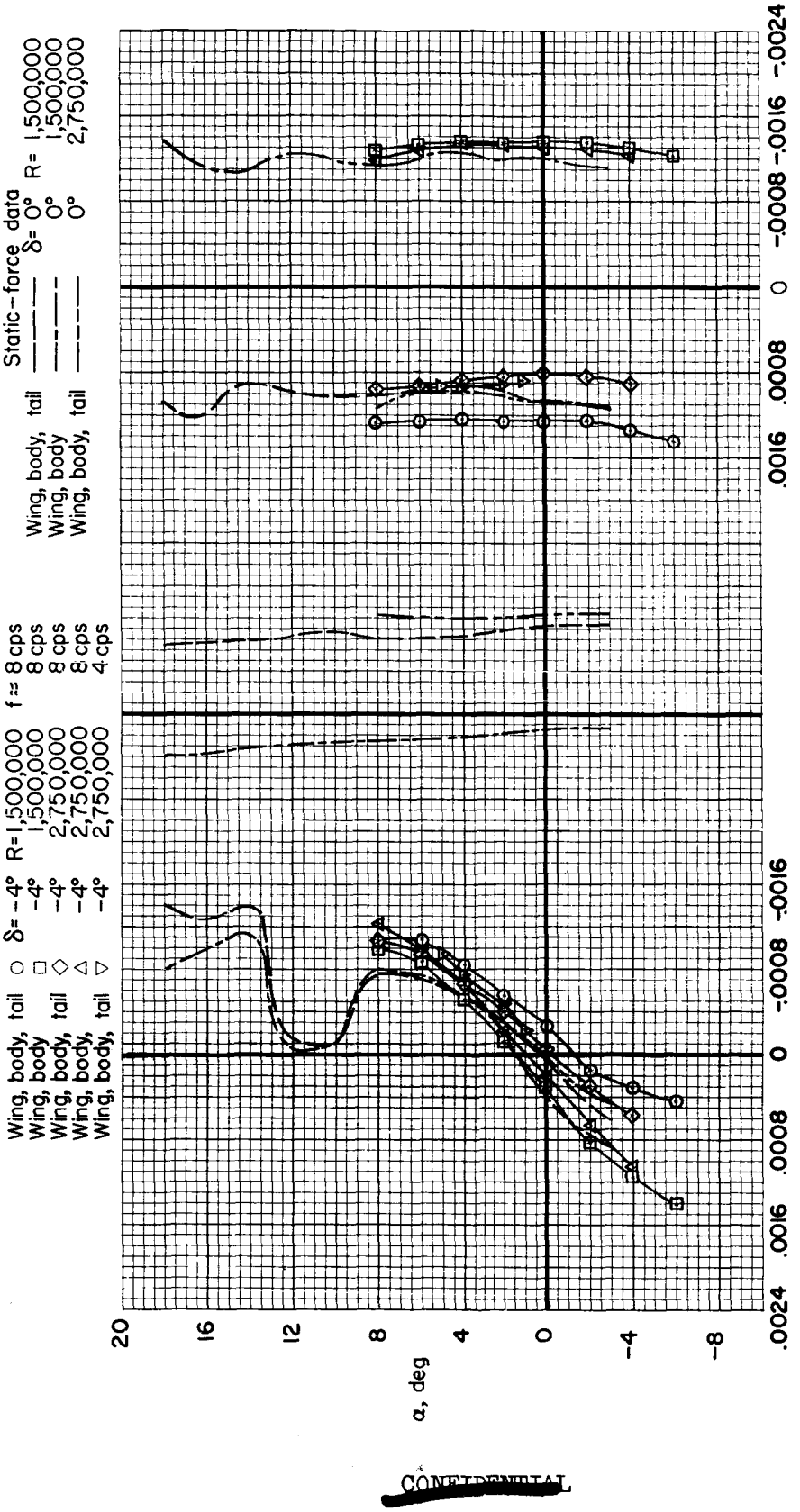

(b) M = 0.80

Figure 18.- Continued.

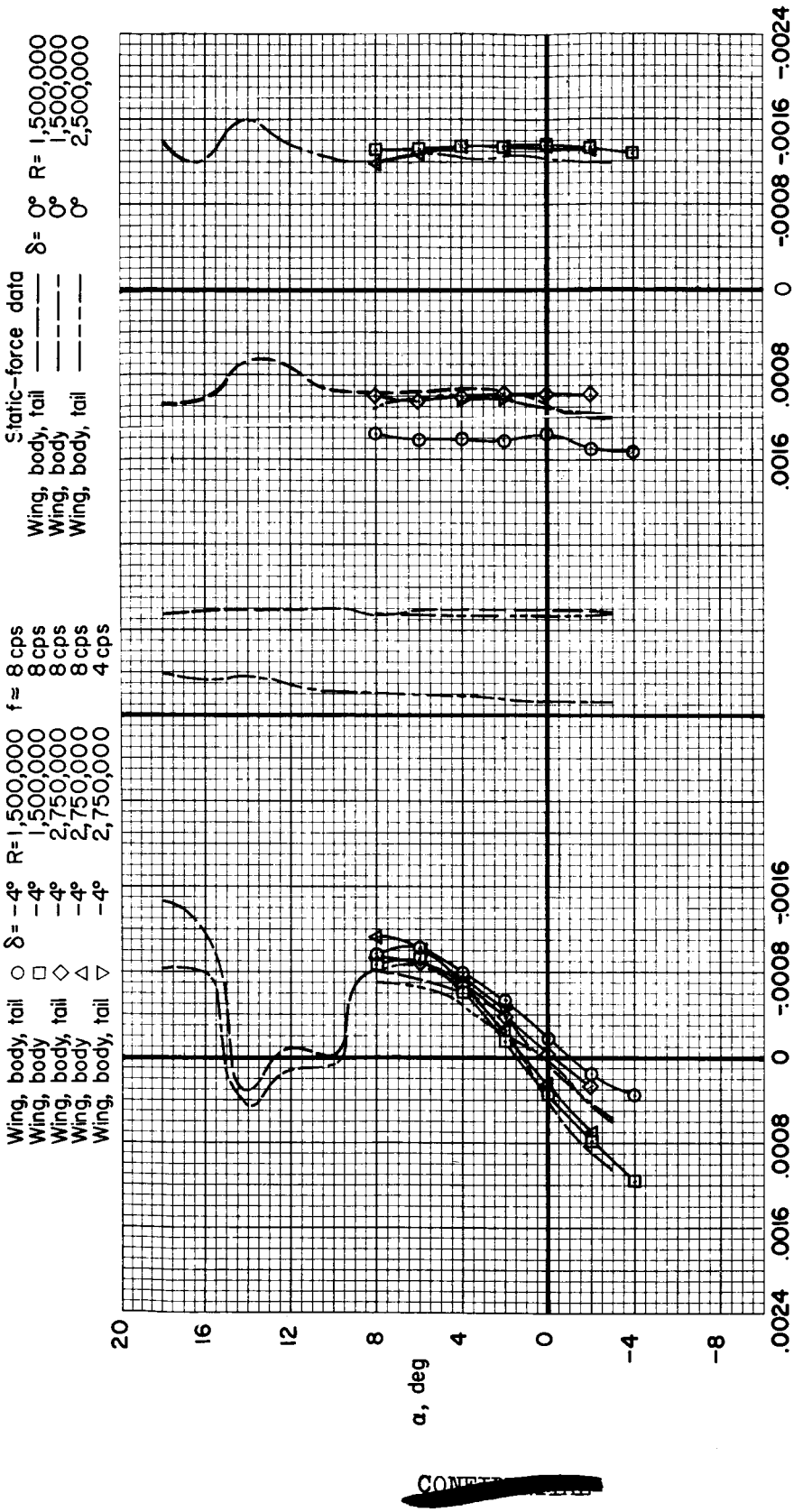

(c) M = 0.85

Figure 18.- Concluded.

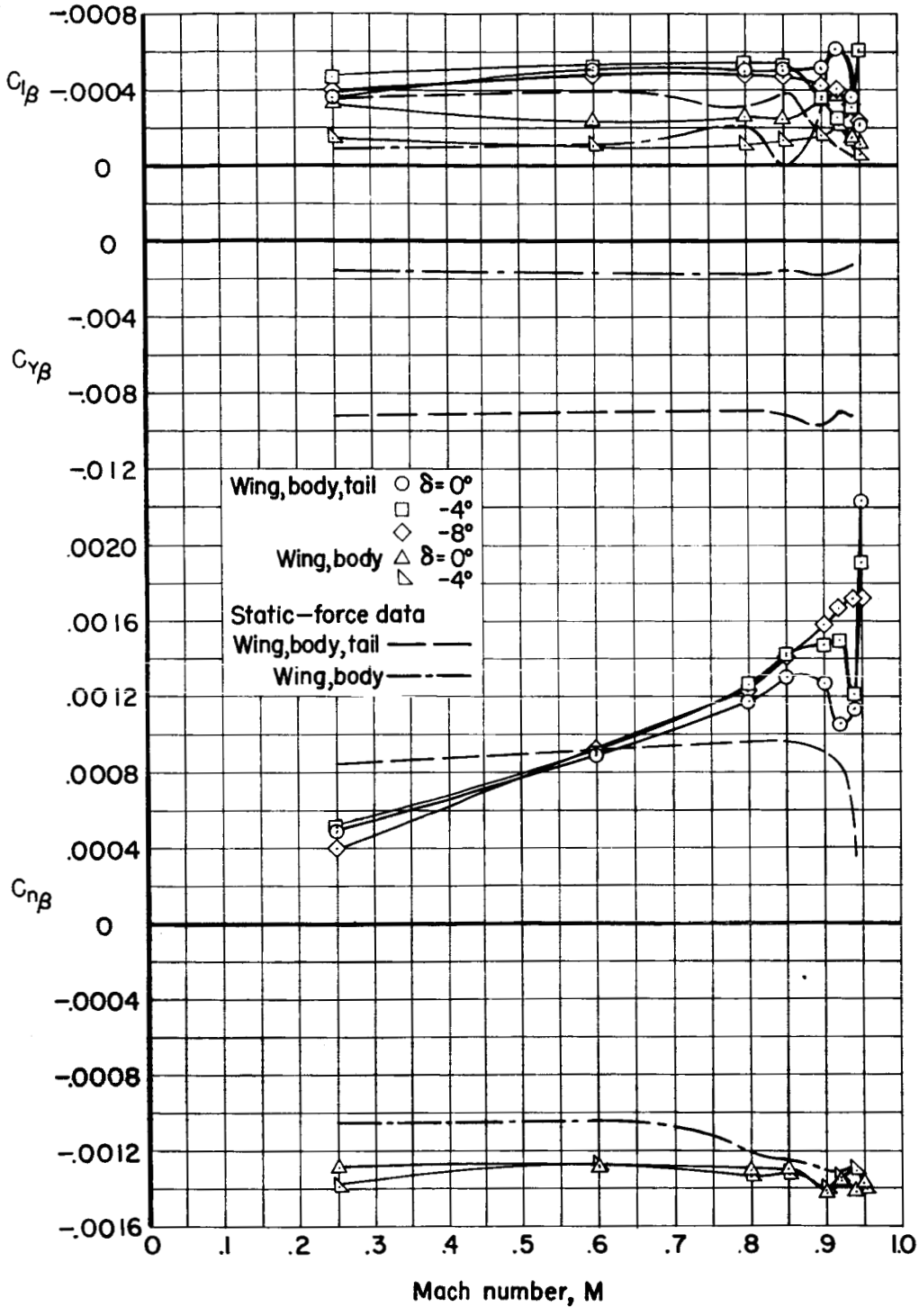

Figure 19.- The variation with Mach number of the sideslip derivatives from the oscillation tests; $\alpha = 2^{\circ}$.

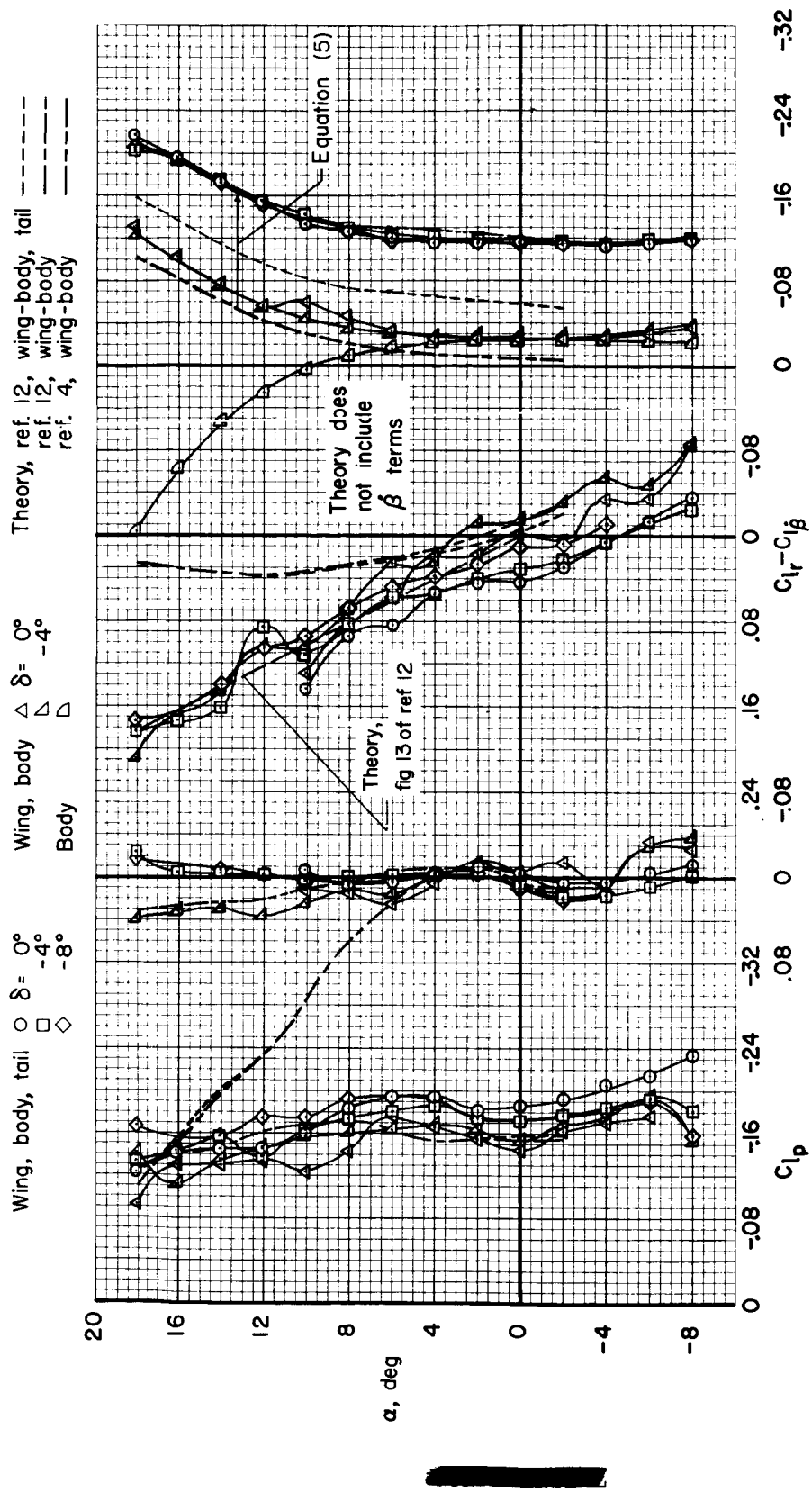

(a) M = 0.25

Figure 20.- The dynamic lateral-directional rotary stability derivatives.

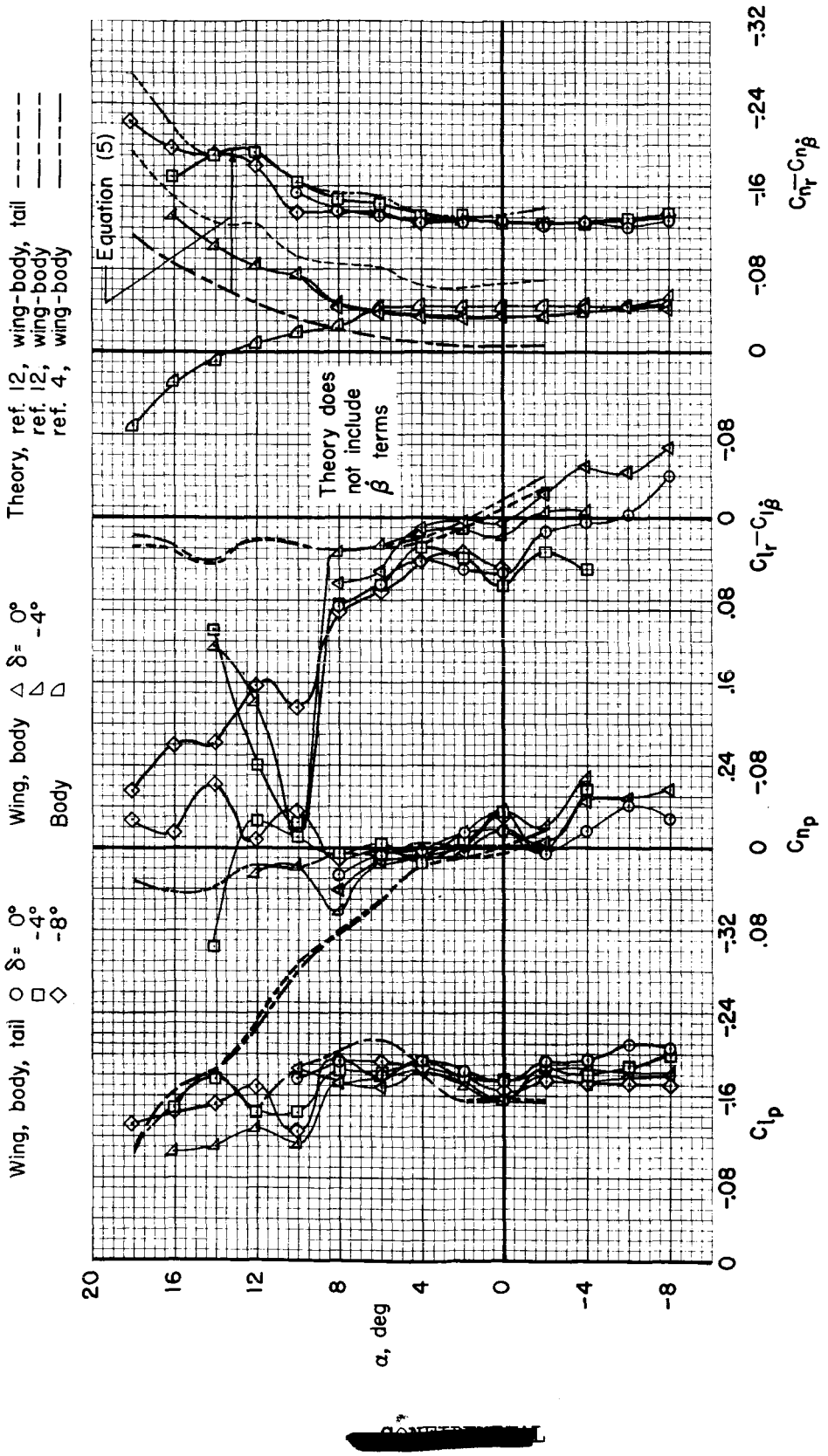

(b) M = 0.60

Figure 20.- Continued.

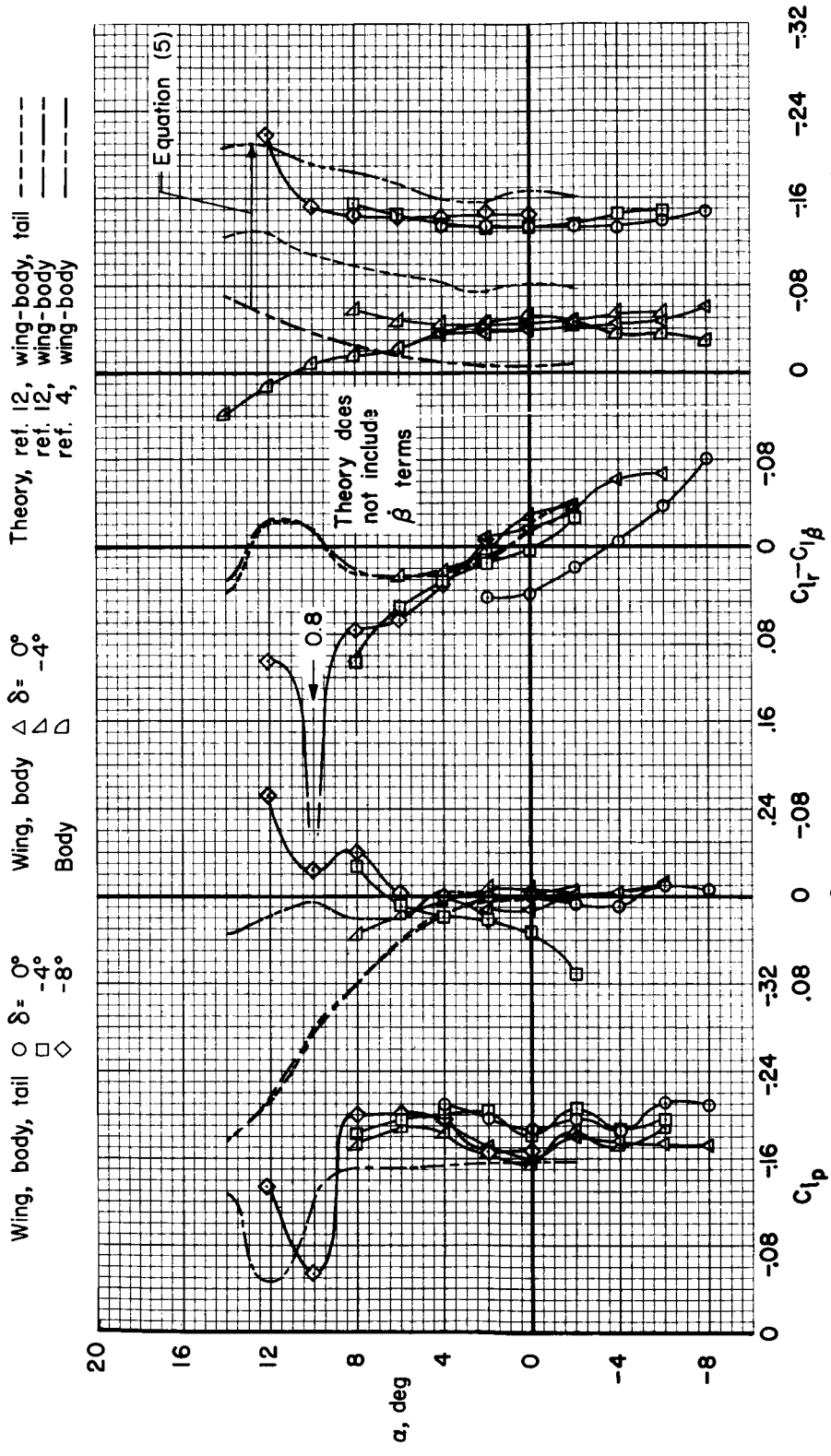

(c) M = 0.80

Figure 20.- Continued.

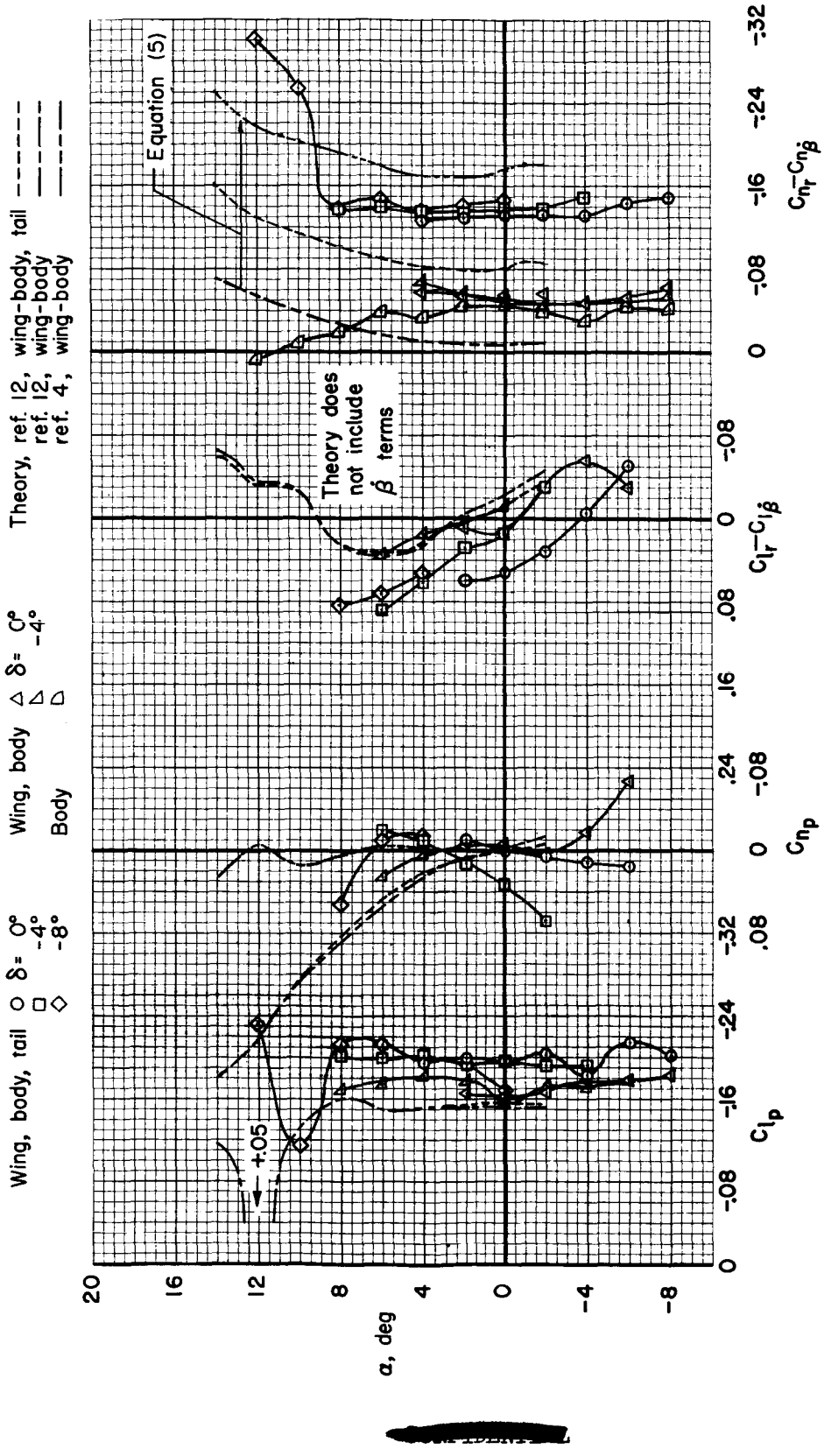

(d) M = 0.85

Figure 20.- Continued.

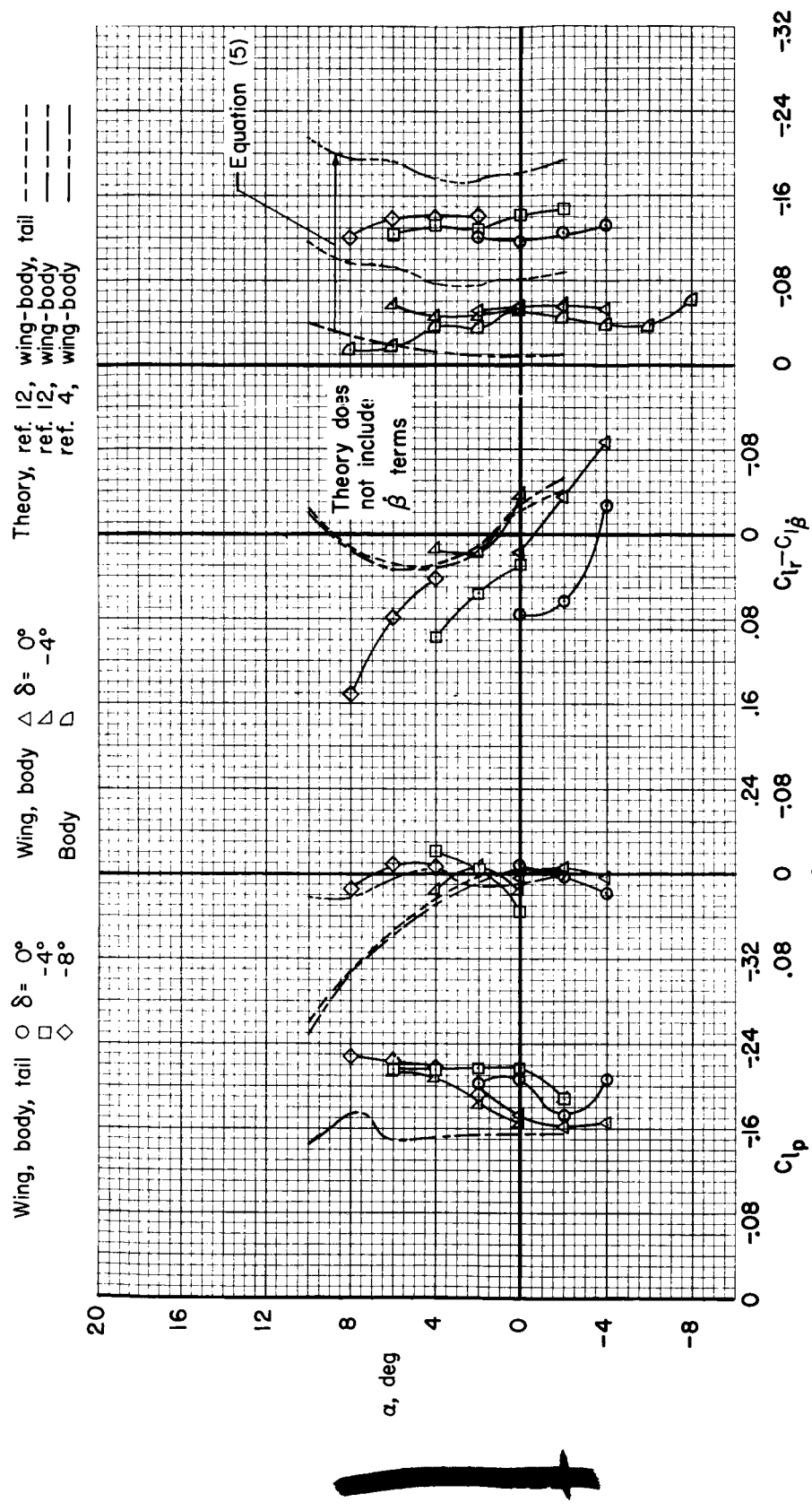

(e) M = 0.90

Figure 20.- Continued.

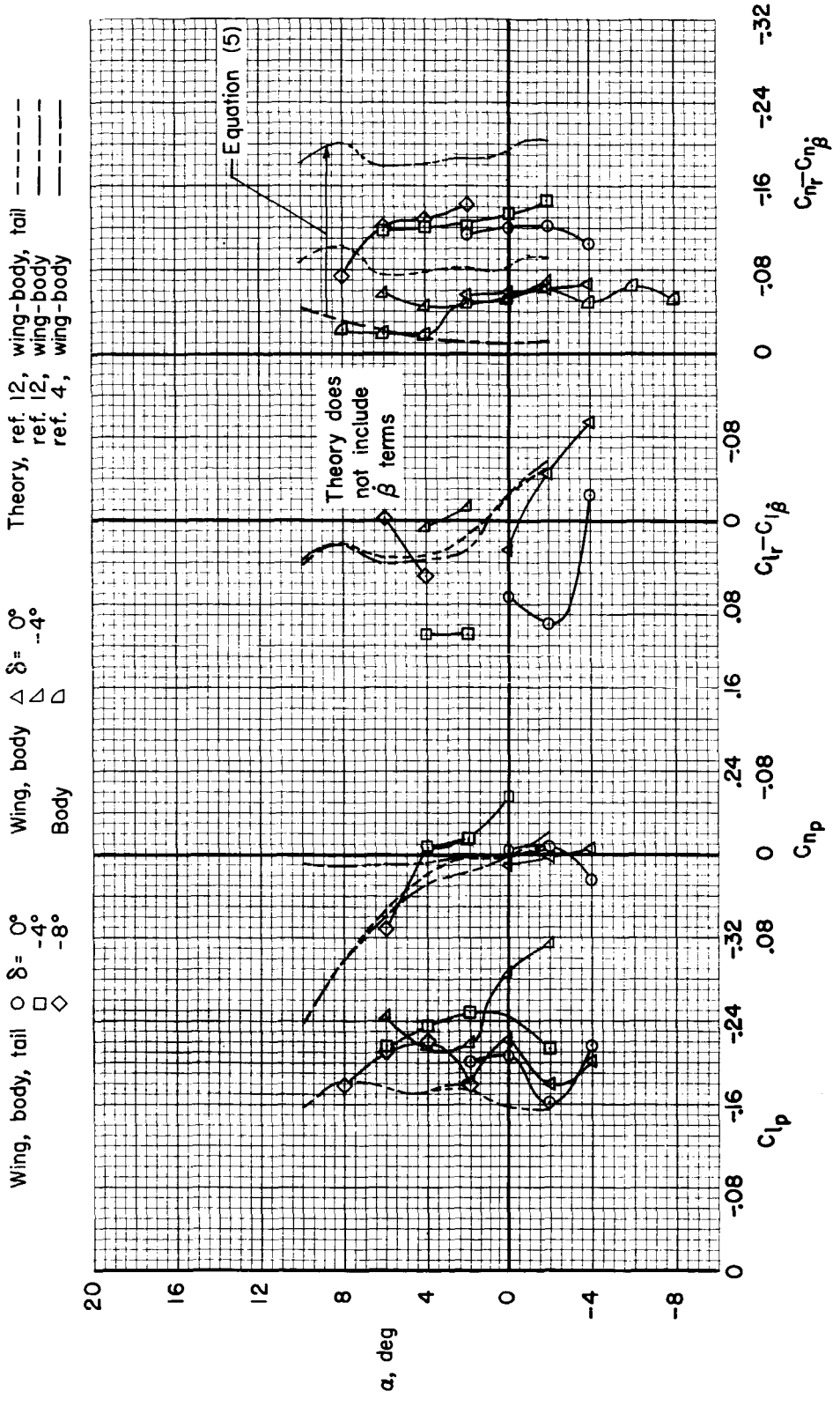

(f) M = 0.92

Figure 20.- Continued.

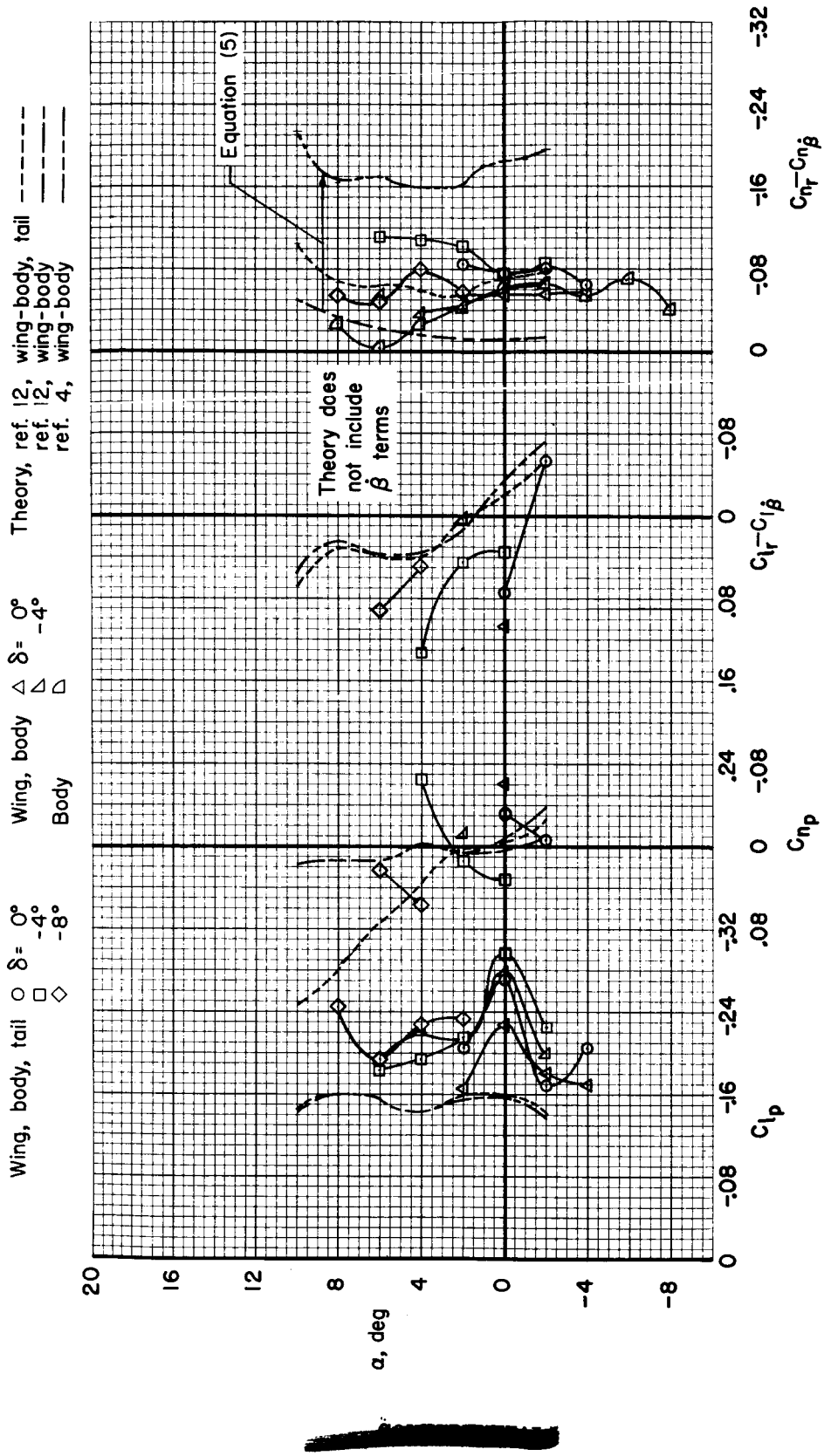

(g) M = 0.94

Figure 20.- Continued.

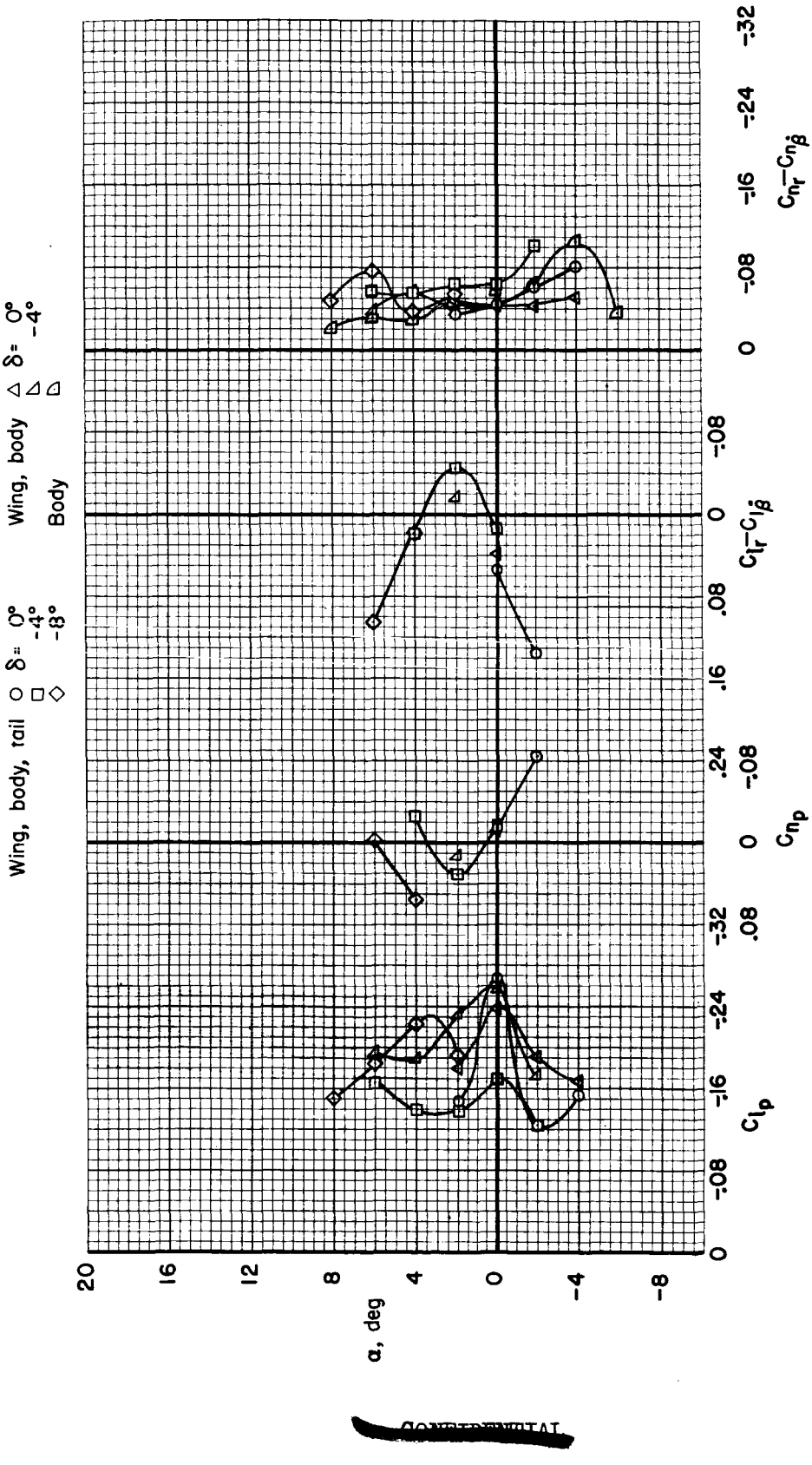

(h) M = 0.95

Figure 20.- Concluded.

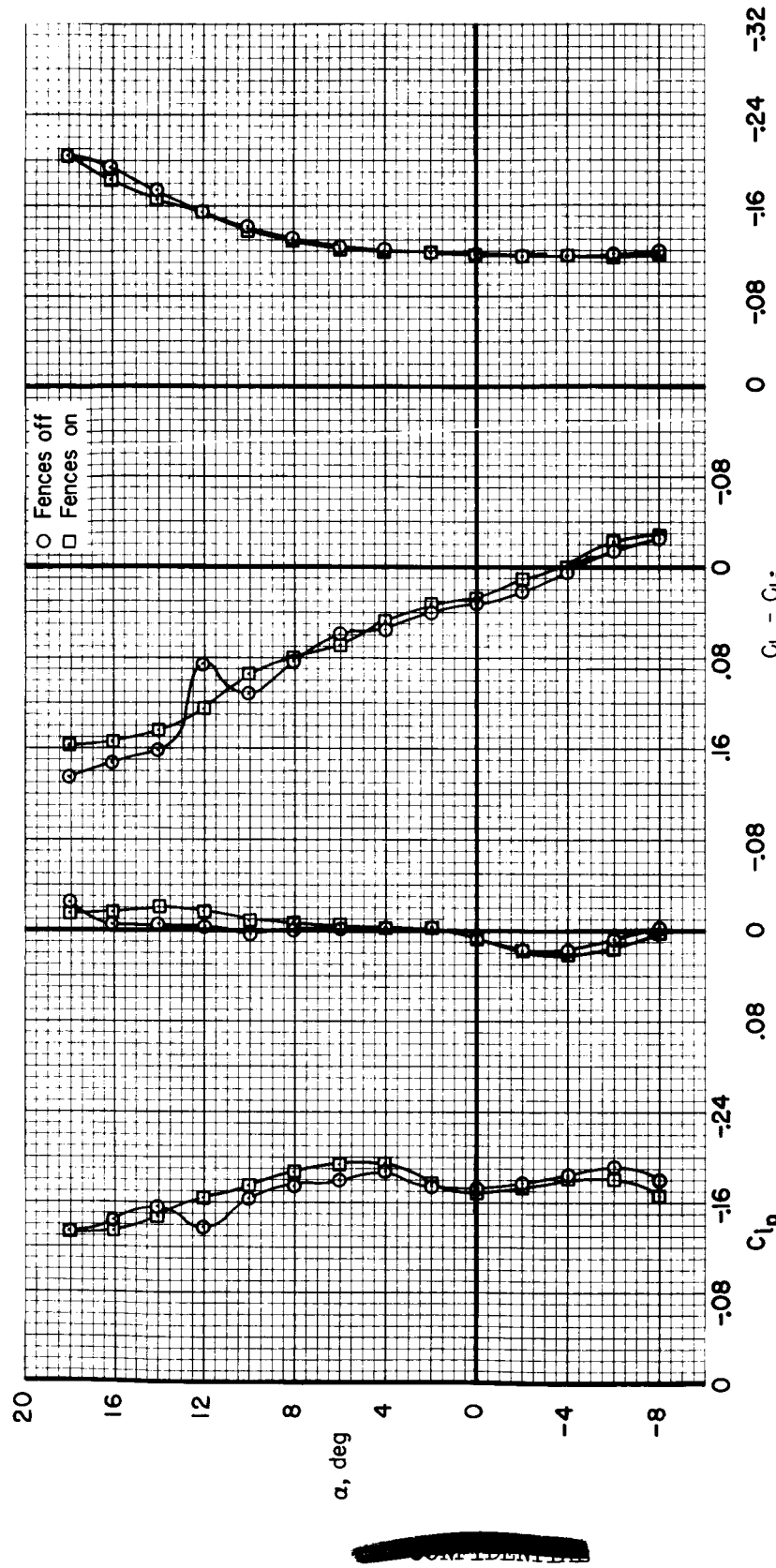

(a) M = 0.25

Figure 21.- The effect of fences on the dynamic lateral-directional rotary stability derivatives; f = approximately 8 cycles per second.

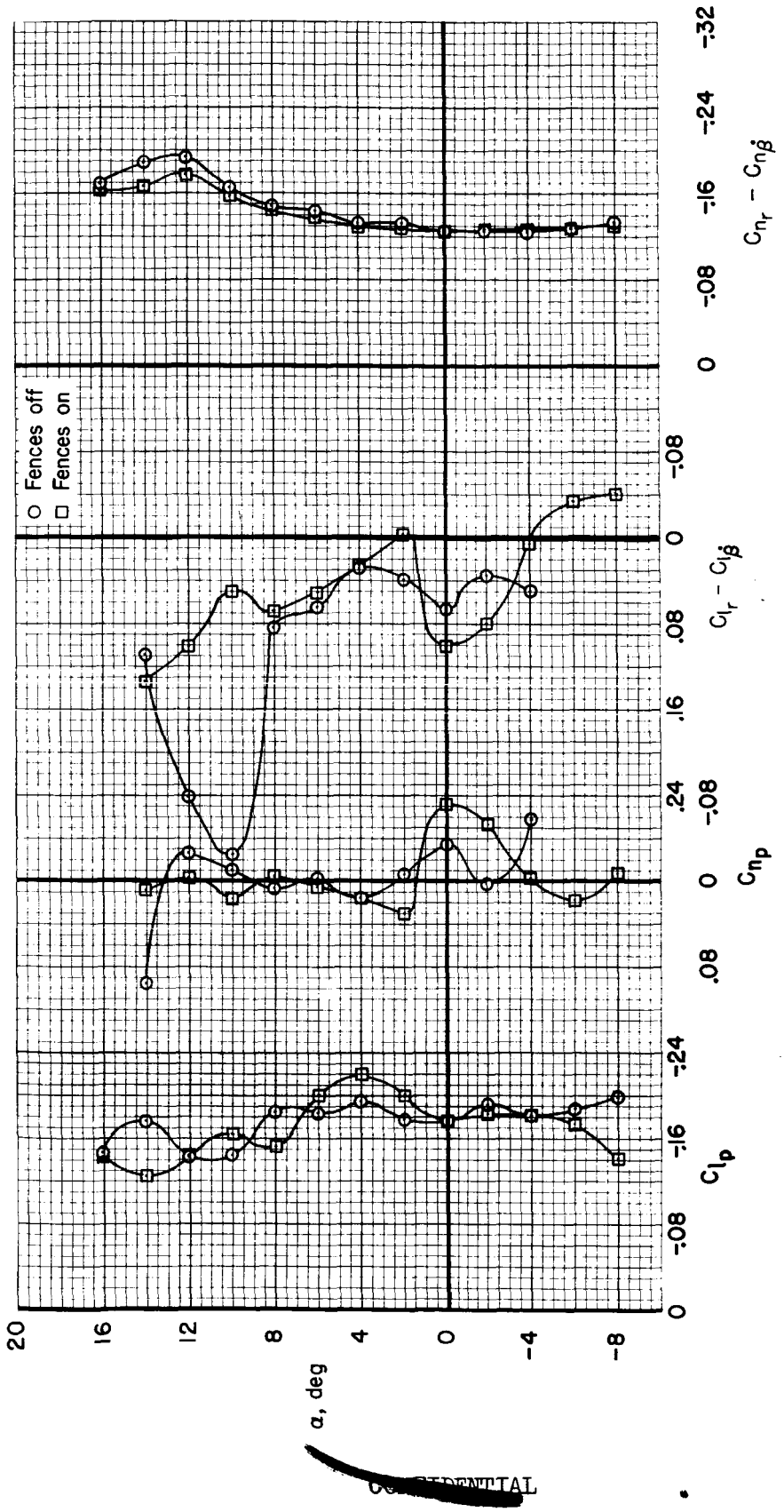

(b) M = 0.60

Figure 21.- Continued.

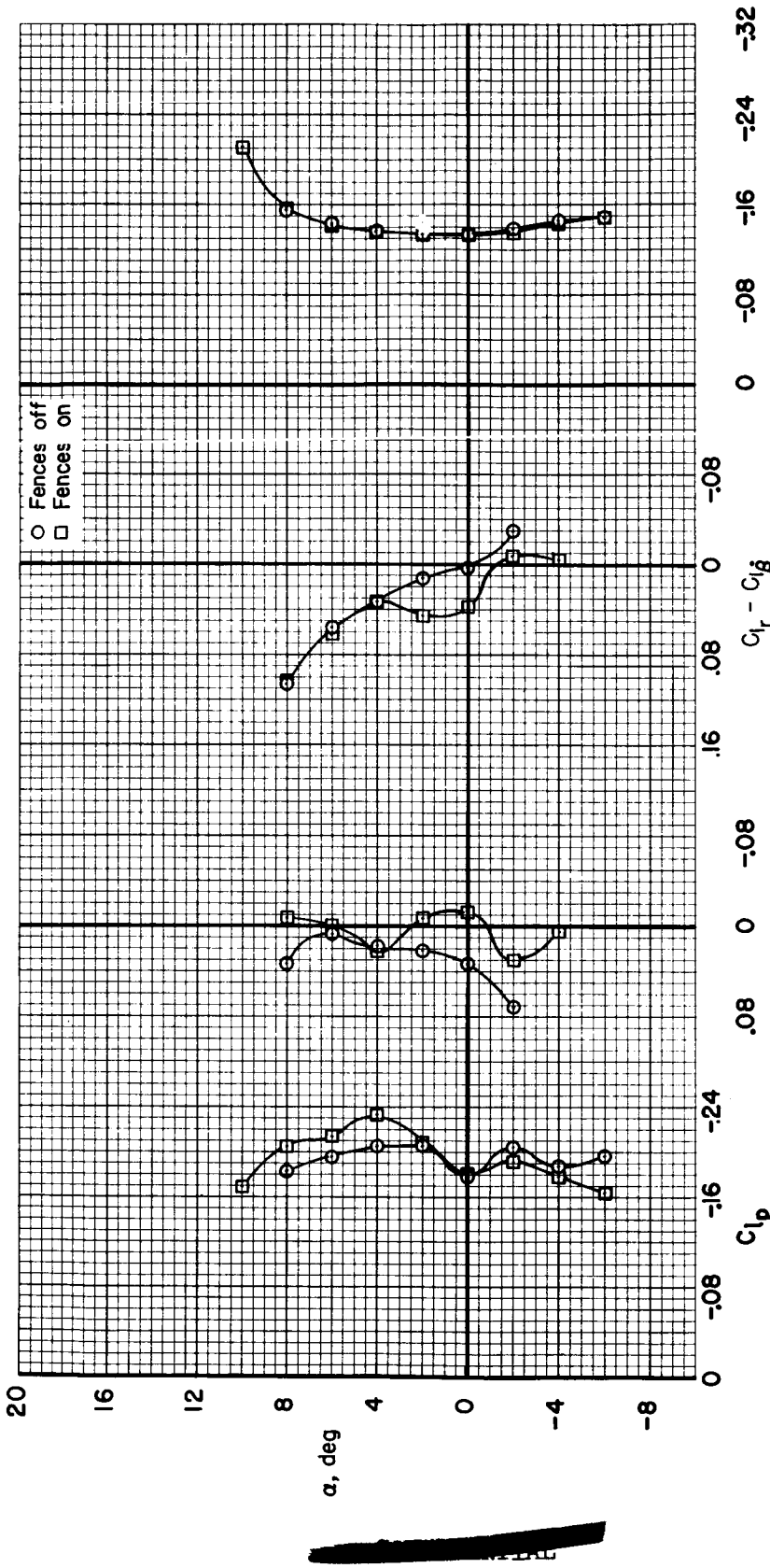

(c) M = 0.80

Figure 21.- Continued.

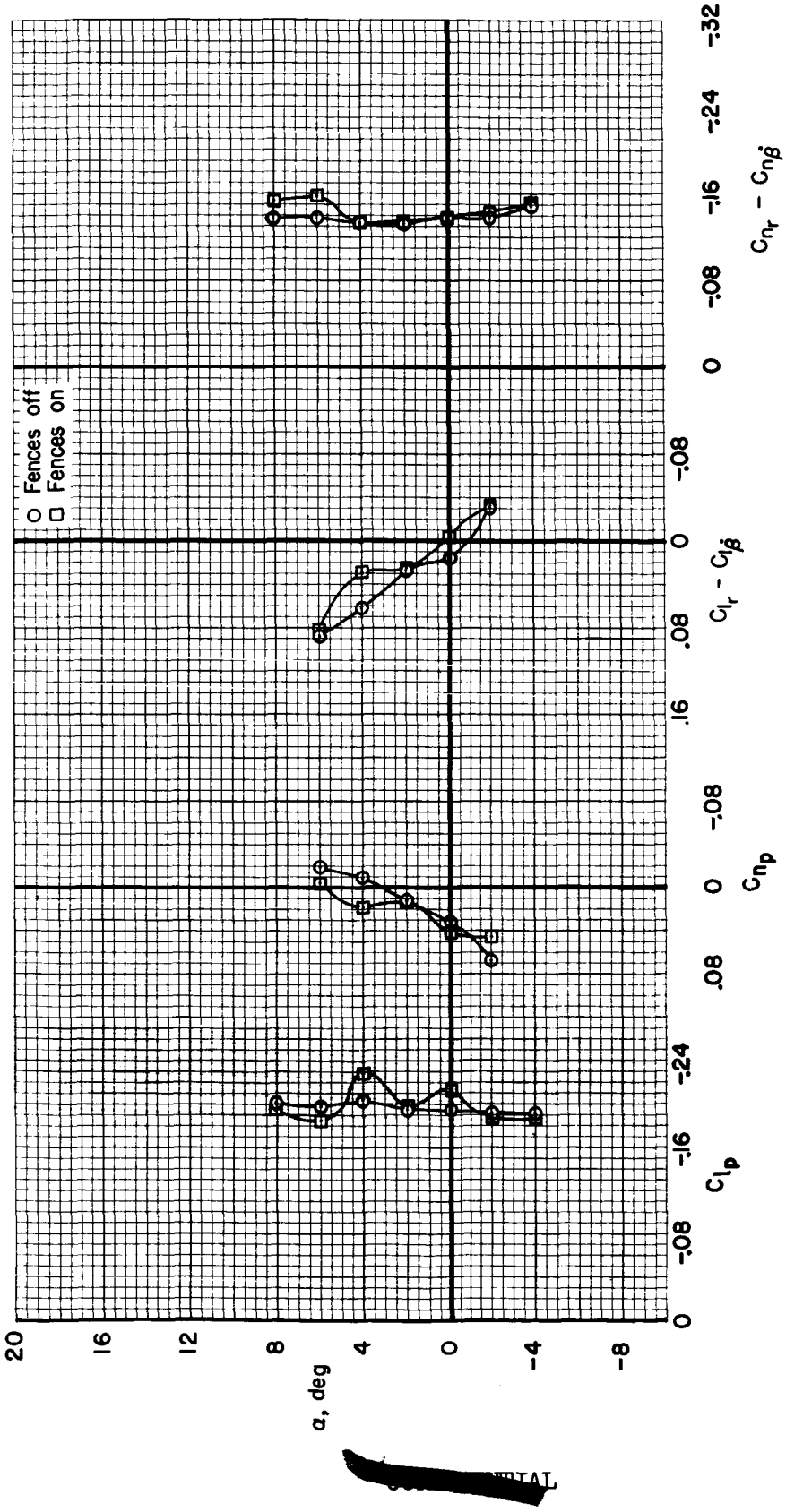

(d) M = 0.85

Figure 21.- Continued.

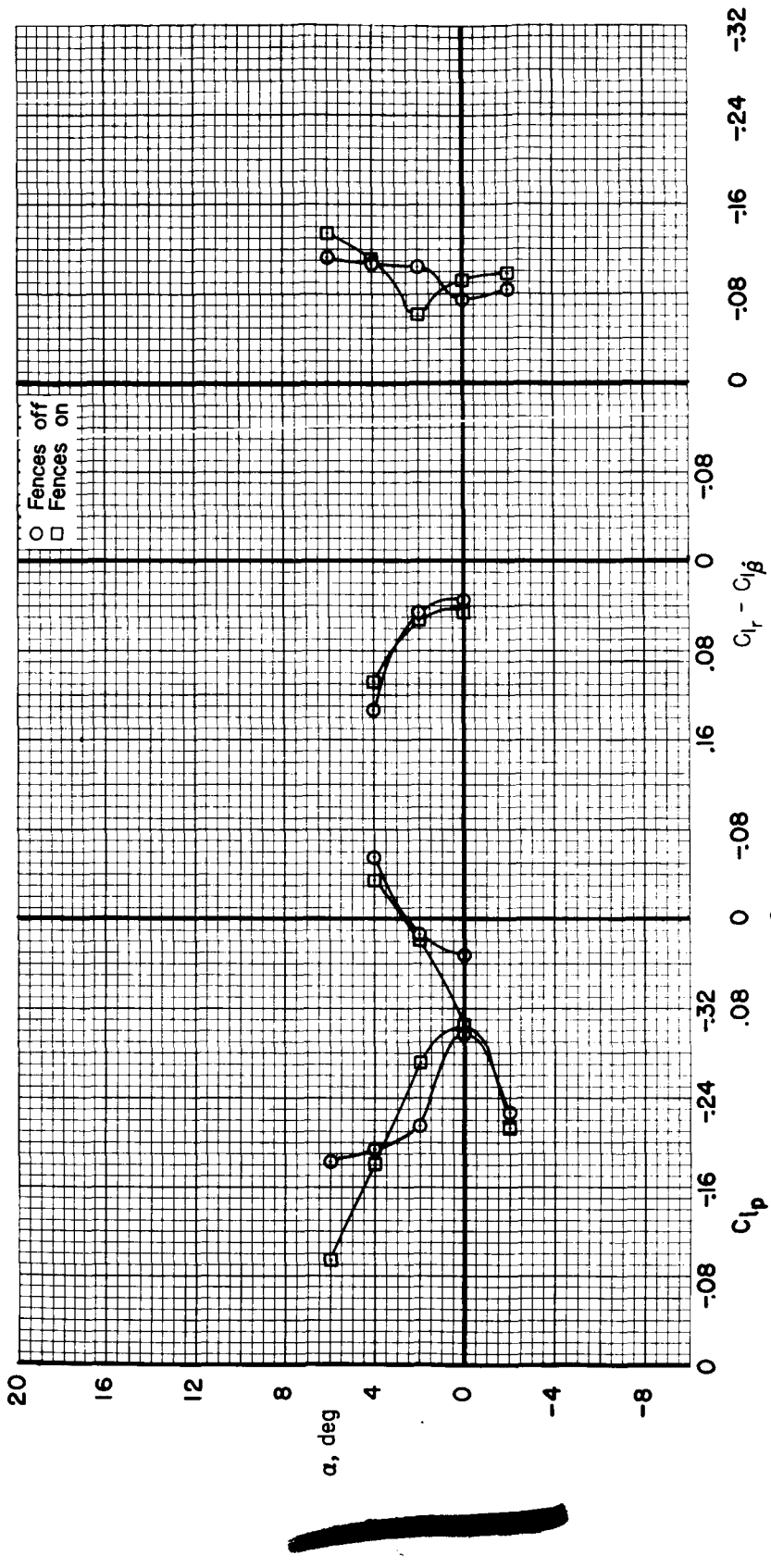

(e) M = 0.94

Figure 21.- Concluded.

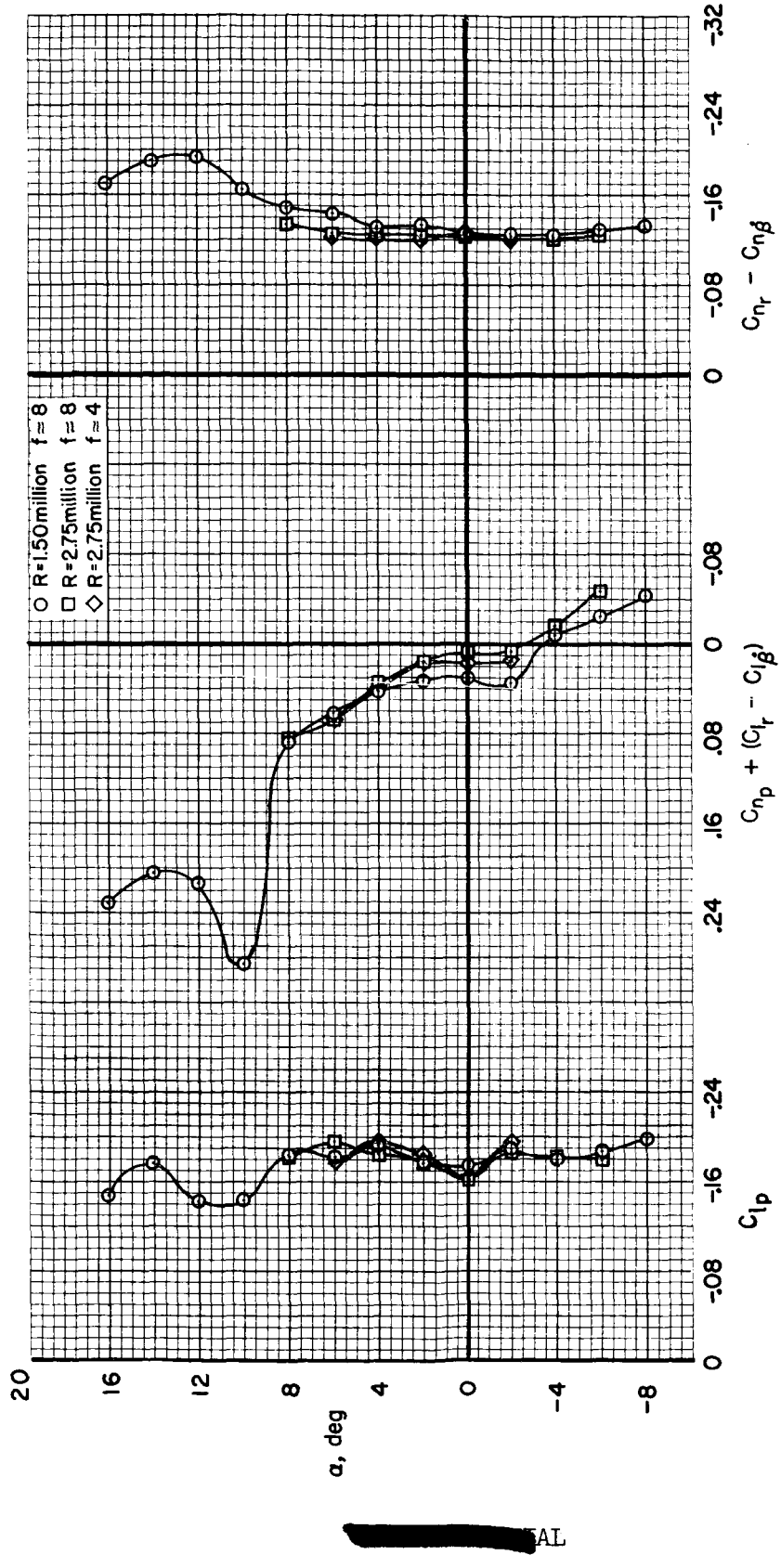

(a) M = 0.60

Figure 22.- The effect of Reynolds number and frequency of oscillation on the dynamic lateral-directional rotary stability derivatives.

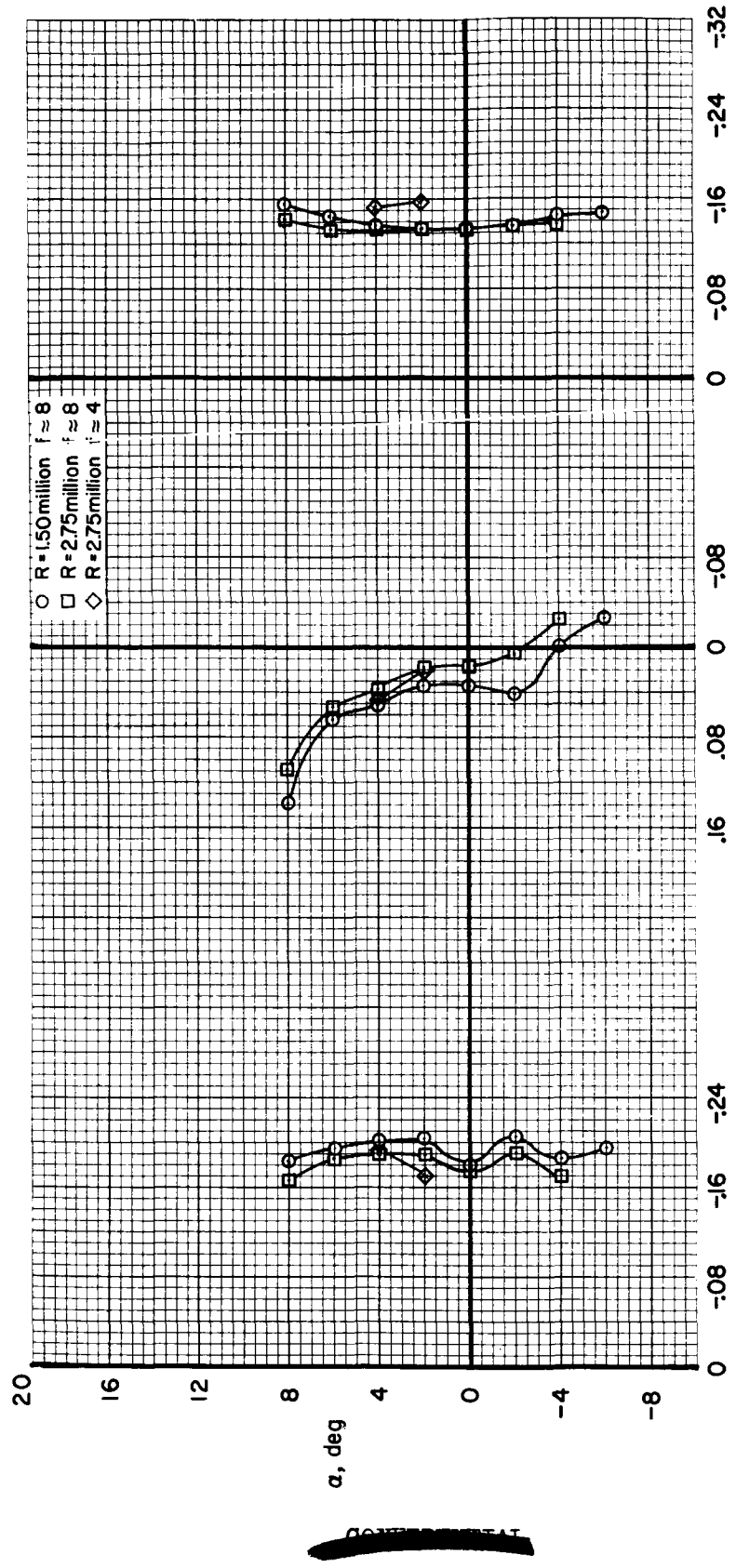

(b) M = 0.80

Figure 22.- Continued.

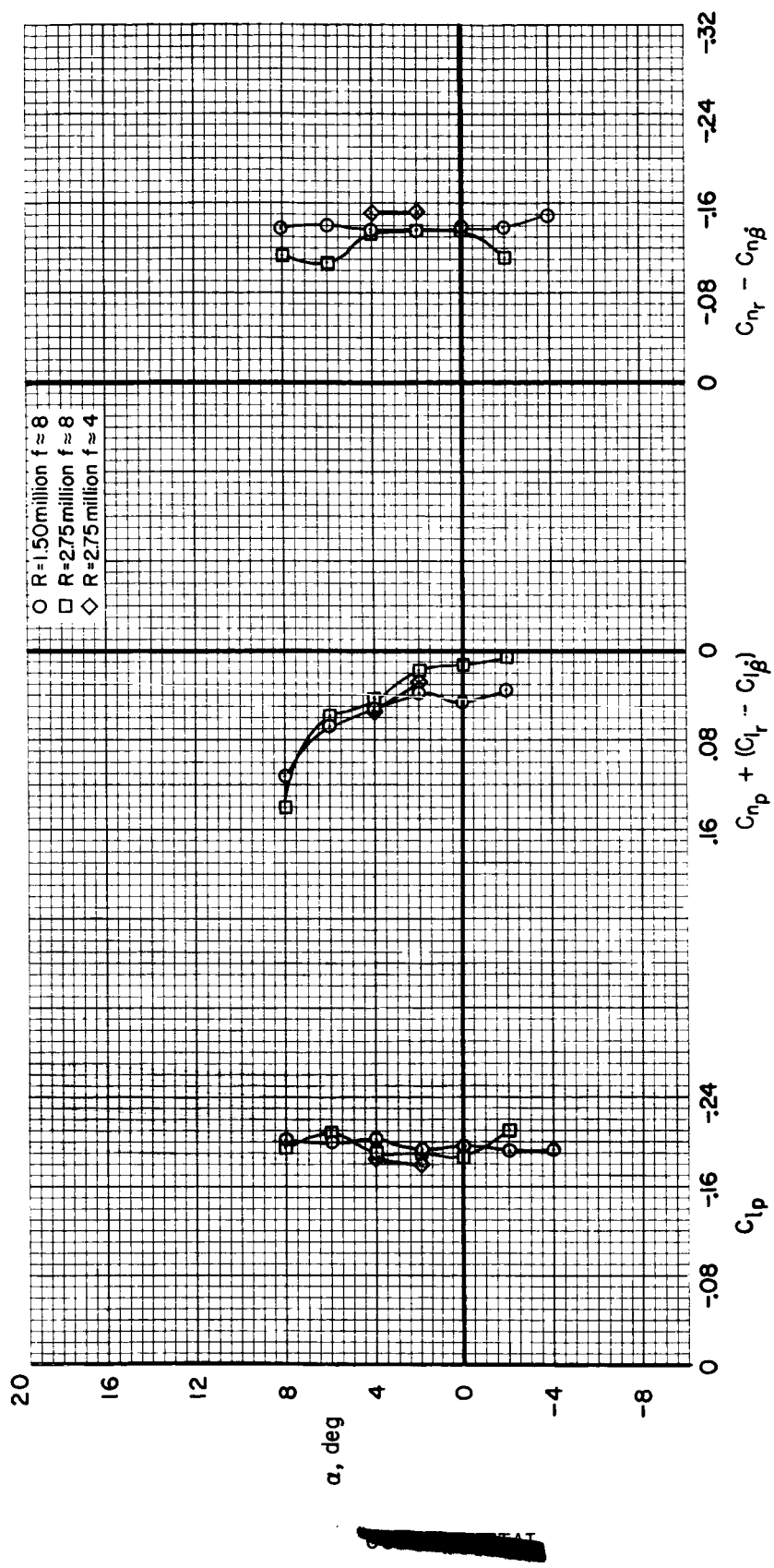

(c) M = 0.85

Figure 22.- Concluded.

[redacted]

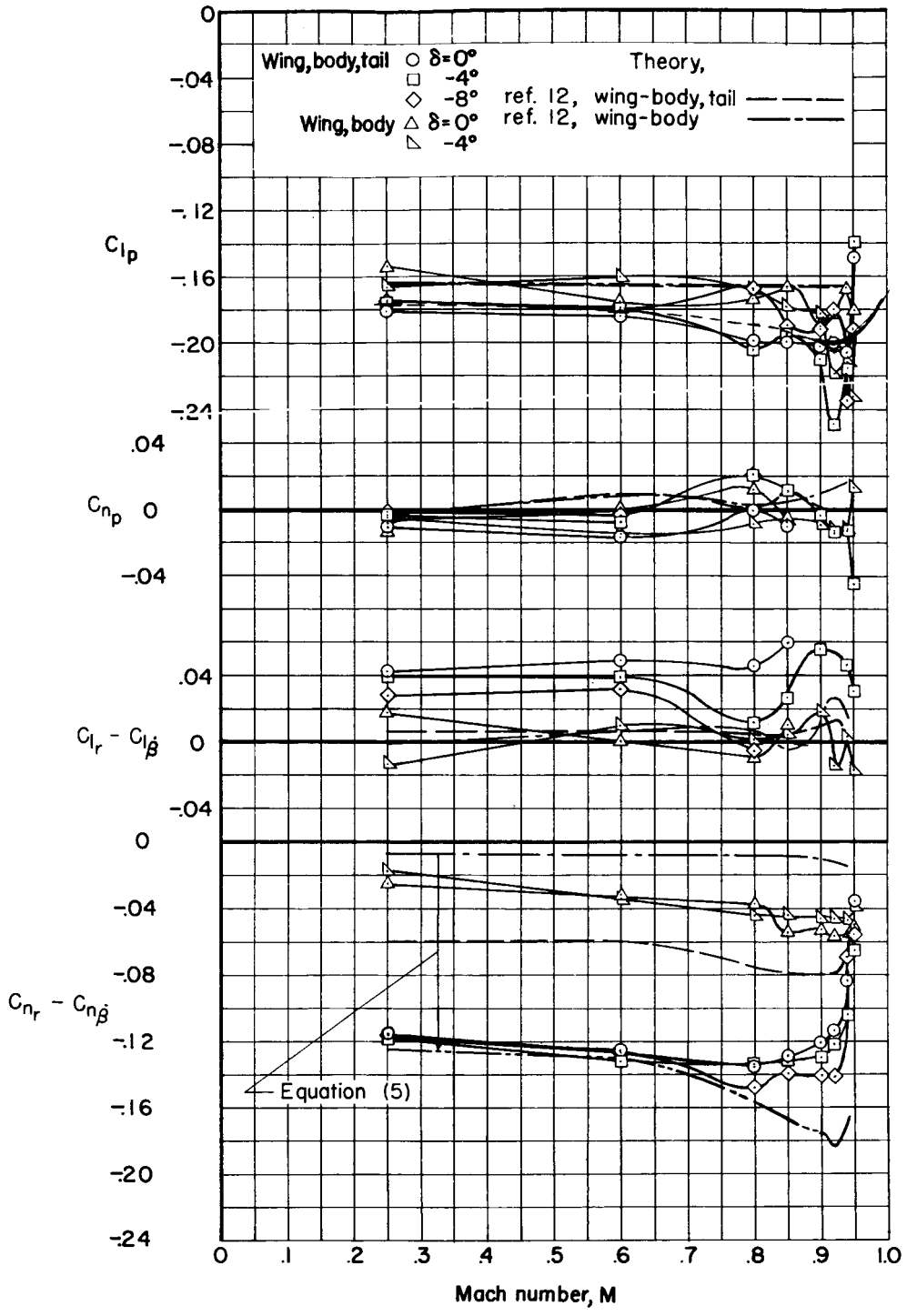

Figure 23.- The variation with Mach number of the dynamic lateral-directional rotary stability derivatives; $\alpha = 2^{\circ}$.

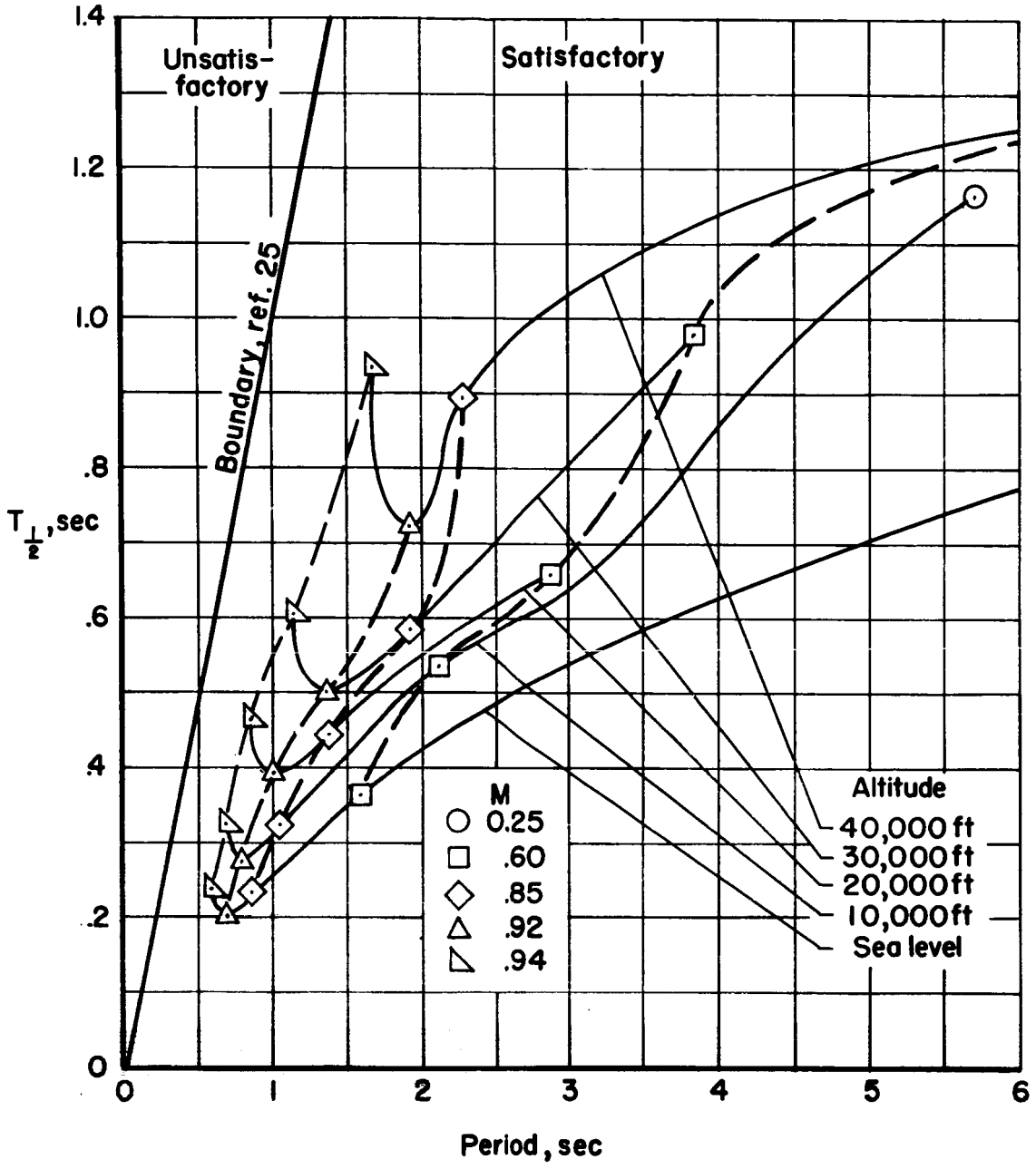

Figure 24.- Estimated period and time to damp of the controls-fixed, short-period, longitudinal oscillation for a representative airplane in level flight.

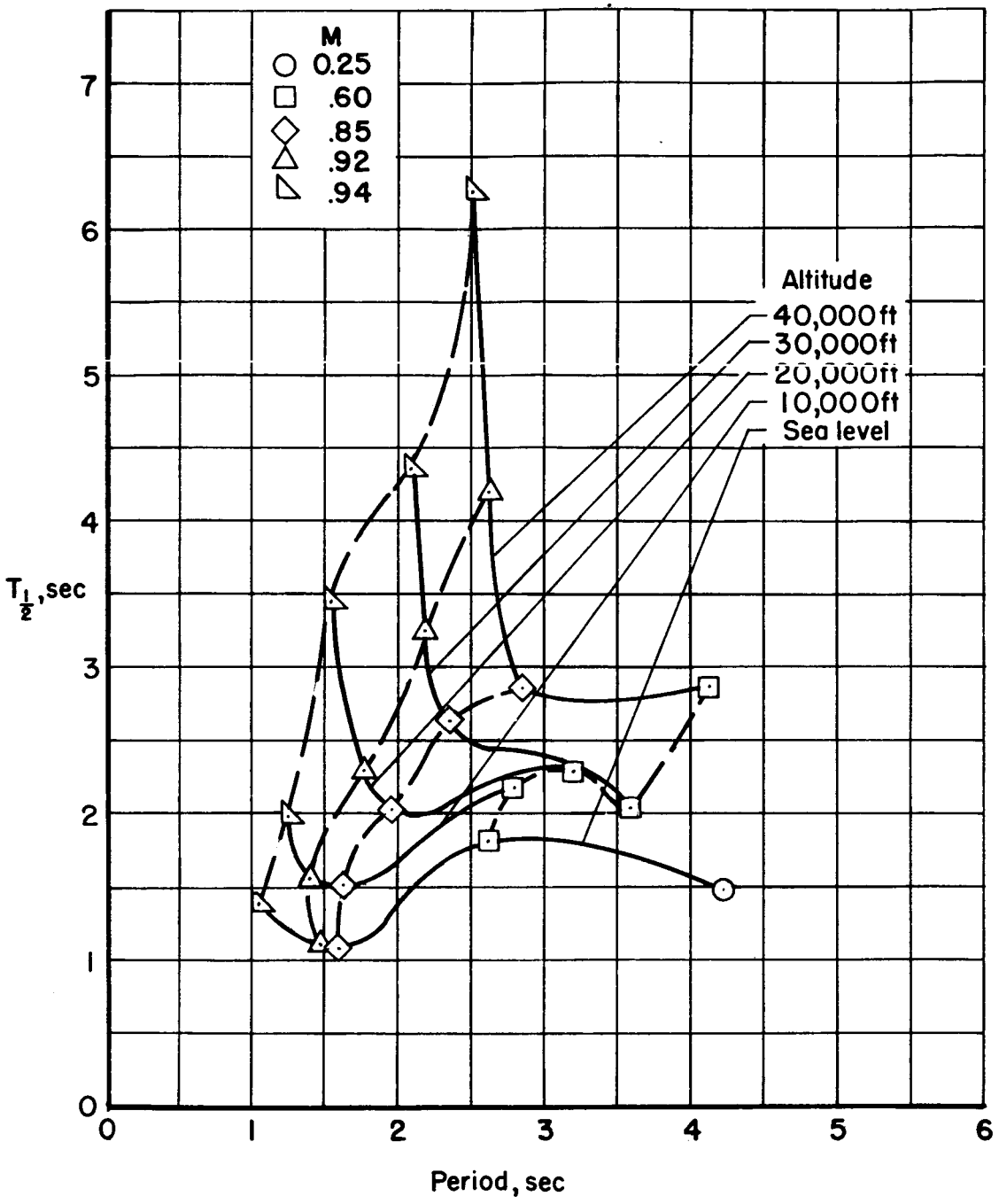

Figure 25.- Estimated period and time to damp of the controls-fixed lateral-directional oscillation for a representative airplane in level flight.

NACA - Langley Field, Va.